NATURAL RADIOACTIVITY IN ANGOLAN ADOBE HOUSES AND BUILDING MATERIALS

by

Judith Salupeto-Dembo

Lithosphere Fluid Research Lab at the Department of Petrology and Geochemistry,

Eötvös Loránd University, Budapest

Ph.D. thesis

submitted to the

Ph.D. Program of Environmental Geology, Doctoral School of Environmental Sciences,

Eötvös Loránd University, Budapest

Director: Imre Jánosi, D.Sc., Program leader: Csaba Szabó, Ph.D.

Supervisor:

Csaba Szabó, Ph.D.

Lithosphere Fluid Research Lab at the Department of Petrology and Geochemistry,
Eötvös Loránd University, Budapest

Consultants:

Zsuzsanna Szabó-Krausz, Ph.D.

MTA Premium Postdoctorate Research Program, Lithosphere Fluid Research Lab at the Department of Petrology and Geochemistry, Eötvös Loránd University, Budapest

Péter Völgyesi, Ph.D.

Nuclear Security Department, Centre for Energy Research, Budapest

2020 April

Budapest

ACKNOWLEDGMENTS

This project was financed by the Higher Education Department of the Angolan Army. The laboratory work was done at the Lithosphere Fluid Research Lab at the Eötvös Loránd University with the participation of the Centre for Energy Research, the Institute of Mineralogy and Geology of the Miskolc University and the Óbuda University. Passive detectors were provided by Radosys Ltd.

To my supervisor Csaba Szabó, no words can express enough my thankfulness, for the trust in me on this project and most of all for all the guidance and support. To my consultants Zsuzsanna Szabó-Krausz and Péter Völgyesi I am exceedingly grateful for your willing to be in this journey with me. Professor Csaba, Zsuzsi and Peti you were the right team, even in uncertain moments you were always there to make this moment happen. My thanks are extended to all the members of the Lithosphere Fluid Research Lab of the Eötvös Loránd University particularly: Nelson, Gorkhmaz, Silvana, László, Ábel, Thomas, Csilla, Levente. A big thanks to Mr. Erik Hulber and the workers of the Radosys Ltd., Hungary, as well as to Dr. Zoltán Kis and to all the colleagues connected to this project from the Centre for Energy Research. To Dr. Ferenc Kristaly from the Miskolc university for his contribution. Professor Éva Kiss from Eötvos Lorand University and Professor Judit Borsa from the Óbuda University, thank you for your kind help.

A special thanks to Mr. Geraldo Sachipengo Nunda and Domingos Lutok Liahuka for all the support. The field campaign was possible thanks to the support of many people in Angola, specially: Regue (with a very special thanks for being everywhere and overcoming all situations together during the whole field campaign), Agostinho, Adelaide, Lelo, Mestre, Bruno, Bemba, Nangueve, Tio Bino, Sr Sapundo, Sr David, Fifi, and all the local people for their trust and letting the work be done in their properties.

I cannot forget my family, my dear mother Mrs. Lizeth Pena, who has been there for me with all kind of support she could give, my grandparents (Judith and Isaac) who taught me valuable principles that are leading my life. Sakala, Justina, Valeria, Maymona and Samy, thank you for helping with the kids so that I could work. Madé "*toi même tu sais*". To my brothers thank you for when you could be there for me. Brothers and sisters in the Lord, thank you for all your prayers. Finally to my kids António, Elias, Sapi and Ezequiel, thank you for the joy you bring to me and most of all to my companion, friend and husband António Dembo, I couldn't have

been more blessed than having you in my life. I do not have enough words to say THANK YOU.

"*Praise the Lord, my soul; all my inmost being, praise his holy name. Praise the Lord, my soul, and forget not all his benefits*"

Psalm 103:1-2

Dedication

To those who are no longer among us, especially my father Elias Salupeto Pena, my grandparents Isaac, Ezequiel, Jonas and grandmother Liliana.

To all people present in my life today with a special thought to my husband, my mother Lizeth, my grandmother Judith and my kids Antonio, Elias, Sapi and Ezequiel.

To my extended family and all the Angolan future generation.

"Olondui vi nene apa vi tundalala, polo ndondo". (Umbundu)

"Os grandes rios nas suas origens não são se não pequenos fios de água". (Português)

"Big achievements come from modest beginnings". (Interpretation)

Umbundu popular saying

Table of contents

1. Introduction and objectives

Radiation exposure originates mainly from natural sources (Eisenbud and Gesell 1997). Human population is exposed to two types of natural radiation: 1) internal exposure is due to inhalation or ingestion of radionuclides, which release alpha, beta and gamma radiation inside the human body, 2) external exposure is mostly due to the more penetrable gamma radiation from surrounding environment. Radionuclides responsible for the internal exposure specifically for inhalation are radon and thoron and their progenies. For a couple of decades, radon (radon-222 from the U-238 decay chain) has been a subject of research due to its potential risk causing lung cancer. It is considered the second most important cause of lung cancer after smoking (World Health Organization (WHO) 2016). In another hand, radon-220, called otherwise thoron, another isotope of radon from the Th-232 decay chain, has been usually ignored given its short half-life of 55.6 s (Gierl et al. 2014). Thoron contribution to the inhalation dose has been already proven (Schery 1990; Doi and Kobayashi 1994; Chung et al. 1998; Tokonami et al. 2001) what further triggered surveys focusing on this isotope (Csige et al. 2013; Saini et al. 2016; Chege et al. 2019; Takoukam S. et al. 2019; Bineng et al. 2020). Many studies have proven high levels of thoron in houses made of unburnt earthen material (like soil or clay), or adobe, a block made of soil and water then dried in ambient conditions in sunlight. In Germany, a recent comprehensive study conducted in houses made of clay, the thoron annual inhalation dose was found to be as high as 4 mSv a^{-1} (Gierl et al. 2014). In China, a research made in traditional houses pointed on a thoron contribution up to 56.6 % to the inhalation dose (Shang et al. 2005). In Hungary, the same contribution was estimated to be 30 % in adobe houses (Szabó et al. 2014).

In Africa, research works mostly have been focusing on radon but not thoron. In some countries like Ghana, Nigeria, Kenya and Cameroon (Ajayi and Olubi 2016; Otoo et al. 2018a; Chege et al. 2019; Takoukam S. et al. 2019), an effort is being made to collect reference data based on which national radon action levels can be derived. Nevertheless, a few studies on both isotopes are reported. In Kenya (at the Coast region), in houses made of soil, 25 % of the surveyed houses showed values above 1 000 Bq m^{-3} of thoron activity concentration and the mean was 652 Bq m^{-3} (Chege et al. 2019). In Cameroon, a study at a high natural radiation area of Bikoue and Ngombas located in the uranium occurrences, in region of Lolodorf, reported a contribution of thoron to the inhalation dose by up to 78.5 % (Saïdou et al. 2015).

As for the external exposures, amongst natural sources the biggest causes are terrestrial radionuclides and cosmic radiation (Eisenbud and Gesell 1997; UNSCEAR 2010). Building materials also significantly contribute to the exposure of the population to natural radioactivity (Trevisi et al. 2010) as they contain terrestrial radionuclides. The main radionuclides responsible for terrestrial radiation are the members of the U-238 and Th-232 series together with K-40 contributor (Eisenbud and Gesell 1997; UNSCEAR 2010).

Numerous investigations on natural radioactivity of building materials have been carried out worldwide. These studies contributed to the elaboration of regulations applicable nationally or regionally (UNSCEAR 2000; ICRP 2007; UNSCEAR 2008, 2010; European Union 2013). It is true that most regulations are made for the technologically enhanced levels of radionuclides in building materials, however purely natural sources are to be spotted in order to prevent excess, unnecessary exposure to natural sources (e.g. by mitigation). In Africa, only a few countries followed the path of detailed study of natural radioactivity. Reviewing studies made in Africa, highly different results can be found depending on the focus of the research. For example, taking as a reference the worldwide median of UNSCEAR (2000), activity concentrations of primordial radionuclides in soil are in the range of the reference in Zambian building materials from Lusaka (Hayumbu et al. 1995), but higher in soils from an uranium ore deposit-rich area at the western part of Namibia (Shimboyo et al. 2016). In terms of dose, an investigation on rocks and soils for outdoor effective dose rates made at different sites in the southern part of Cameroon, showed variable results depending on the geology of the studied area, reaching values three to four times higher than the estimated average of 0.07 mSv y^{-1} by the UNSCEAR 2000 (UNSCEAR 2000; Ateba et al. 2010). In Kenya, studies have also shown annual effective doses higher than the reference in high background areas like the Ruri Hill (Mustapha et al. 1999; Achola et al. 2012). As seen above, natural radiation in Africa varies considerably depending on the geographical location and the geological background.

Adobe is one of the most used building materials in Angola, both in villages and suburban areas, and it is the most widespread building material of families with low income. It is easily accessible and it has an advantage of keeping a favorable indoor temperature in tropical climate. Likewise, adobe houses are popular in Africa mostly in the sub-Saharan part. Nevertheless, research on their natural radiation is scarce. A survey in a modern suburb of Ghana where most houses were built from the 90's to date shows that 28 % of houses are still made of adobe (Kitson-Mills et al. 2019). In Angola, no recorded studies were made on radon

and thoron, or generally on natural radiation and especially not in adobe houses where the inhalation and external doses received by residents are potentially elevated.

The main objective of this research is to get information about potential radiological risks of the Angolan population living in adobe houses by evaluating the external and internal exposure separately. To achieve this goal, examination was conducted in the field with in-situ measurements and in the laboratory investigating the building material itself. As this is the first time such investigation is done in the country, three areas with different geological background and microclimate were chosen. One at the north, one at the center and the last more toward the southern part. The aim of doing so is to have an idea on the spatial distribution of the radionuclides in the country. Besides evaluating the external and internal exposure of residents, further laboratory investigations were performed on the building material samples evaluating their structure, mineralogy and radon and thoron sources and emanation properties. The outcome of this research is a useful contribution to the African database in terms of natural radiation in general, but most of all, it provides essential information for further investigations in Angola.

2. Environmental radioactivity in adobe houses

2.1. Naturally occurring radionuclides in the environment and their geochemistry

2.1.1. Natural ionizing radiation

Human population is exposed to ionizing radiation everywhere in its environment. Radiation can be originated from natural or from man-made sources. Natural radioactivity is far the major source for human exposure to ionizing radiation with a worldwide average contribution of 2.4 mSv y^{-1} (UNSCEAR 2008). The major sources, contributing to natural radiation, are cosmic radiation, cosmogenic isotopes such as, for instance, carbon-14, aluminium-26 and beryllium-7 and -10, produced by the interaction of cosmic radiation with gas constituents and terrestrial radionuclides (Figure 1).

The amount of radiation received by humans is described by different dose definitions, all of which related to the amount of energy deposited into a given part of the body. Summing up all the terrestrial radionuclides, they go over 83 % in terms of contribution to the human annual average dose (UNSCEAR 2008). The intake of radionuclides can be internal via ingestion, inhalation. In this case radionuclides release alpha, beta and gamma radiation inside the human body. Another way is the external radiation mostly due to the more penetrable gamma radiation from surrounding environment. Radionuclides mainly responsible for the internal radiation are radon and thoron, when it comes to inhalation. Potassium-40, Ra-226, U-238 and Th-232 are mainly responsible for doses received through ingestion. All gamma emitting radioactive nuclides, including the ones from cosmic radiation, contribute to the external radiation.

Concentrations of terrestrial radionuclides depend on geology and geographical situation. They are found essentially in rocks, soils and building materials. Those materials are usually called NORM because they contain only naturally occurring radioactive materials (NORM). The contribution of cosmic radiation to the external dose mostly depends on the location of the exposed population on the Earth, more precisely mainly relates to the altitude.

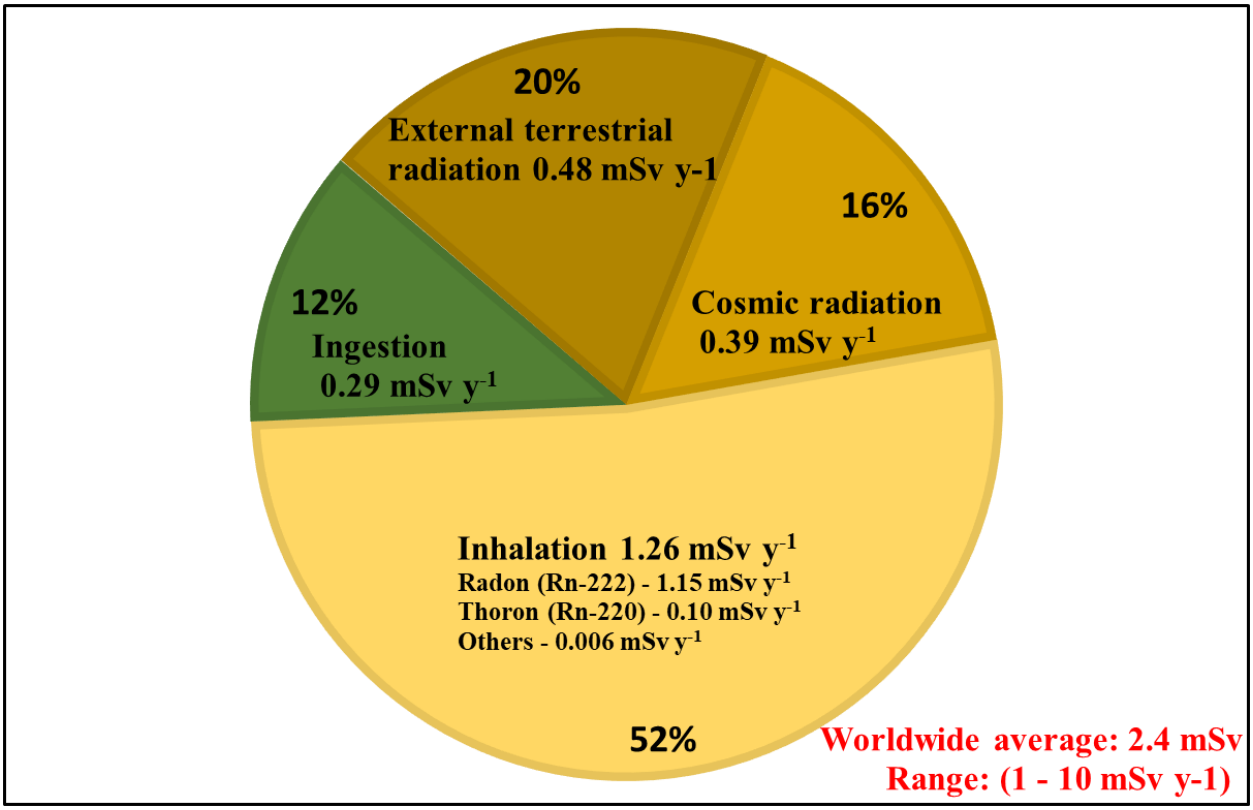

Figure 1. Exposure of human to radiation from natural sources (data from UNSCEAR 2008).

2.1.2. Geochemistry of radionuclides in the interest of this study

The focus of the present study falls on adobe building material, which is made of local soil. Therefore, in this chapter a special attention will be given to the radionuclides present in adobe, which account for human radiation exposure. Those radionuclides are radon and thoron responsible for the internal exposure, and Ra-226 (assumed in equilibrium with U-238), Th-232, their gamma emitting descendants and K-40 responsible for the excess external exposure due to building materials.

2.1.2.1. Radium and radon

Radium

Radium is an alkaline earth metal, with the atomic number Z = 88. In nature, radium occurs as 4 radioactive isotopes being part of decay series of primordial radionuclides, therefore, there is not stable radium. Radium-226 with the longest half-life of 1600 years is part of the U-238 series (Figure 2), Ra-223 (half-life = 11.43 days) is part of the U-235 series and Ra-224 (half-life = 3.63 days) and Ra-228 (half-life = 5.75 years) are part of the Th-232 series. The most

abundant radium isotope is Ra-226. Isotopes of radium are widely distributed in the Earth's crust. The estimated average U-238 concentration in the continental crust is 32.9 Bq kg^{-1} and, assuming radioactive equilibrium with U-238, the crustal Ra-226 activity is expected to be similar (IAEA 2014).

However, in some environments and because of their different geochemical behaviors, such as mobility, disequilibrium is expected between Ra-226 and U-238. This can occur for instance during chemical weathering process. The highest Ra-226 concentrations were observed in shale, bitumen slate and volcanic and phosphate rocks followed by granites, clay rocks and sandstone and, finally, sedimentary rocks, lime and carbonate (IAEA 2014). Radium-226 concentrations in soil in normal areas (i.e. areas without high natural background) vary from 3.7 to 126 Bq kg^{-1} (IAEA 2014). This variation of the concentration of radium in soils depends on the concentration in the source or bedrock, the kind of weathering process and the type of generated soil.

Radium-226 decays by emitting alpha particle to the Rn-222 isotope of radon. From radiological point of view, the relatively long half-life and the widespread abundance in environment of biological activity (in lithosphere and hydrosphere) make Ra-226 and its decay products the most important isotopes in the U-238 decay chain. Therefore, concentrations of these radionuclides are directly connected to the radiation exposure of the population, which varies from place to place depending mostly on the geology of the studied areas.

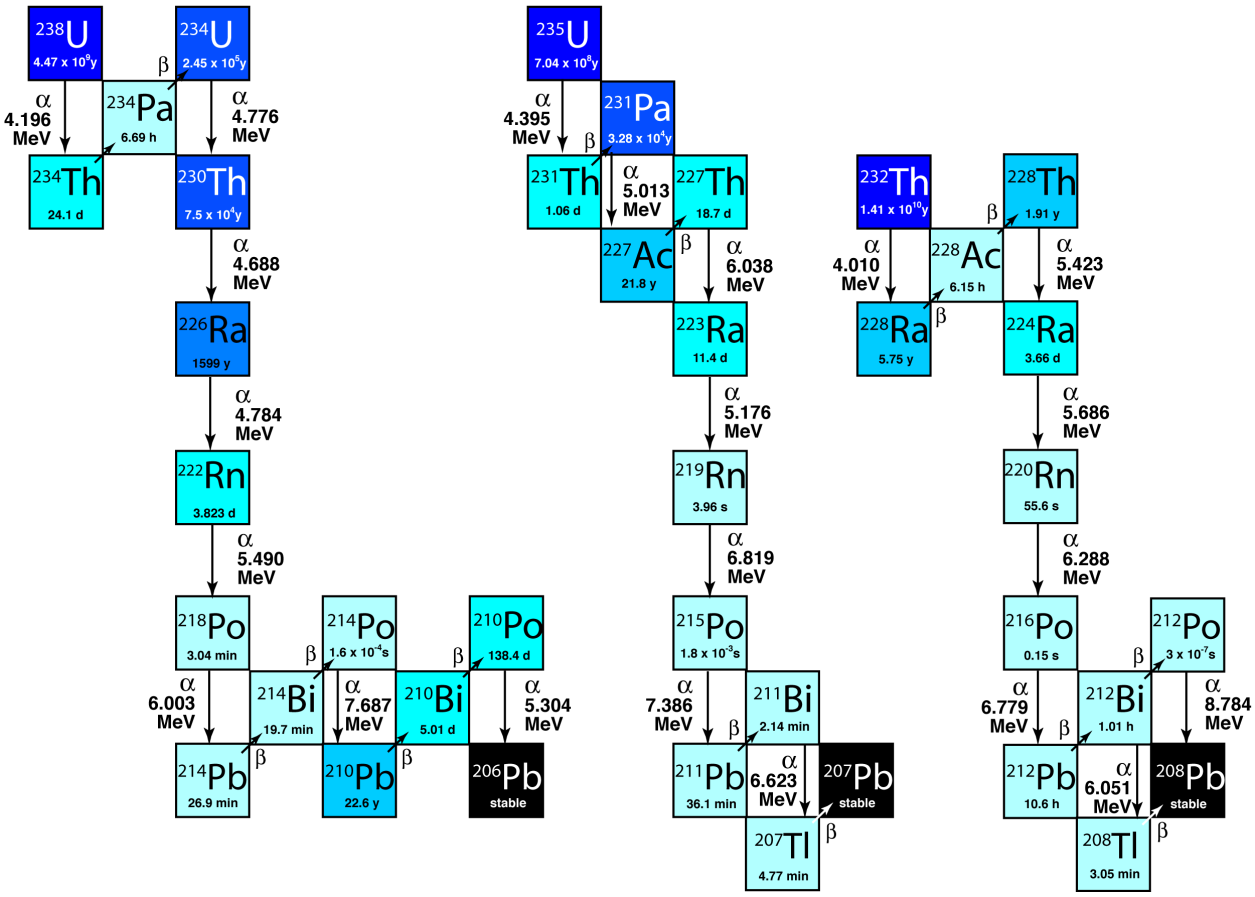

Figure 2. U-238 and Th-232 decay series specifying half-lives, decay type and energy of the isotopes (Bourdon et al. 2003).

Radon

Radon is a noble gas with the atomic number Z = 86. Radon has three known natural isotopes, Rn-222 (half-life = 3.8 days) from the U-238 series (Figure 2), Rn-219 (half-life = 3.96 seconds) from the U-235 series and Rn-220 (half-life = 55.6 seconds) from the Th-232 series (Bourdon et al. 2003). Two isotopes are of particular interest in this study, Rn-222 and Rn-220. The most common radon isotope is Rn-222 generally called radon, which is the 7th daughter isotope in the decay chain of U-238. Its direct parent is Ra-226 and forms by alpha decay and it decays to Po-218 by alpha decay. Because of its relatively short half-life (3.8 days), in nature radon existence exclusively depends on that of radium, its immediate parent. Radon is the only element present as gas phase in natural radioactive series in our environment. Once radon is produced inside a mineral, it can either be stuck inside the grain or recoiled to the pore space. Once in the pore space radon migrates by diffusion or convection and it migrates until reaching the atmosphere. Because of its solubility in water, radon can also be transported by subsurface water (i.e. ground water). The recoil length of radon is typically 30-

50 nm in solid materials, 95 nm in water and 64 000 nm in air (Szabó 2013). Radon is hazardous because of its mobility and due to its 3.8 day half-life what consequently leads to accumulation in closed places (Smith and Cothern 1987).

2.1.2.2. Thorium and thoron

Thorium

Thorium is a metal belonging to the actinide series with the atomic number 90. Thorium has 6 naturally occurring isotopes. In each of the natural decay chains we find 2 isotopes of thorium. Thorium-234 and Th-230 belong to the U-238 series (Figure 2), Th-231 and Th-227 are from the U-235. Finally, Th-232 is the first member of the decay chain where it belongs and Th-228 is a member of this series. The most abundant and long lived isotope of thorium is Th-232. It decays to Ra-228 by emitting an alpha particle. It has two oxidation states, 3 and 4, however in nature is essentially found in the 4^+ oxidation state, which is unsolvable in water. The other one is rare and unstable in aqueous solution (Boyle 1982). Among the heavy radioactive metals (with Z>83), including uranium, thorium is the most abundant. It is a highly lithophile element consequently more abundant in continental crustal rocks (9.6 – 12 mg kg^{-1}). It is oxyphile in nature and it occurs manly as oxide, silicate and phosphate. It has some biophilic affiliation and is found in various living organisms like phytoplankton, some fungi, algae and bacteria (Boyle 1982). It also tends to concentrate under certain conditions in organic compounds like petroleum, coal and humus. The main thorium minerals are thorite $ThSiO_4$, thorianite ThO_2 and monazite $(Ce,La,Nd,Th)(PO_4,SiO_4)$. It can also be found as an accessory element in mineral of zircon, sphene, epidote, uraninite, allanite and apatite occurring in igneous rocks. In soils, thorium concentrations show a wide range from 0.1 to 50 ppm. Thorium is strongly adsorbed onto mineral surfaces mostly on clay minerals what can considerably increase its concentration in some soils (Boyle 1982; Bourdon et al. 2003). In the Th-232 decays series a radon isotope (Rn-220) is found which is commonly called thoron.

Thoron

Thoron is a radon isotope generated by Ra-224 via an alpha decay with a half-life of 55.6 seconds. Thoron decays to Po-216 by emitting an alpha particle (Figure 2). From the six thoron daughter isotopes, two needs special attention, which are the Pb-212 because of its longest half-life among thoron daughters and the Po-212 because of the high alpha energy generated by its decay (Figure 2). Like radon, thoron is a threat to human health when its progenies are inhaled from the concentrated indoor air. Unlike radon, thoron mainly

accumulates indoors deriving from the building material. The reason for that is its much shorter half-life (55.6 seconds vs. 3.8 days), which does not allow thoron to reach the indoor environment from the bedrock or soil. When thoron generates inside a mineral, the recoil length for thoron is considered to be the same as radon. However it, indeed, should be slightly higher due to the more elevated alpha energy generated when it is formed (5.69 MeV vs. 4.78 MeV, Figure 2, as it was studied, for instance, in thesis of Szabó (2013).

2.1.2.3. Potassium

Potassium is an alkali metal with the atomic number Z = 19. Three naturally occurring K isotopes are known as K-39 (93.3 %), K-40 (0.011 %) and K-41 (6.7 %). Among the isotopes only K-40 is radioactive with a half-life of 1.28×10^9 years. In 89.1 % of cases, K-40 decays with an emission of a negative beta particle (i.e. electron) yielding Ca-40 stable isotope and in 10.9 % of cases it produces stable Ar-40 by electron capture. The decay to Ar-40 is always followed by a measurable gamma ray at 1460.8 keV (e.g. Völgyesi 2015). The average K-40 activity concentration in soil is 420 Bq kg^{-1} (UNSCEAR 2000). Potassium is known as one of the major chemical elements in the Earth's crust (~2 m/m %). Its oxidation state is K^+, which is highly soluble in aqueous system. It is easily incorporated in particularly in structure of sheet minerals (like clay minerals). Potassium is an essential micro element for living organisms. It is readily ingested by plants from soils and gets into human body by nutrition.

2.2. Radon and thoron emanation of adobe building material

2.2.1. Adobe building material

Adobe is one of the oldest building material used by humankind (Pacheco-Torgal and Jalali 2012). It is found worldwide and it is widely used nowadays (Avrami et al. 2008; Fratini et al. 2010; Pacheco-Torgal and Jalali 2012; Szabó et al. 2013; Gomes et al. 2014; Saïdou et al. 2015). Over half of the Earth's population is estimated to live in houses constructed by unburned earthen material (Avrami et al. 2008).

Adobes are made of soil and water, sometimes mixed with organic matter, and dried at ambient conditions (Figure 3). Because of the simple manufacturing of adobes, they preserve the radionuclide content of the source soil. It is important to note that one of the main factors that determines soil composition is the geological composition of the county/bed rock. Studied building material (adobe) is made of the local soil, which develops via chemical weathering

process from the surrounded rocks. The composition of the source rock eventually controls the natural radioactivity of the soils of the area (Navas et al. 2011) and, therefore, of adobes. Consequently, mineralogical and physical (grain size and shape) composition of adobe widely depends on the place of its origin. As a result of the above stated, the type of soil and with it the clay content of the adobe also highly varies (Coffman et al. 1990). One important parameter affected by the difference in mineralogical composition is the porosity. Adobe containing a low portion of clay mineral tends to be more porous. On top of that, as the adobe gets dehydrated by water evaporation, small cracks are formed around and inside the block, which increases considerably the gas-permeability of adobe.

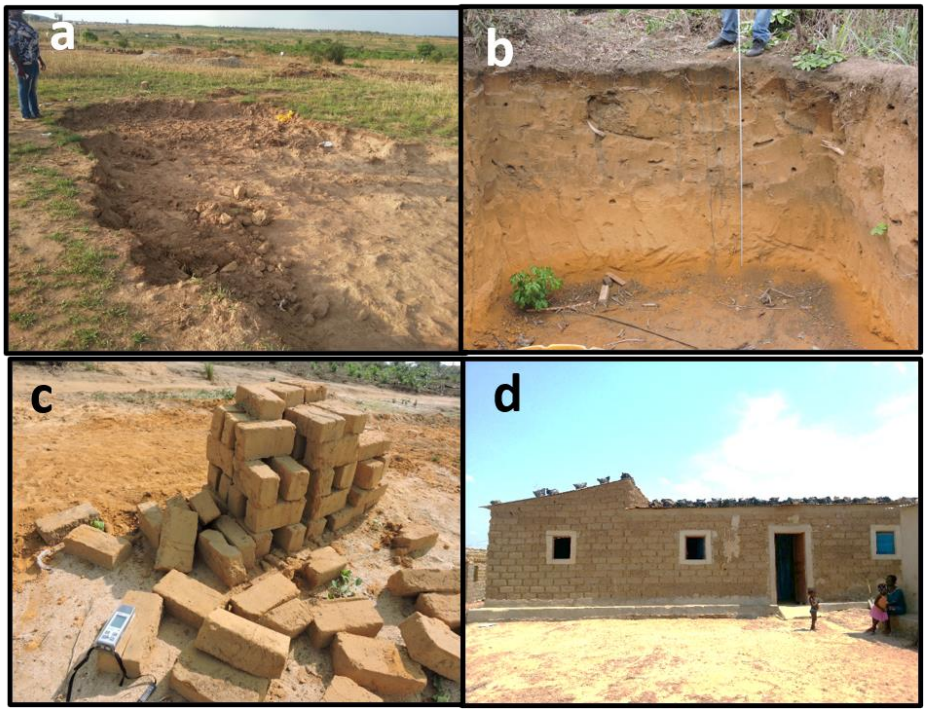

Figure 3. Illustration of a) source site for adobe manufacturing in Menongue b) source site for adobe manufacturing in Huambo, c) adobe building material in Huambo, d) adobe house in Cabinda (Pictures taken by Judith Salupeto-Dembo).

2.2.2. Radon and thoron emanation processes

Radon and thoron indoor accumulation depends on many factors. First, both radionuclides need to be generated by the decay of the mother nuclides radium-226 and radium-224, respectively. Secondly, they need to be transported, mainly by diffusion or convection from the host material to the surrounding space. If the surrounding space is a closed one, as it is the case of dwellings, then it will be accumulated. Two main processes are important to understand

from the moment radon/thoron[1] is decayed to the moment it moves into the indoor space. Emanation is when radon/thoron leaves the mineral grain and reaches to the pore space. Exhalation is when it leaves the pore space of the host material to the surrounding space. Throughout the process of emanation, not all radon is able to leave the grain to the pore space. The amount of radon/thoron leaving the grain depends on the location of the mother nuclide in the grain. This amount that can leave the grain to the pore space is called emanation coefficient. The emanation coefficient is influenced by several factors. The first is the radium or thorium content and distribution in the grain (Nazaroff 1992; Porstendörfer 1994), the water content in the pore space (Thamer et al. 1981), the grain size distribution in the material (Nazaroff 1992), and, as some studies also suggest, the influence of the temperature (Nazaroff 1992; Eakin et al. 2016). Radon emanation coefficient in soils is reported to be very high, 1 to 50 %, and in building materials, 0.2 to 30 % (Porstendörfer 1994), whereas thoron emanation coefficient is shown to be 5 times less, 0.2 to 6 % in building materials. As seen above, adobe building material behaves like soil, given the fact that it keeps most of the soil properties. Moreover, the way it is manufactured increases the chance that the porosity is high. Consequently, radon/thoron emanation fraction in adobes is likely to be identical or similar to that of the soils (Szabó 2013), meaning that it is expected to be high compared to other building materials. In Africa, it is difficult to find reported studies on emanation. Nevertheless, a study carried out on variability of disequilibrium and the emanation fraction made in 1978, reported an emanation fraction of 26 to 79 % in South African soils from a uranium mine located in an arid area (Levinson and Bland 1978).

[1] When the information is applied to both radon and thoron they will be written as "radon/thoron" hereafter.

3. Study areas

Angola is the sixth biggest African country with a 1 246 700 km^2 area. The western part of the country is surrounded by the Atlantic Ocean along a 1650 km long coastline. The geographical landscape of the country varies from north to south as follows: a tropical forest at the north part, a fine coastal line along the ocean, an interior plateau in the center, and a dry savannah from south to south east.

Three geologically and climatically different areas, Cabinda, Huambo and Menongue have been chosen for this study from the north, central and south parts of Angola, respectively (Figure 4). These three localities belong to three different provinces. Below an overview of each province is provided. Information about geological features described in this section was taken from "*Notícia Explicativa da Carta Geologica de Angola*", a summary of the geology of Angola made by the National Institute of Geology in 1977, reviewed and updated in 1992 (De Araújo 1992). It is important to note that the reconstitution of the Angolan Geological map is still ongoing.

In general about the climate, Angola is a tropical country and only two main seasons are identified, the rainy (November-May) and the dry (June-October) seasons. Weather data detailed are taken for the monitoring period between November 2014 and October 2015 from the "*OpenWeather"* website history (OpenWeatherMap 2016), which uses data from local weather stations.

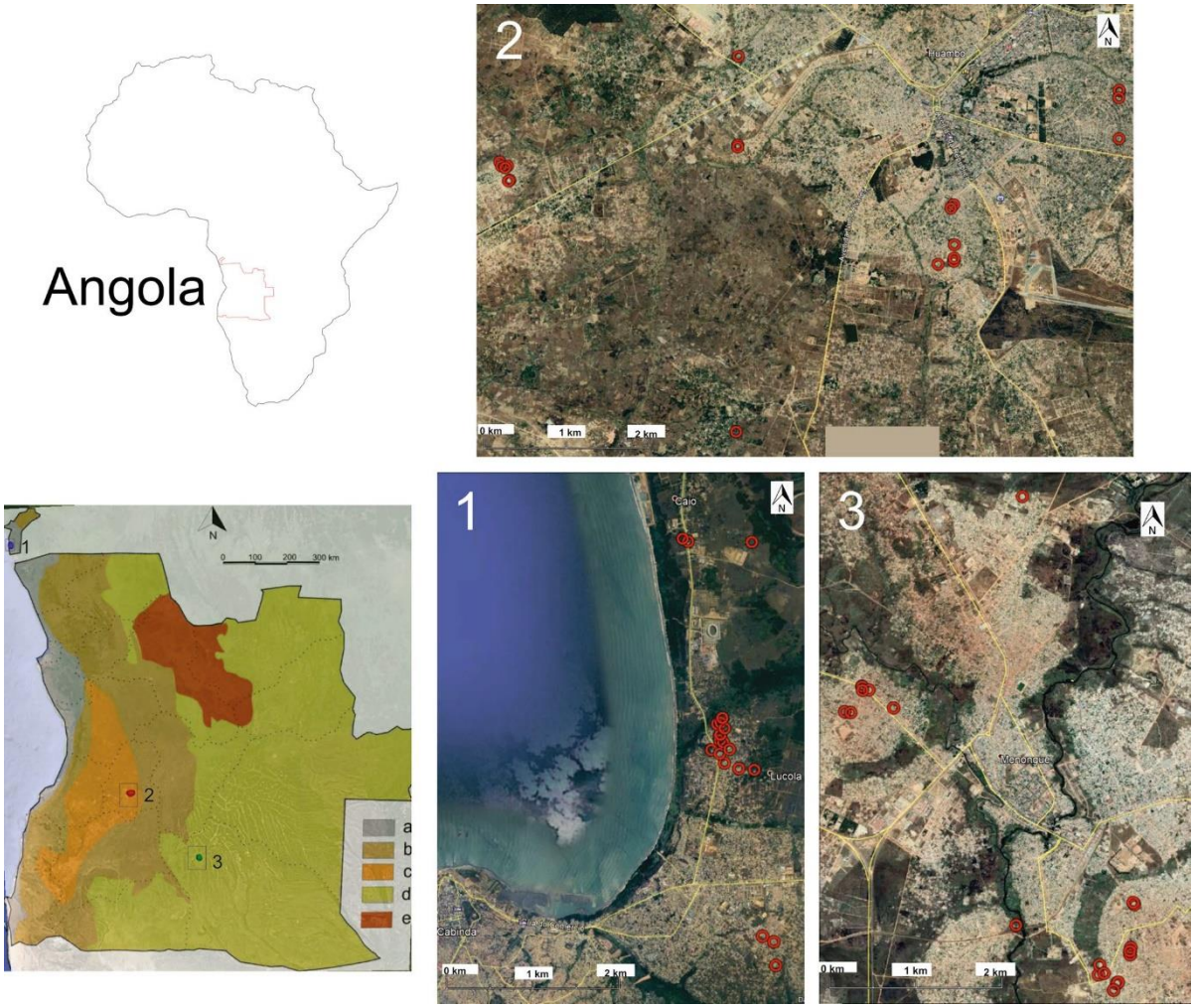

Figure 4. Sampling sites in 1 - Cabinda, 2 - Huambo and 3 -Menongue on the sketch of the geological map of Angola taken from Geologia de Angola by De Araujo (1992). Geological features on the map are as follows a) Cretaceous to Pleistocene marine sediments, b) Archean to Proterozoic metamorphic and igneous rocks, c) Belts of the upper Proterozoic (Pan-African of age), d) Sedimentary formations from Tertiary to Quaternary, e) Paleozoic to Mesozoic sedimentary rocks.

3.1. Cabinda

In Angola most of the main cities have the same name as the province they belong to. This is the case of Cabinda which is the main city of the Cabinda province. It is located at 12° 12'E and 5° 30'S with a mean altitude of 1 m above sea level (Figure 4). The province of Cabinda is an enclave located at the North-West part of the country between Zaire and Congo. Its climate is tropical humid.

The geology of Cabinda province is characterized by various formations aging from Precambrian to Holocene, including Pleistocene marine deposits at the coastal area. Soils in Cabinda province are mostly alluvional soils, calsisoils, ferralsoils, paraferrallitic,

psammaferralitic and psammitic soils (Diniz 2006). Psammitic soils corresponds to the arensoils following the FAO/UNESCO classification (FAO 1977). The radon and thoron activity concentration measurements were done at the coastal part of the main city (zone corresponding to psammitic soils), where the humidity is very high in both seasons around 85 % (Figure 5a). Higher temperatures are registered during the rainy season with an average of 27 ℃ than in the dry season with an average of 23 ℃ (Figure 5b). During the monitored year (2014-15), total precipitation was 244 mm for the rainy and 2 mm for the dry season (Figure 5c).

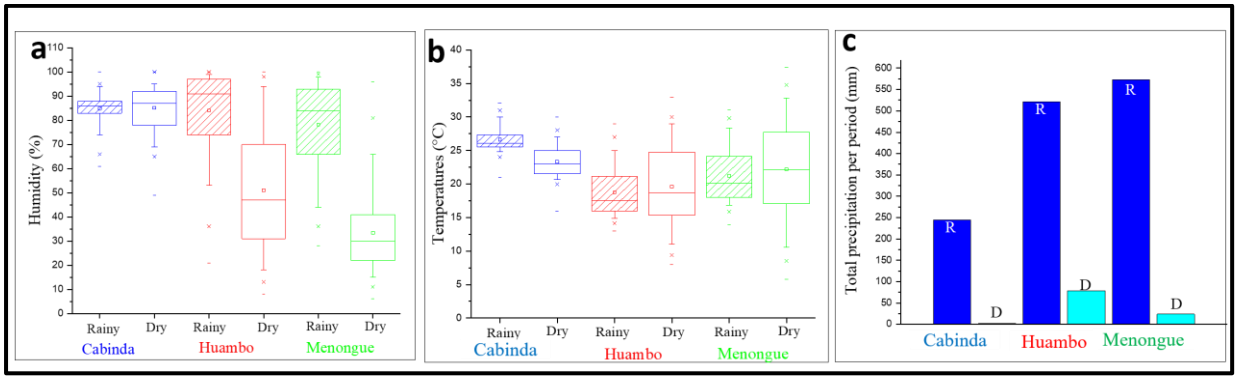

Figure 5. Box and whisker plots of (a) humidity, (b) temperature values and (c) bar chart of total precipitation in rainy (R) and dry (D) seasons (OpenWeatherMap 2016) at the studied areas during the survey period.

3.2. Huambo

Huambo is the capital city of the Huambo province. It is located 1700 m above the sea and the coordinates are 15° 45'E and 12° 48'S (Figure 4). The province of Huambo is located at the central part of the country. Its climate is tropical highly influenced by the altitude and the cold current of Benguela.

The geology of Huambo province consists of old (Archean to Proterozoic) metamorphic (gneiss, micaschist, metasediments) and igneous (granite, rhyolite to andesites) rocks. At Huambo city, Paleocene-Eocene laterites were also mapped. The most common unit of soil in this area is the ferrosoils in different varieties. Local units are identified, influenced by the microclimate, relief and draining system. The main types of soils are: oxilithic dark gray, oxipsammitic darkish, paraferrallitic, red ferralsoils, yellow and darkish ferrasoils, typical ferrasoils, psammaferralitic, psammahydromorphic, shallow laterite soils, lithosoils with rocky outcrops (Diniz 2006). The climate is highly influenced by the altitude, i.e. 1700 m above the sea. In the rainy season, the average humidity is 84 % and in the dry season, it is 51 % (Figure

5a). The average temperature during the rainy season is 19 ℃ and during the dry season is 20 ℃ (Figure 5b). Precipitation registered during the monitoring period was 522 mm for the rainy and 79 mm for the dry season (Figure 5c).

3.3. Menongue

Menongue is the main city of the Cuando Cubango province. It is located at 17°41'E and 14°39'S with an elevation of 1300 m above sea level (Figure 4). The province of Cuando Cubango is located at the southwest part of the country.

The geology of Menongue study area is based on Archean gneiss, Proterozoic rhyolitye-andesite and Tertiary-Quaternary Kalahari sediment formations. The most representative soils are arenosoils. Nevertheless, small localized unites are grouped as follow: fluvisoils, psamma-regosoils, calcisoils, oxipsammitic darkish, psammaferralitic, psammahydromorphic, humic psammahydromorphic, arensoils and lithosoils (Diniz 2006). Menongue has a semi-desert climate influenced by the desert of Namibia. The humidity is much higher during the rainy (78°%) than during the dry season (33 %, Figure 5a). The temperature difference between daytime and night is around 10 ℃ during the rainy season and 20 ℃ during the dry season. The average temperature in the rainy season is 21 ℃ and in the dry season is 22 ℃ (Figure 5b). Precipitation data registered during the monitored period gives a total of 573 mm and 24 mm for the rainy and the dry seasons, respectively (Figure 5c).

4. Methods

4.1. In-situ techniques

In-situ measurements were done in houses located in suburban areas. Adobe houses in Angola are abundantly found in suburban areas and villages. As for the houses, the willingness of the owners to participate in the campaign was determinant. The very low level of education of local population made the fieldwork rather difficult. Dwellers were suspicious about the used material. Therefore, an effort was made to have measurements in houses where an adobe building material sample could be collected as well, even though it was not always possible. Two kinds of measurements were done in-situ. The ambient gamma dose equivalent rate by a portable device and the radon and thoron activity concentration measurements with the help of passive detectors.

4.1.1. Ambient gamma dose equivalent rate determination by a portable device

The portable device FH 40 G-L10 (Thermo Fisher Scientific Inc.) was used to perform the in-situ ambient gamma dose equivalent rate measurements. The detection limit of the mentioned survey goes from 10 nSv h^{-1} to 100 mSv h^{-1} and from 30 keV to 4.4 MeV regarding the gamma energies. The investigation was done in 45 houses (15 per area). In living rooms 3 different points were measured taking two opposed corners and the center of the living room. At each place two measurements were done, one on the floor and the other one at a height of 1 m. As for the background radiation, measurements were taken outdoors at 1 meter exclusively, at 10 randomly chosen points per area. A total of 300 measurements were taken. The ambient gamma equivalent dose rate is given in nSv h^{-1}. For the annual effective dose from the external sources, the given value was converted to mSv y^{-1}.

4.1.2. Radon and thoron activity concentration monitoring by etched track detectors

A pair of passive radon and thoron detectors were used separately for the rainy and dry seasons in a year monitoring period in 2014-2015. The rainy season was recorded by a measurement campaign from the beginning of November 2014 to the end of April 2015, whereas the dry season campaign took from the beginning of May to the end of October 2015. The exposure time was 180 +/- 5 days. Fifteen houses per area, in total 45 houses were monitored. Only

those results were analyzed where values were available about both radon and thoron in both rainy and dry seasons, making a total of 40 dwellings. For the placement of the detectors, two aspects were considered. The first one is the possibility of disturbance of the measurement by the residents or visitors of the surveyed dwellings and the second one is the efficiency of measuring thoron. The distance of the detector from the wall, therefore, was around 8-10 cm and the height around 2 m (when not placed behind a cupboard). All detectors were placed in living rooms as the only place made available by the owners.

In this study, etched track passive detectors were used to monitor radon and thoron activity concentrations. This is a detector composed of two electroconductive cylindrical plastic chambers containing CR-39 plastic nuclear track detector (PNTD). The mentioned chambers are made in a way that one is restricted to detect thoron and the other can detect both radionuclides. Radon and thoron activity concentrations are determined after the PNTDs are etched and alpha tracks are identified and counted with a proper reading system (Tokonami et al. 2005). Analysis of etched track passive detectors, reading results as well as radon and thoron activity concentration calculations were all performed by the manufacturer, Radosys Ltd. (Budapest, Hungary).

4.1.3. Estimation of annual inhalation doses

To evaluate the health risk of the population living in the monitored houses, inhalation dose from radon and thoron were calculated based on Eq. 1 (UNSCEAR 2000).

$$D_i = 10^{-6} * C_{av} * F_{eq} * F_c * O \qquad \text{(Eq. 1)}$$

where D_i is the estimated annual inhalation dose from radon or thoron (mSv y^{-1}), C_{av} is the annual average radon or thoron activity concentration (Bq m^{-3}), F_{eq} is the equilibrium factor which is 0.4 for radon (UNSCEAR 2000) and 0.04 for thoron (Harley et al. 2010), F_c is the dose conversion factor which is 9 nSv (Bq h m^{-3})$^{-1}$ for radon and 40 nSv (Bq h m^{-3})$^{-1}$ for thoron (UNSCEAR 2000) and finally, O is the annual indoor occupancy time (7012.8 h y^{-1}). It is important to note that the direct determination of decay product activity concentrations and equilibrium factors were not possible within this study. Therefore, average values were used. Like this, for radon, it is accepted to provide a comparably good estimation for the dose, however for thoron, the doses estimated with a discrete F_{eq} = 0.04 will be loaded with high uncertainty.

4.2. Laboratory methodologies

4.2.1. Adobe building material sampling

A total of 60 adobe samples were collected in the three study areas, making 20 per area. The materials were sampled from (i) pieces of remaining adobes after construction, (ii) pieces took directly from houses, and (iii) soil used to make the adobe, in a few cases. The sampling sites were selected randomly within the studied cities (Figure 6).

Figure 6. Adobe building material sampling in Cabinda, Huambo and Menongue. (Pictures taken by Judith -Dembo)

4.2.2. Radium-226, Th-232 and K-40 content determination by gamma-ray spectroscopy

4.2.2.1. Sample preparation for gamma-ray spectroscopy

The sample preparation was carried out in the Lithosphere Fluid Research Lab at the Eötvös Loránd University, Budapest. Samples were dried at lab temperature (around 20 °C) at least for a month. Then they were powdered and sieved below 0.5 mm diameter to ensure homogeneity. Afterwards, the homogeneous samples were dried in an oven at 40 ºC until constant weight is reached.

The dry, homogeneous samples were poured into sample holders made of High-Density Polyethylene (HDPe), which are proven to be radon-tight (Figure. 7, Kis et al. 2013). There was a need to artificially compact the sample in the sample holder in order to avoid a later self-compaction because it could have led to an empty space inside the sample holder where radon can accumulate. Such inhomogeneity leads to false results (Kis et al. 2013). After the filling, samples were left on rest for a minimum of 30 days to ensure the secular equilibrium between Ra-226, Rn-222 and its daughters.

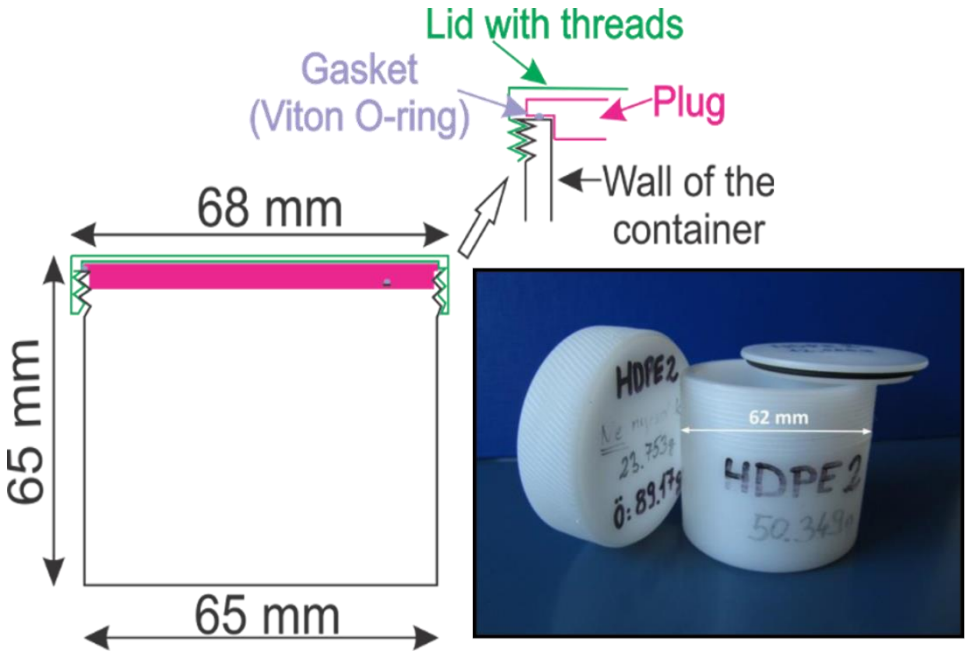

Figure 7. Sample holder made of High-Density Polyethylene (HDPE) and Viton O-ring.

4.2.2.2. Gamma-ray spectroscopy measurements

Gamma-ray spectroscopy measurements were carried out at the Centre for Energy Research, Hungarian Academy of Sciences, Budapest. An n-type HPGe detector (Canberra GR1319) with a relative efficiency of 13 %, and a Canberra DSA-2000 acquisition system were used with a low background chamber (Figure. 8, Kis et al. 2013). The energy resolution (FWHM) is 1.53 and 1.99 keV at 662 and 1332 keV, respectively. The peak-to-Compton ratio is 42.8:1 at 1332 keV. Dead-time losses during the experiments never exceeded 0.05 %. The efficiency transfer method was applied for the determination of the full-energy-peak efficiency for the extended samples in close-in geometry. More details on the measurement method are explained by Kis et al. (2013).

Samples were measured for 42 to 120 hours (samples with lower radioactivity needed more time) to reach good statistics. The determination of Ra-226 was made from gamma lines of

radon daughters, Pb-214 (242, 295 and 352 keV) and Bi-214 (609, 1120 and 1765 keV), assuming the secular equilibrium inside the sample holder. This followed previous experiences with Hungarian coal slag samples, which results were published in a methodological paper with the participation of the author (Völgyesi et al. 2016). Thorium-232 was evaluated using gamma lines of Pb-212 (239 and 300 keV) and Ac-228 (338, 463, 911, 965 and 969 keV) assuming the secular equilibrium in the Th-232 chain as well. Potassium-40 was evaluated from its own peak (1461 keV).

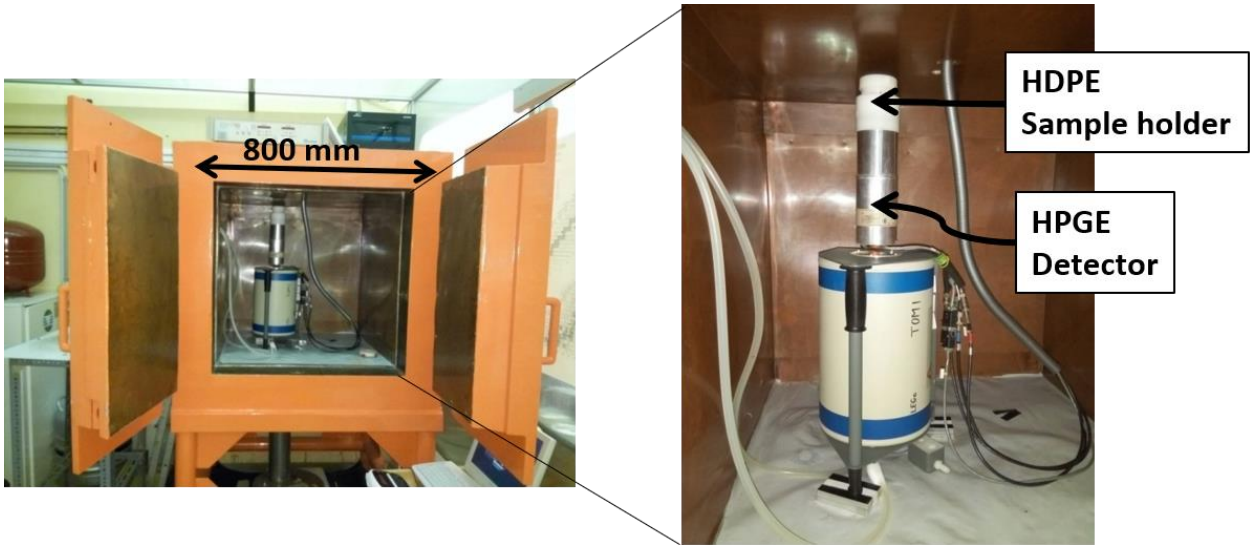

Figure 8. N-type HPGe detector (Canberra GR1319, 13 %).

4.2.3. Hazard index and external dose calculations due to building materials

For the qualification and classification of building materials, hazard indexes were determined from the activity concentrations of Ra-226 ($C_{Ra\text{-}226}$), Th-232 ($C_{Th\text{-}232}$) and K-40 ($C_{K\text{-}40}$). Annual external dose was also accessed from the mentioned activity concentrations as well as from the measured ambient gamma dose equivalent rate.

4.2.3.1. Radium Equivalent Index (Ra_{eq})

Radium equivalent index (Ra_{eq} in Bq kg^{-1}) is one of the most commonly used indexes in literature. This index allows to calculate the specific activity concentration of the sample and to evaluate the radiation hazard associated to it. The equation below (Eq. 2), determining the Ra_{eq} index, is established considering that 370 Bq kg^{-1} of Ra-226, 299 Bq kg^{-1} of Th-232 and 4810 Bq kg^{-1} of K-40 produce the same ambient gamma dose equivalent rate. Limit values of Ra_{eq} are the following: for building materials 370 Bq kg^{-1} (OECD 1979) to keep the external

dose below 1.5 mSv y^{-1}, for industrial use 740 Bq kg^{-1}, for roads and railways 2200 Bq kg^{-1}, for landfill materials 3700 Bq kg^{-1}.

$$Ra_{eq} = C_{Ra-226} + \frac{10}{7} C_{Th-232} + \frac{10}{130} C_{K-40} \quad \text{(Eq. 2)}$$

4.2.3.2. Activity Concentration Index (I)

The unitless activity concentration index (I, Eq. 3) recommended by the Radiation Protection (RP)112 (EC 1999), was applied for further comparison purposes. Calculation of this index is based on the following assumptions: the room size is 4m × 5m × 2.8m, all structures (walls, floor and ceiling) are made of the same material with density of 2350 kg m^{-3}, no windows or doors exist, and it also takes into account a background cosmic and terrestrial dose rate of 50 nGy h^{-1} (EC 1999). The main aim of this index is to show whether the annual dose due to the excess external gamma radiation in a building may exceed 1 mSv y^{-1} (EC 1999). For materials used in bulk amounts the recommended limit of this index is $I \leq 1$, whilst for materials with restricted usage it is $I \leq 6$.

$$I = \frac{C_{Ra-226}}{300\ Bq\ kg^{-1}} + \frac{C_{Th-232}}{200\ Bq\ kg^{-1}} + \frac{C_{K-40}}{3000\ Bq\ kg^{-1}} \quad \text{(Eq. 3)}$$

4.2.3.3. External dose estimations

In this work annual effective doses (AED) were determined in two distinct ways: in the first method it was determined from the in-situ ambient gamma dose equivalent rate measurements (AED-measured), and in the other it was calculated from the activity concentrations of Ra-226, Th-232 and K-40 of the building material (AED-calculated).

- *In situ ambient gamma dose equivalent rate measurements (AED-measured)*

The AED-measured was determined by converting the ambient gamma dose equivalent rate values measured in-situ from nSv h^{-1} to mSv y^{-1}.

- *Calculated annual effective dose (AED-calculated)*

The AED-*calculated* (D_e in mSv y^{-1}; Eq. 4) was determined from the absorbed dose rate (D_a in nGy h^{-1}) taking into account the annual indoor occupancy time (T = 0.8×24 h×365.25 d = 7012.8 h y^{-1}) and the dose conversion factor (F = 0.7 Sv Gy^{-1}, EC

1999). According to the RP 112 (EC 1999), D_a can be calculated from the equation below (Eq. 5) if we consider a room with dimensions of 4 x 5 x 2.8 m, wall thickness of 20 cm and wall density of 2350 kg m^{-3}. A 50 nGy h^{-1} background radiation is assumed.

$$D_e = 10^{-6}\, T\, F\, D_a \qquad \text{(Eq. 4)}$$

$$D_a = 0.92C_{Ra-226} + 1.1C_{Th-232} + 0.08C_{K-40} \qquad \text{(Eq. 5)}$$

4.2.4. Radon and thoron emanation measurements

The emanation determination, measurements of adobe samples were done at the Lithosphere Fluid Research Lab at the Eötvös Loránd University using the RAD7 detector with a calibrated induced air flow rate of q = 11 cm^3 s^{-1} (Durridge Co. 2013). An aluminum container with a height of H = 9.5 cm and a cross-sectional area of A = 38.48 cm^2 was used as sample holder. To reduce humidity in the RAD7, a drying unity filled with desiccant ($CaSO_4$ with 3 % $CoCl_2$, as indicator) was added to the measurement setup (Figure 9). An aerosol filter to protect the device from dust was the part of the setup as well. All the elements were connected using plastic tubes insulated with parafilm at each connection (product of the Pechiney Plastic Packaging Company).

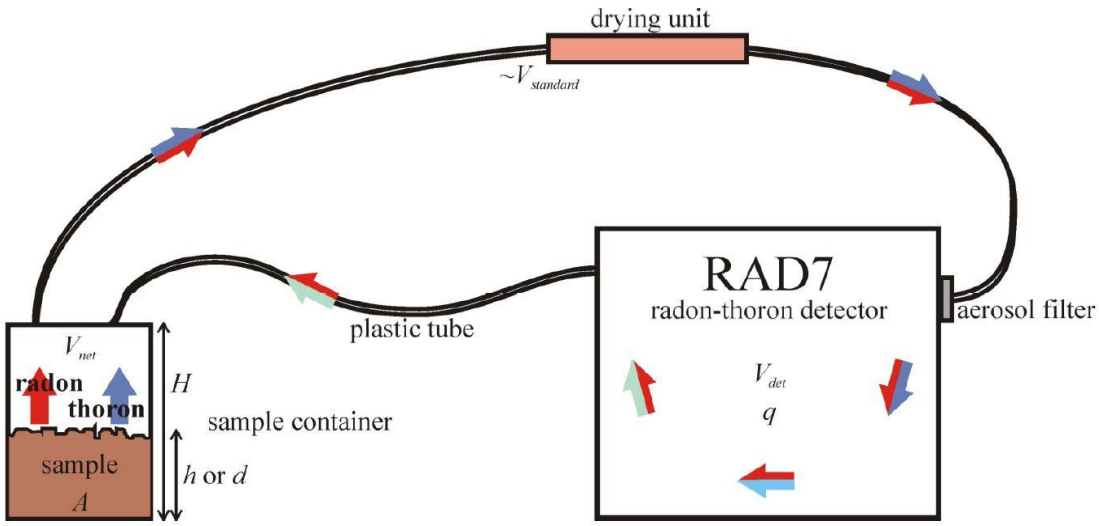

Figure 9. Radon and thoron emanation measurement setup with RAD7 detector. Arrows with different colors indicate the radon and thoron activity concentrations circulating in the setup (Szabó 2013; Csige et al. 2013). In case of thoron, its decay has to be taken into account as well in the evaluation of the results.

4.2.4.1. Radon emanation measurements

The growth curve method was chosen to better handle problems with the radon leakage from the setup as explained by Szabó (2013). Following this method, a sample with known weight is placed into the sample holder and the system is closed, starting the measurement right away. At each measurement, a single block of sample with weights between 80 and 250 g, depending on the available amount, was placed in the sample holder and measured with an integration time of 30 minutes for 5 days. According to Szabó (2013), the best duration of the measurement would be 10 days. In this study, measurements lasting 5 days were satisfying and given the number of measured samples that was the best time. In theory, the equilibrium concentration is reached in 21 days without any leakage from the setup. The leakage decreases both the equilibrium concentration and also the time needed to reach it (Szabó 2013), which makes it possible to measure its level as well.

4.2.4.2. Thoron emanation measurements

Unlike for radon, in case of thoron the sample was split into small pieces of about maximum 1-2 cm and measured with an integration time of 5 minutes for 4 hours per sample. This was done because thoron has a much shorter half-life which means that equilibrium is reached in 5 minutes, therefore, it cannot leak from the measurement setup. However, it also means that if the sample is too big, not all emanated thoron could leave the sample (get exhaled). The method and dimensions of the samples were selected based on an experiment carried out on a Hungarian adobe sample (Csige et al. 2013; Szabó 2013).

4.2.5. Radon and thoron emanation fraction calculations

4.2.5.1. Radon emanation fraction calculation

Evaluation of the results was possible using the "Microcal Origin" software. Growing concentrations were plotted in function of time and the equation (Eq. 6) below was fitted on the radon activity concentration curve.

$$C(t) = (C_{max} - C_{bg})(1 - e^{-(\lambda+\alpha)t}) + C_{bg} \quad \text{(Eq. 6)}$$

where C(t) is the increasing radon activity concentration above the sample in the air volume of the experimental setup (Bq m^{-3}), C_{max} is the maximum of radon activity concentration reached during the measurement (Bq m^{-3}), C_{bg} is the radon activity concentration of the background, λ

is the decay constant of radon (or later also thoron, s^{-1}), α is the measure of radon leakage giving the proportion of radon atoms leaving the experimental setup within a unit time (s^{-1}), and t is the accumulation time. From the fit we get the values of C_{max} and α which can be used in the calculation of the emanation. Radon emanation then is determined by the equation below (Eq. 7).

$$E = \frac{1}{M}\frac{\lambda+\alpha}{\lambda}C_{max}(V_{net} + V_{standard} + V_{det}) \quad \text{(Eq. 7)}$$

where E is the radon (or later also thoron) emanation (kg^{-1} s^{-1}) and M is the sample mass placed into the sample container (kg). The $V_{standard}$ represents a volume equal to that of a "standard RAD7 inlet filter, a 3-foot long, 3/16 inch inner diameter vinyl hose, and a small (6 inch) drying tube" (Durridge Co. 2013) and V_{det} is the 750 cm^3 detector volume of RAD7 (Durridge Co. 2013). The V_{net} is the rest of the volume of the sample container above the sample. Dividing the radon emanation results by the activity concentration of Ra-226 in the sample, we obtain the radon emanation fraction (%).

4.2.5.2. Thoron emanation fraction calculation

The calculation of thoron emanation from the measured data has to take into account the decay of thoron in the setup (Figure 9), which means that the measured activity concentrations in the RAD7 detector are lower than the concentration above the sample in the sample holder. It also has to be taken into account that the diluted air goes back to the sample holder, which further reduces the measurable concentrations. The calculation then can rely on the work of Szabó (2013) and Csige et al. (2013). Based on their model, the following equation (Eq. 8) can be applied, which describes the RAD7 displayed thoron activity concentration as a function of the sample thickness in the sample holder and takes into account above processes.

$$C_{meas}(h) = \frac{G}{\lambda\beta + \frac{\gamma(\lambda(H-h)+q/(\beta A))}{\tanh(\gamma h)}} \quad \text{(Eq. 8)}$$

where $C_{meas}(h)$ is the measurable thoron activity concentration (Bq m^{-3}) depending the sample thickness, G is the thoron generation rate (Bq m^{-3} s^{-1}), λ is the decay constant of thoron (s^{-1}), β is the partition corrected porosity of the sample taken to be 0.56, γ is a sample parameter (m^{-1}), which is reciprocating the diffusion length of thoron in the sample and was taken to be 73 m^{-1}, H is the height of the sample container (9.5 cm), h is the height of the sample (cm), q is the air flow rate of RAD7 (11 cm^3 s^{-1}) and A is the cross-sectional area of the sample container (38.48 cm^2, Figure 9). The values of β and γ are fixed and taken from the work of Szabó (2013)

and Csige et al. (2013) estimated based on a Hungarian adobe sample. The value of h was calculated for each sample from the M sample mass (kg), ρ density (1800 kg m^{-3}) and A cross sectional area (38.48 cm^2). The value of ρ is estimated based on the method detailed in Sections 4.2.5.3. Afterwards, reordering the Eq. 8, the values of G can be calculated from, which the thoron emanation is described by Eq. 9.

$$E = \frac{G}{\lambda \rho} \quad \text{(Eq. 9)}$$

where E is the thoron emanation (kg^{-1} s^{-1}), G is the thoron generation rate (Bq m^{-3} s^{-1}) and ρ is the density of the sample (1450 kg m^{-3}).

Dividing the thoron emanation results by the activity concentration of Th-232 in the sample, we obtain the thoron emanation fraction (%).

4.2.5.3. Bulk density determination

One of the important parameters in the emanation fraction calculations is the bulk density (ρ). It is known that the density equals to the mass of a sample divided by its volume. Determining the volume of the Angolan adobe samples used for these aims needed some adaptation. The classical method where the volume is determined by submerging the sample into a liquid was used. However, in this case, the liquid should not fill the pores of adobe samples because we are interested in the bulk density and not the grain density. Thus, an adequate liquid had to be used. A cosmetic gel with a viscosity equals to 2.6 mPa s^{-1} was found to be the perfect liquid for this propose. The viscosity of the gel was determined by a rheotest rotational viscometer at the Óbuda University (Bongenaar 1973).

4.2.6. Grain size distribution measurement

The grain size distribution measurements of the studied Angolan adobe soil samples were performed at the Eötvös Loránd University. Samples were analysed by laser diffraction with a Horiba Partica 950-V2 LA Analyzer at the Laser Diffraction Particle Size Distribution Analyzer Laboratory of the Research and Instrument Core Facility at Eötvös Loránd University. For the determination of the grain size distribution, laser diffraction is a highly accepted method in the (e.g. Varga et al. 2019 and references therein). Laser diffraction technique is based on the interaction between the light and the grain. When the light hits the grain, it diffracts, refracts, reflects or absorbs the light. The size of the grain is calculated from the angle and the intensity of the refracted or diffracted light.

For the classification of the samples, the Soil Texture Utility from the he USDA soil taxonomy (USDA 1999) was used. This is a triangle with sand, silt and clay fractions on its extremities. Each extremity corresponds to the 100 % of the defined grain size category. For example, if a plotted result of a sample falls at the sand extremity of the triangle, that means the sample is composed of 100 % of sand. Usually, soils have different proportions of sand, silt and clay. Depending on the position where the results of the samples fall on the triangle, the type of the soil is defined. The USDA soil taxonomy soil classification systems uses 12 textural classes (USDA 1999).

4.2.7. X-ray diffraction analysis (XRD)

The Angolan adobe soil samples were prepared and measured by X-ray diffraction analysis at the Institute of Mineralogy and Geology of the Miskolc University.

4.2.7.1. Sample preparation for XRD

As soil samples usually prepared for XRD, samples were powdered. As tropical soil samples generally contain large amount of finely dispersed Fe-oxide-hydroxide (e.g. Segalen 1971; Dossetto et al. 2006) , caution has to be taken that this material is not removed from the samples by sticking to the mortar surface. Thus, powdering by hand was applied, crushing in steel mortar with W-carbide pestle to < 0.1 mm, powdering in porcelain mortar to < 0.05 mm and fine grinding in agate mortar to < 0.005 mm. However, adobe samples from Angola are characterized with a relatively high amount of coarse (> 250 μm, as shown later in results) grains/aggregates. As a result, if the conventional dry grinding is used, the clay fraction gets amorphized as proven by the tests (Figure 10) made prior to the ultimate measurements of all the samples. To solve this problem, during the powdering process samples were powdered under acetone starting from the porcelain mortar. In the agate mortar, the sample was continuously rinsed with acetone and the fine fraction in the suspension was gradually collected with a pipette and moved to the next agate mortar (Figure 11). The collected fraction was then further grinded under acetone until obtaining the desired grain size. Finally, the sample was dried and homogenized by stirring with the pestle. The powder samples were then prepared in the top-loaded sample holders of the XRD instrument.

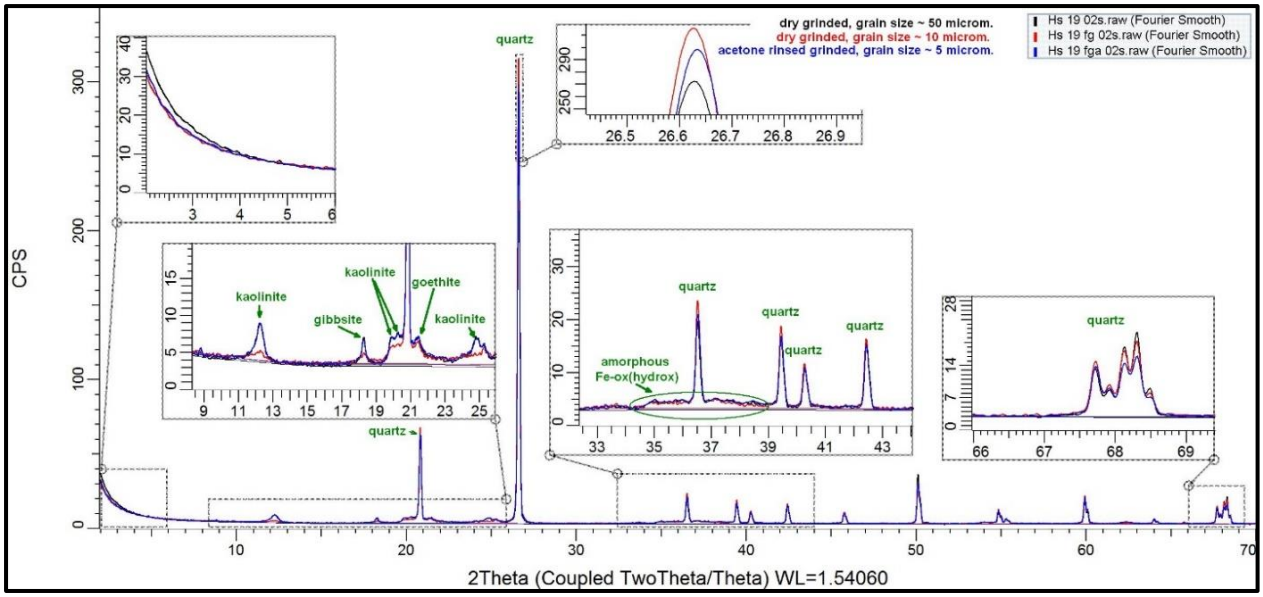

Figure 10. Results of the test run to check the best grinding method. Dry grinding shows in black and red color more amorphous material and less clay mineral, whereas acetone rinse grinding shows in purple the more proper proportion of amorphous material and clay mineral.

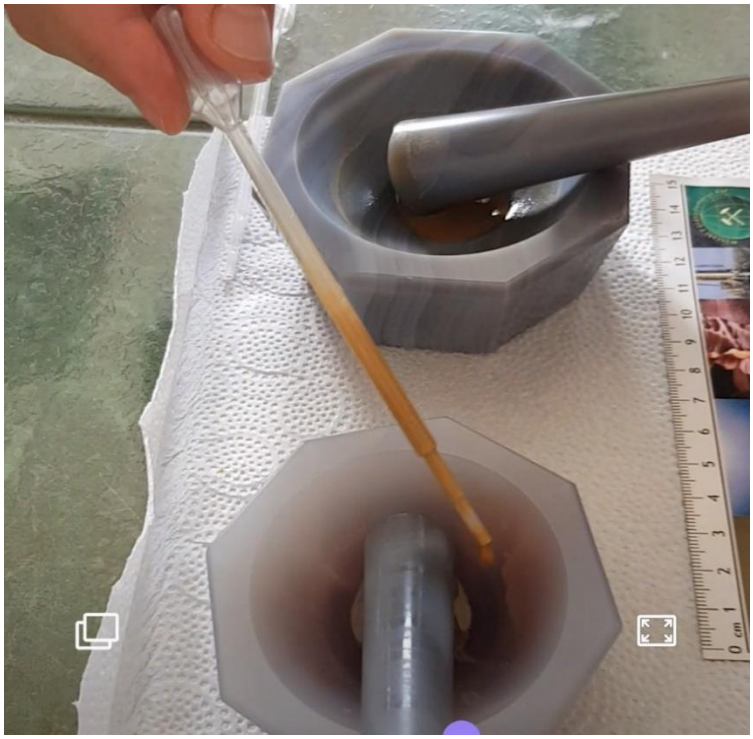

Figure 11. Acetone grinding in an agate mortar. (Picture taken by Judith Salupeto-Dembo in the Lab of the Institute of Mineralogy and Geology of the Miskolc University)

4.2.7.2. XRD measurements

Adobe soil samples were measured with a Bruker D8 Advance powder diffractometer, equipped with Cu-Kα source (40kV, 40mA), Göbel mirror (0.6 mm exit slit) and Våntec1 PSD detector, on a 250 mm radius θ-θ vertical goniometer installed at Miskolc University. Measurements were run in the 2-70 °(2θ) range with 0.007 °(2θ)/48 sec counting time.

Evaluation of recorded patterns was done in Bruker DiffracPlus EVA software, applying Search/Match algorithm for ICDD PDF2 (2005) database, on Fourier-polynomial smoothed (Wells and Brown 2009) and background removed curves. Quantitative composition was calculated by Rietveld refinement in TOPAS4 using instrumental profile obtained by empirical parametrization on NIST SRM 640d Si standard. Crystal structure data were obtained from 'Crystallography Open Database' (Graulis et al. 2009) and 'American Mineralogist Crystal Structure Database' (Downs and Hall-Wallace 2003). Amorphous content was calculated by the amorphous hump method. The applied solution is a combined deconvolution of measured pattern with the Rietveld calculated patterns and a Pawley fit single peak, allowed to fit the hump, whereas the background is restricted to the 4^{th} degree Chebyshev polynomial, determined on the Si standard as a baseline characteristic for the instrument on the given sample holders, identical measurement conditions to the samples. The model is applied under the assumption that average chemical composition of the amorphous fraction is similar to the bulk chemical composition of the sample. Amorphous amount can be refined to +/- 1 m/m % accuracy, whereas crystalline phases are quantified to +/- 10 % relative error.

4.3. Statistical methods

4.3.1. Software

Various statistical methods have been used to allow variable analyses, data comparison and interpretation. The "*Origin*" and "*Statgraphics*" software have been used as well as the Microsoft excel.

4.3.2. Basic statistics

Descriptive statistics as count, minimum, lower quartile, median, upper quartile, maximum average, standard deviation, range, standard skewness and standard kurtosis have been

determined, presented in tables and represented in box and whisker plots. Simple regression was plotted to check the relationship between different variables.

4.3.3. Correlation

Pearson correlation coefficients (Rodgers and Nicewander 1988) have been determined for the variables using the software program "*Statgraphics*". Correlations were performed at the 95 % confidence level in this program.

4.3.4. Hypothesis tests

Statistical distributions of annual radon and thoron activity concentrations were analyzed by the cumulative frequency histogram and tested for normality and lognormality by the Shapiro-Wilk hypothesis test. Lognormality was tested using the natural logarithm of the data following international research works (Szabó et al. 2014). If the P-value is less than 0.05, we can reject the idea that the sample comes from the suggested distribution with 95 % confidence level.

For comparison of medians of sample groups and for checking if the differences are statistically significant, the Mann-Whitney hypothesis test was performed. The null hypothesis is that the median of a chosen group of samples is equal to the median of the other one. The alternative hypothesis is that the medians are different. For P-values, less than 0.05, the alternative hypothesis is accepted, whereas for P-value greater or equal to 0.05, it is rejected at the 95 % confidence level.

5. Results

5.1. In-situ ambient gamma dose equivalent rate

In-situ ambient gamma dose equivalent rate measurements were performed on the floor and at 1 m height as explained in Section 4.1.1. The difference between values measured on the floor and the one measured at 1 m height was checked with the Mann-Whitney test. Statistically, there was no significant difference between the measured values in all areas with P-values equal to 0.62, 0.84, and 0.84 in Cabinda, Huambo and Menongue, respectively. Consequently, used data are the average ambient gamma dose equivalent rate in each dwelling. Summary statistics of all measured values are shown in Table 1. Results of the indoor annual effective dose from external sources are visualized in Figure 12.

Measured in-situ ambient gamma dose equivalent rates give the following averages and respective standard deviations of 78 ± 15, 175 ± 42 and 117 ± 19 nSv h^{-1} in Cabinda, Huambo and Menongue, respectively. Transforming the unit, external annual effective dose and respective standard deviations are 0.69 ± 0.13, 1.53 ± 0.37 and 1.03 ± 0.16 mSv y^{-1} in Cabinda, Huambo and Menongue, respectively (Table 1; Figure 12).

Background radiation was checked as well and the outdoor ambient gamma dose equivalent rates give the following averages and respective standard deviations of 71 ± 15, 166 ± 37, 117 ± 23 nSv h^{-1}. After unit transformation, background external annual effective dose and respective standard deviations are 0.62 ± 0.13, 1.36 ± 0.34 and 1 ± 0.19 mSv y^{-1} in Cabinda, Huambo and Menongue, respectively (Table 1, Figure 13).

Area	Place of measurement		Count	Min.	L. quartile	Median	Av.	St. dev.	U. quartile	Max.	Range	St. skewness	St. kurtosis
Cab[1]	Indoors	G. D. R. (nSv h^{-1})	15	58	61	78	78	15	90	102	44	-0.01	-1.14
		E. E. D. (mSv y^{-1})		0.50	0.54	0.68	0.69	0.13	0.79	0.89	0.39	-0.05	-1.13
	Outdoors	G. D. R. (nSv h^{-1})	10	45	60	70	71	15	80	100	55	0.46	0.78
		E. E. D. (mSv y^{-1})		0.39	0.52	0.61	0.62	0.13	0.70	0.87	0.48	0.46	0.78
Hbo[2]	Indoors	G. D. R (nSv h^{-1})	15	133	139	154	175	42	220	242	109	0.91	-1.24
		E. E. D (mSv y^{-1})		1.16	1.22	1.35	1.53	0.37	1.93	2.12	0.96	0.92	-1.23
	Outdoors	G. D. R (nSv h^{-1})	10	110	130	152	155	39	170	240	130	1.25	0.70
		E. E. D (mSv y^{-1})		0.96	1.14	1.33	1.36	0.34	1.49	2.10	1.14	1.25	0.70
Mge[3]	Indoors	G. D. R (nSv h^{-1})	15	73	108	122	117	19	129	142	69	-1.67	0.97
		E. E. D (mSv y^{-1})		0.64	0.95	1.07	1.03	0.16	1.13	1.24	0.60	-1.63	0.89
	Outdoors	G. D. R (nSv h^{-1})	10	90	100	110	115	22	130	150	60	0.41	-0.95
		E. E. D (mSv y^{-1})		1.31	0.88	0.96	1	0.19	1.14	1.31	0.53	0.42	-0.95
All[4]	Indoors	G. D. R (nSv h^{-1})	45	15	78	98	105	39	127	196	181	1.19	0.0081
		E. E. D (mSv y^{-1})		0.12	0.62	0.78	0.84	0.31	1.01	1.57	1.45	1.18	0.019

Table 1. Summary statistics for all measured ambient gamma dose equivalent rates (G.D.R. in nSv h^{-1}) and external annual effective doses (E.E.D. in mSv y^{-1}) in study areas of Cabinda[1], Huambo[2] and Menongue[3]. Averages from all places[4] are represented as well.

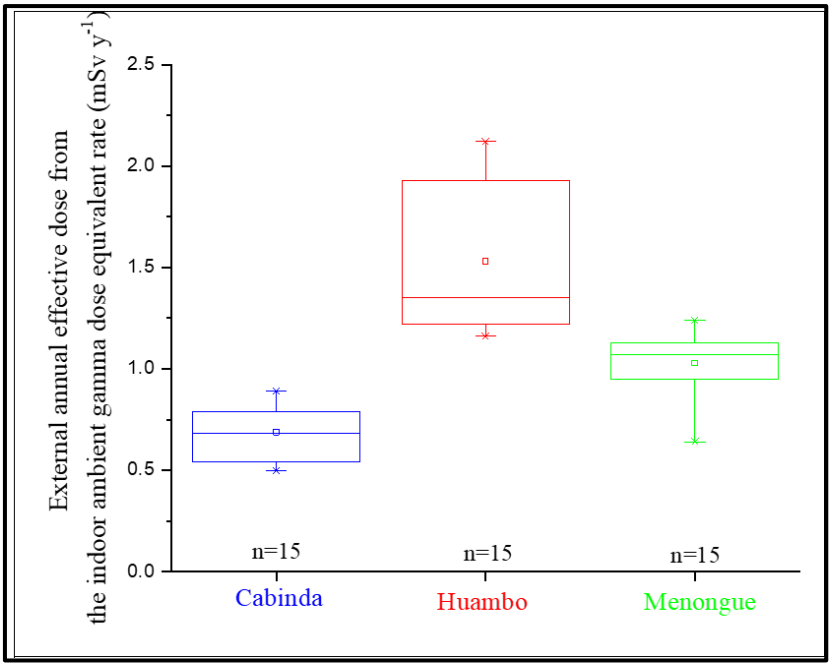

Figure 12. Box and whisker plot of the measured indoor external annual effective dose ($mSv\,y^{-1}$) at the three studied areas

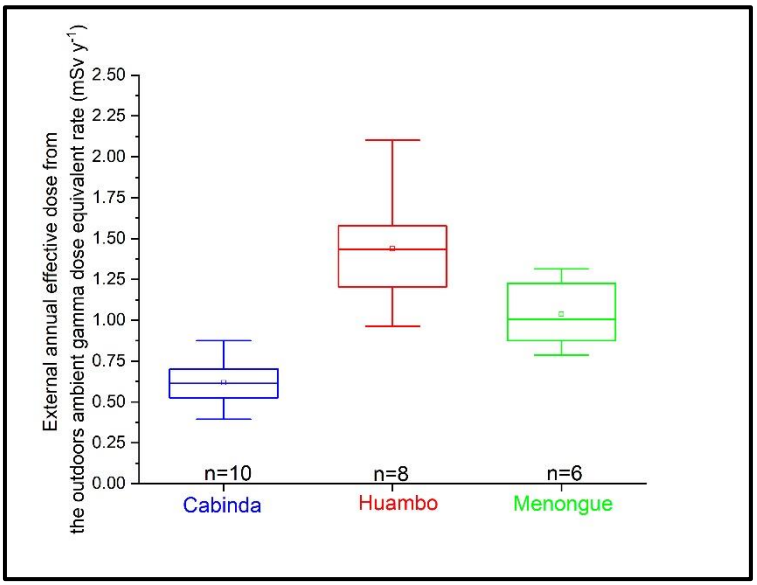

Figure 13. Box and whisker plot of the outdoors external annual effective dose from the in-situ ambient gamma dose equivalent rate ($mSv\,y^{-1}$) at the three studied areas

5.2. Indoor radon and thoron activity concentrations

5.2.1. Seasonal indoor radon and thoron activity concentrations

Basic statistics of radon and thoron activity concentrations are summarized in Table 2 and the box and whisker plots of Figure 14. Averages with corresponding standard deviations and medians in brackets [average±standard deviation(median)] of radon during rainy and dry seasons, respectively, are 38±11(36) and 22±8(20) Bq m^{-3} in Cabinda, 130±39(118) and 94±31(83) Bq m^{-3} in Huambo, and 65±19(62) and 53±15(52) Bq m^{-3} in Menongue. For thoron, the same results are as follows: 155±92(164) and 169±97(159) Bq m^{-3} in Cabinda, 262±137(236) and 293±136(240) Bq m^{-3} in Huambo, and 83±54(60) and 101±59(76) Bq m^{-3} in Menongue, respectively, for rainy and dry seasons. To check if the medians of the activity concentrations are different between the seasons and if the differences are statistically significant, the Mann-Whitney test was performed. Results of the P-values for radon and thoron, respectively, are as follows, <0.05 and 0.73 in Cabinda, <0.05 and 0.74 in Huambo and 0.067 and 0.92 in Menongue. Accordingly, for radon, differences are statistically significant between the two seasons, except in Menongue. For thoron, activity concentrations, the differences between rainy and dry seasons are statistically not significant in all areas.

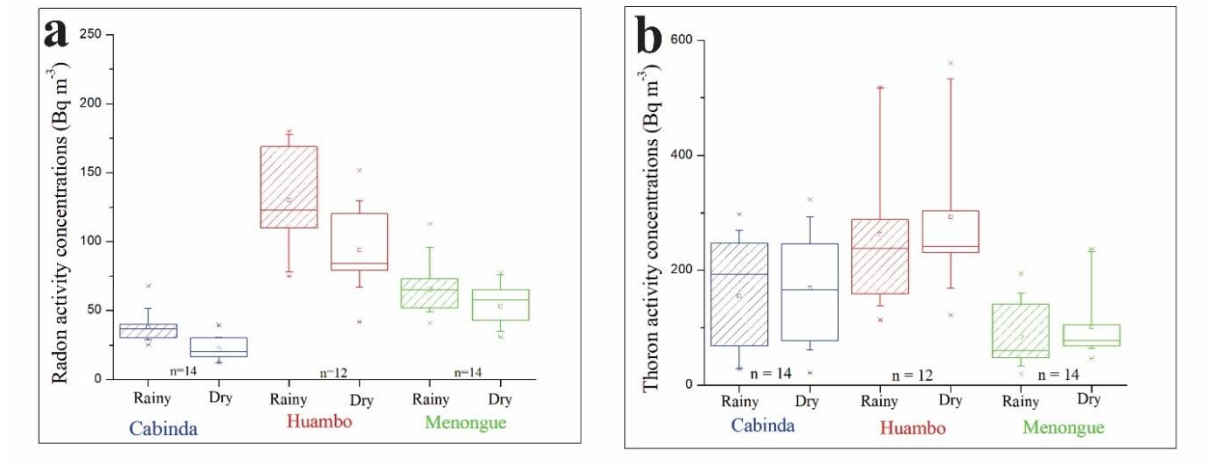

Figure 14. Box and whisker plots of measured (a) radon and (b) thoron activity concentrations (Bq m^{-3}) in both rainy and dry seasons in the study areas of Cabinda, Huambo and Menongue.

		Season	Count	Min.	L. quartile	Median	U. quartile	Max.	Range	Mean	St. dev.	St. skewness	St. kurtosis
Cab[1]	Rn	Rainy	14	26	26	36	40	68	42	38	11	2.90	3.40
		Dry	14	12	12	20	29	39	27	22	8	0.71	-0.14
	Tn	Rainy	14	28	28	164	235	297	269	155	92	0.01	-1.46
		Dry	14	22	22	159	244	323	301	169	97	0.06	-1.42
Hbo[2]	Rn	Rainy	12	75	108	118	171	180	105	130	39	0.07	-1.47
		Dry	12	42	77	83	120	152	110	94	31	0.36	-0.26
	Tn	Rainy	12	113	156	236	302	518	405	262	137	1.09	0.28
		Dry	12	122	229	240	327	560	438	293	136	1.13	0.41
Mge[3]	Rn	Rainy	14	41	52	62	72	113	72	65	19	1.35	1.78
		Dry	14	31	43	52	64	77	46	53	15	0.22	-1.08
	Tn	Rainy	14	20	49	60	128	194	174	83	54	0.91	-0.46
		Dry	14	47	69	76	103	237	190	101	59	1.87	2.54

Table 2. Basic statistics of radon (Rn) and thoron (Tn) (in Bq m^{-3}) for both seasons (rainy and dry) in the study areas of Cabinda[1], Huambo[2] and Menongue[3].

5.2.2. Annual average indoor radon and thoron activity concentrations

Results of the annual average indoor radon and thoron activity concentrations are summarized in box and whisker plots (Figure 15). Radon and thoron averages, respective standard deviations and medians in brackets are $30\pm8(29)$ and $163\pm93(161)$ Bq m^{-3} in Cabinda, $112\pm31(103)$ and $278\pm134(242)$ Bq m^{-3} in Huambo, and $55\pm13(53)$ and $98\pm57(76)$ Bq m^{-3} in Menongue, respectively. In the box and whisker plots, Huambo shows the highest annual average radon and thoron activity concentrations. The lowest median is measured in Cabinda for radon and in Menongue for thoron. The Mann-Whitney hypothesis test was performed comparing the medians of the activity concentrations among all areas. The P-values comparing medians of radon and thoron for Huambo vs. Cabinda, Huambo vs. Menongue and Menongue vs. Cabinda are all <0.05. These results show significant differences among medians of all studied areas for both annual radon and thoron activity concentrations.

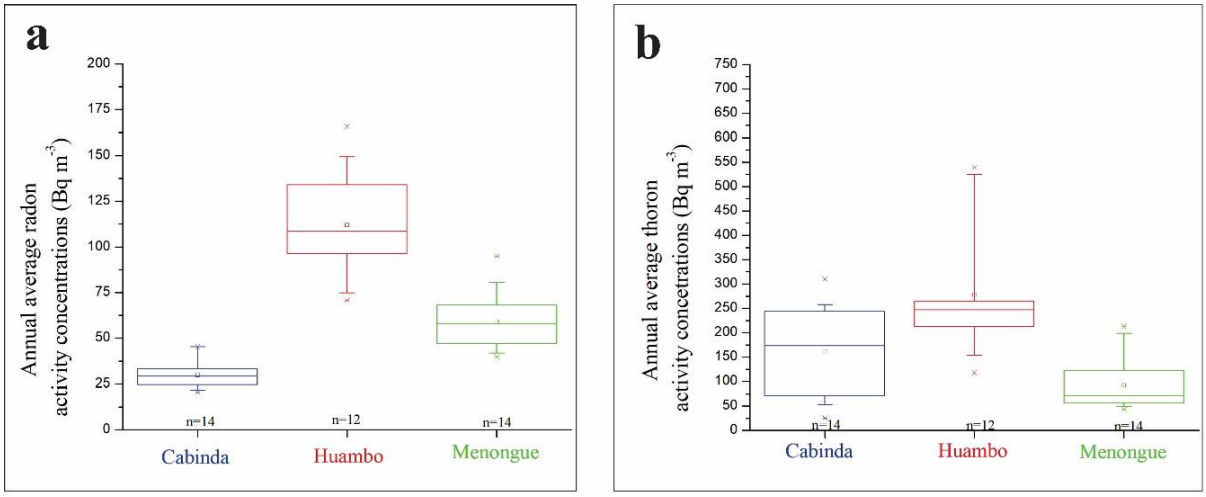

Figure 15. Box and whisker plots of annual average (a) radon and (b) thoron activity concentrations (Bq m^{-3}) in study areas of Cabinda, Huambo and Menongue.

5.2.3. Statistical distributions of annual averages

The sample distribution was ascertained by the frequency histogram (Figure 16) and Shapiro-Wilk test. For both radon and thoron, normal distribution was rejected by the Shapiro-Wilk test that shows a P-value <0.05 for both radon and thoron. On the other hand, the test does not reject the hypothesis of radon and thoron coming from a lognormally distributed population with P-values equal to 0.14 for radon and 0.09 for thoron. Both tests are performed with 95 % confidence level.

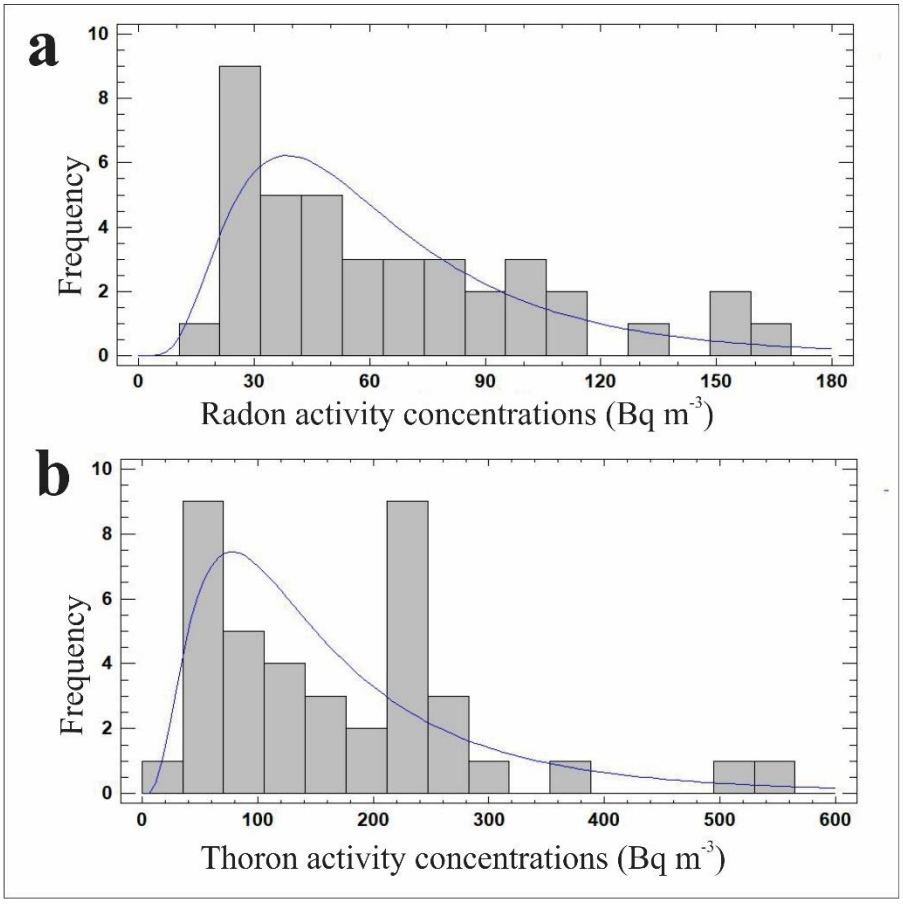

Figure 16. Frequency histogram showing the distribution of all annual average (a) radon and (b) thoron activity concentrations for all sampling sites.

5.3. Estimated annual inhalation doses

Estimated annual inhalation doses of radon and thoron at the three areas are 0.75±0.19 and 1.82±1.04 mSv y^{-1} in Cabinda, 2.83±0.8 and 3.12±1.5 mSv y^{-1} in Huambo, and 1.49±0.4 and 1.03±0.6 mSv y^{-1} in Menongue, respectively (Table 3, Figure 17a). The total inhalation doses per area are 2.0±0.8, 4.5±1.5 and 2.0±0.6 mSv y^{-1} in Cabinda, Huambo and Menongue, respectively (Table 3, Figure 17b). Note the significant uncertainty of thoron inhalation dose estimation due to the use of an average equilibrium factor.

	Radon inhalation dose (mSv y^{-1})	Thoron inhalation dose (mSv y^{-1})	Total inhalation dose (mSv y^{-1})
Cabinda	0.75±0.19	1.82±1.04	2.0±0.8
Huambo	2.83±0.8	3.12±1.5	4.5±1.5
Menongue	1.49±0.4	1.03±0.6	2.0±0.6

Table 3. Inhalation dose of radon, thoron and 'total' in (mSv y^{-1}) in study areas of Cabinda, Huambo and Menongue.

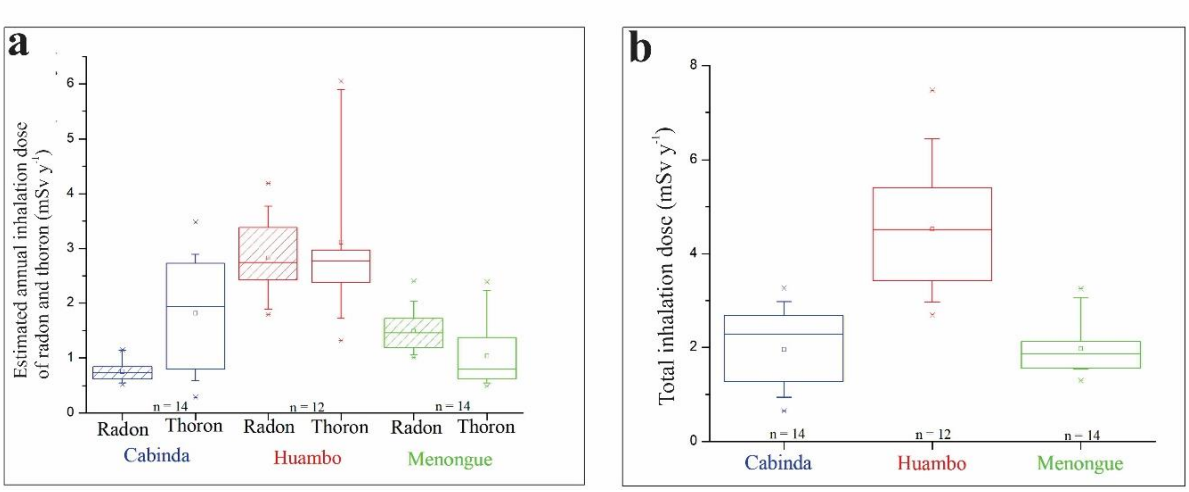

Figure 17. Box and whisker plots of (a) estimated annual inhalation doses from radon and thoron, separately, (mSv y^{-1}) and (b) total inhalation doses (mSv y^{-1}) from the study areas of Cabinda, Huambo and Menongue.

5.4. Ra-226, Th-232 and K-40 contents of adobes

5.4.1. Measured Ra-226, Th-232, K-40 activity concentrations

Average and standard deviations of the activity concentrations in Bq kg^{-1} are 26 ± 7, 36 ± 5, 45 ± 17 in Cabinda, 87 ± 20, 81 ± 21, 82 ± 15 in Huambo and 27 ± 10, 30 ± 10, 73 ± 40 in Menongue for Ra-226, Th-232 and K-40, respectively (Table 4; Figure 18).

Location		Activity concentrations (Bq kg^{-1})		
		Ra-226	Th-232	K-40
Cabinda	Average	26 ± 7	36 ± 5	45 ± 17
	Range	15-45	27-49	28–92
Huambo	Average	87 ± 15	81 ± 21	82 ± 15
	Range	49-116	39-121	50–105
Menongue	Average	27 ± 10	30 ± 10	73 ± 40
	Range	15-56	17-57	21–155

Table 4. Summary of averages, standard deviations and ranges of Ra-226, Th-232 and K-40 activity concentrations in adobe samples of the study areas.

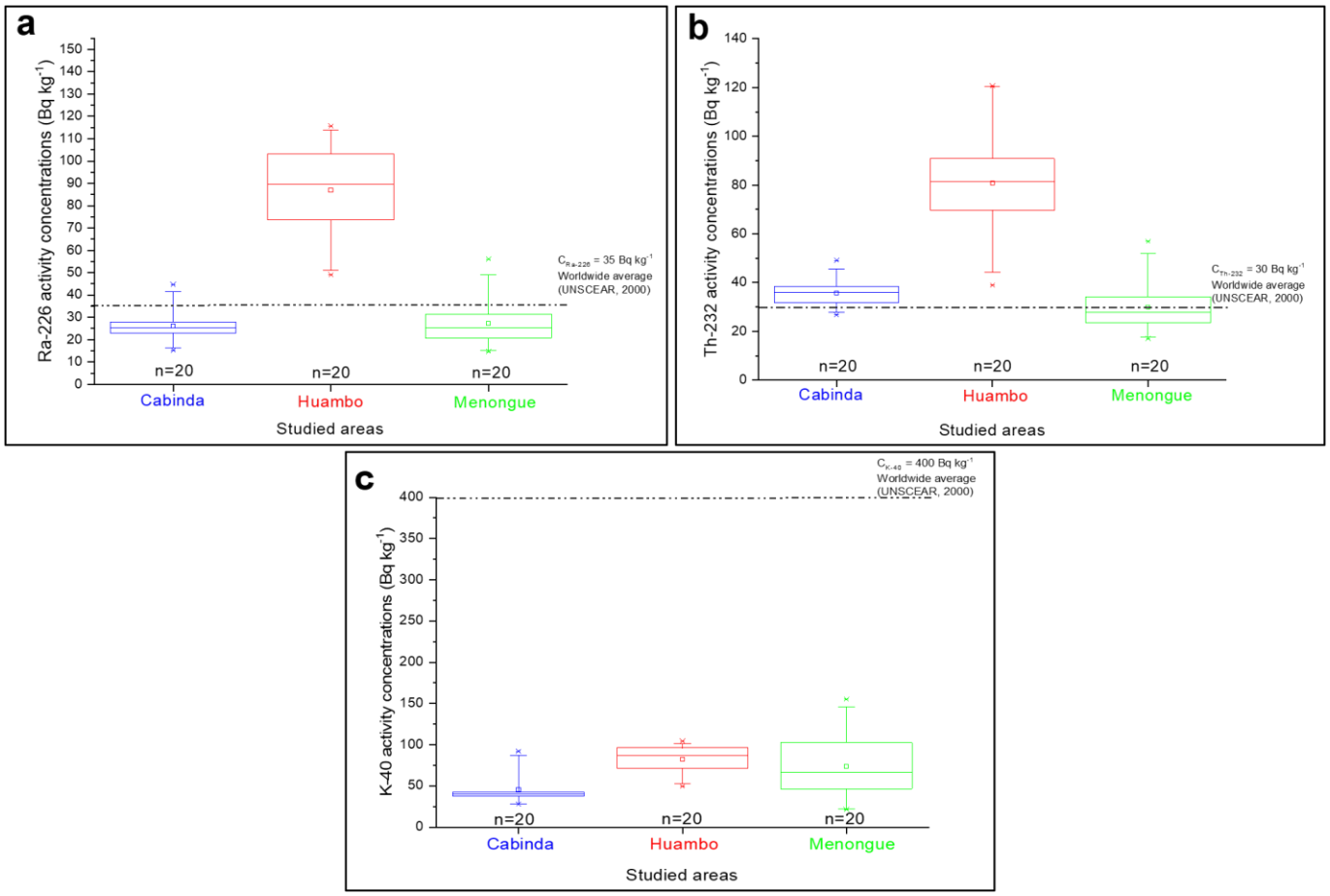

Figure 18. Box and whisker plots of (a) Ra-226, (b) Th-232 and (c) K-40 activity concentrations (Bq kg^{-1}) of the studied adobes from the three study areas from Cabinda, Huambo and Menongue.

5.4.2. Correlations among Ra-226, Th-232 and K-40 activity concentrations

Correlations between Ra-226 and Th-232 was found to be 0.66 in Cabinda with a P-value <0.05 (Table 5; Figure 19a), 0.55 in Huambo with a P-value of <0.05 (Table 5; Figure 19b) and 0.80 in Menongue with a P-value of <0.05 (Table 5; Figure 19c). According to this result, in all study areas the mentioned radionuclides have a statistically significant linear relationship.

Correlations between Ra-226 and K-40 show the following results: 0.62 with a P-value <0.05 in Cabinda (Table 5; Figure 20a), 0.19 with a P-value of <0.05 in Huambo (Table 5; Figure 20b) and 0.23 with a P-value of 0.338 in Menongue (Table 5; Figure 20c). Statistically significant linear relationship is found in Cabinda, but not in the two other study areas.

Results of correlations between Th-232 and K-40 are as follow: 0.36 with a P-value of 0.115 in Cabinda (Table 5; Figure 21a), 0.50 with a P-value of 0.023 in Huambo (Table 5; Figure 21a) and 0.48 with a P-value of 0.0312 in Menongue (Table 5; Figure 21a). Here, statistically significant linear relationship exists in correlation values of sampling sites in Huambo and Menongue, but not in Cabinda.

Location	Ra-226 and Th-232 correlation	Ra-226 and K-40 correlation	Th-232 and K-40 correlation
Cabinda	R = 0.66 P-Value = 0.0014	R = 0.62 P-Value = 0.0036	R = 0.36 P-Value = 0.115
Huambo	R = 0.55 P-Value = 0.012	R = 0.19 P-Value = 0.41	R = 0.5 P-Value = 0.023
Menongue	R = 0.8 P-Value = 0.0001	R = 0.23 P-Value = 0.338	R = 0.48 P-Value = 0.0312

Table 5. Correlations among the three studied radionuclides (Ra-226, Th-232 and K-40) in the studied areas of Angola.

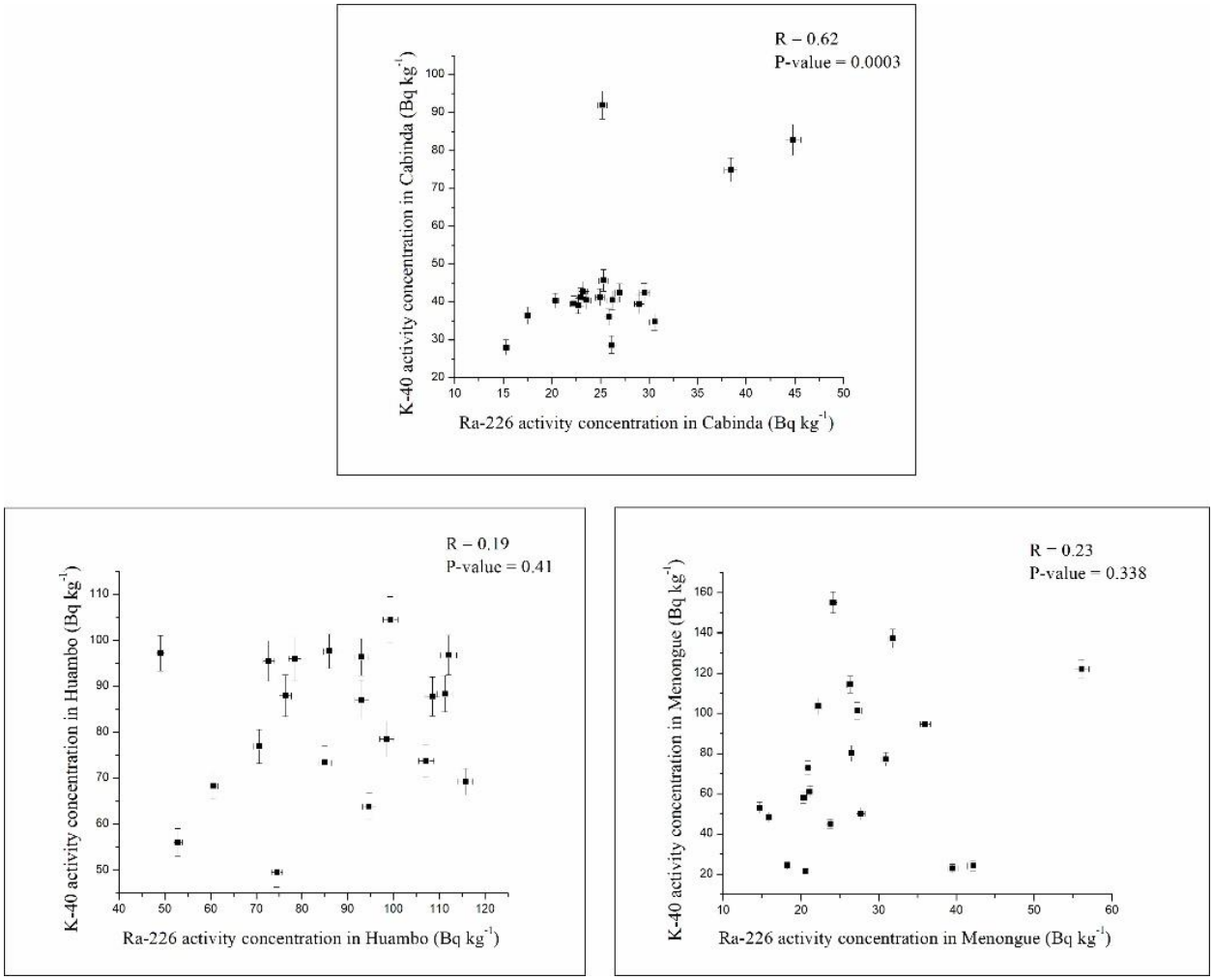

Figure 19. Correlation between Ra-226 and Th-232 activity concentrations in adobe of the study areas (a) Cabinda, (b) Huambo and (c) Menongue.

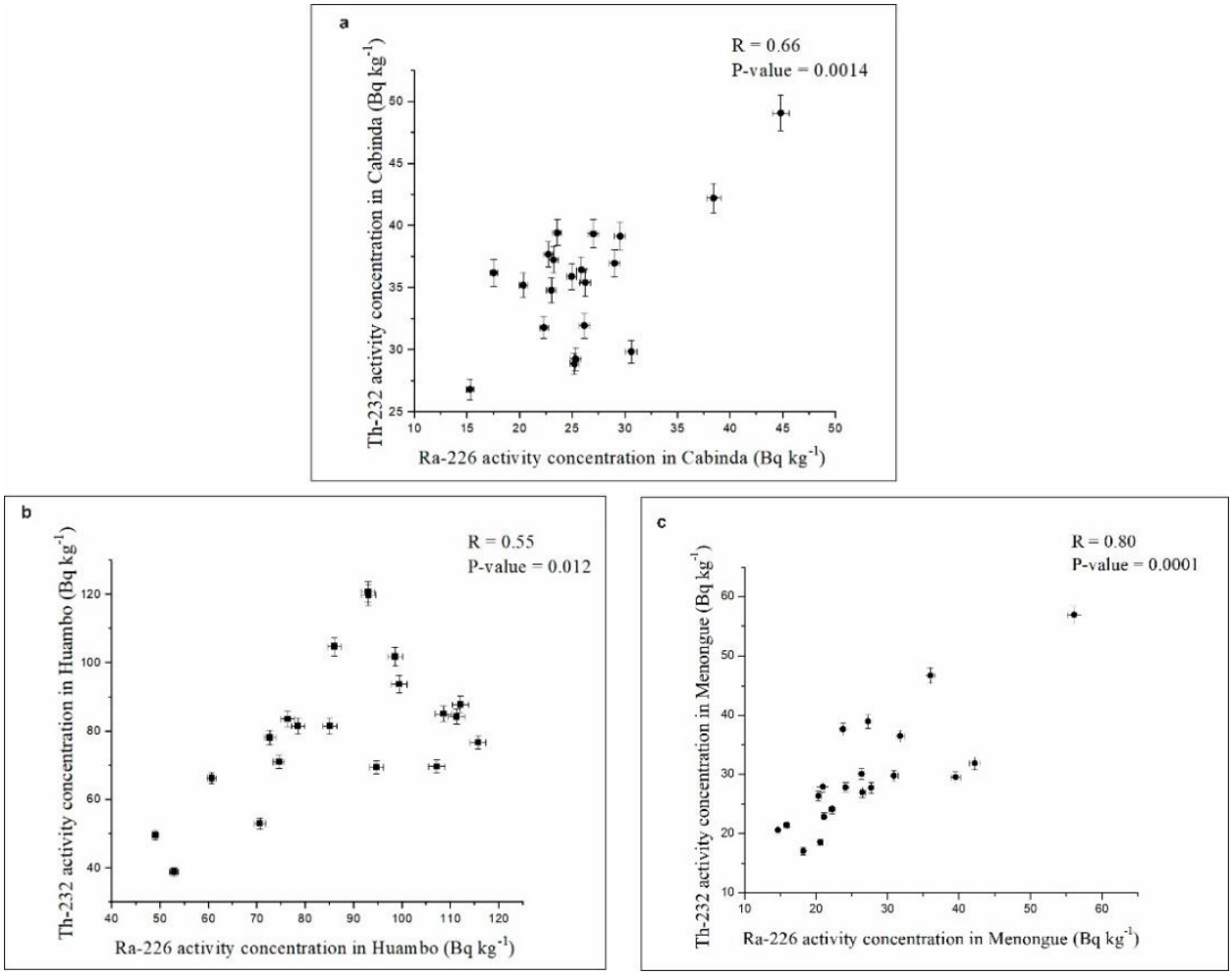

Figure 20. Correlation between Ra-226 and K-40 activity concentrations in adobe of the study areas (a) Cabinda, (b) Huambo and (c) Menongue.

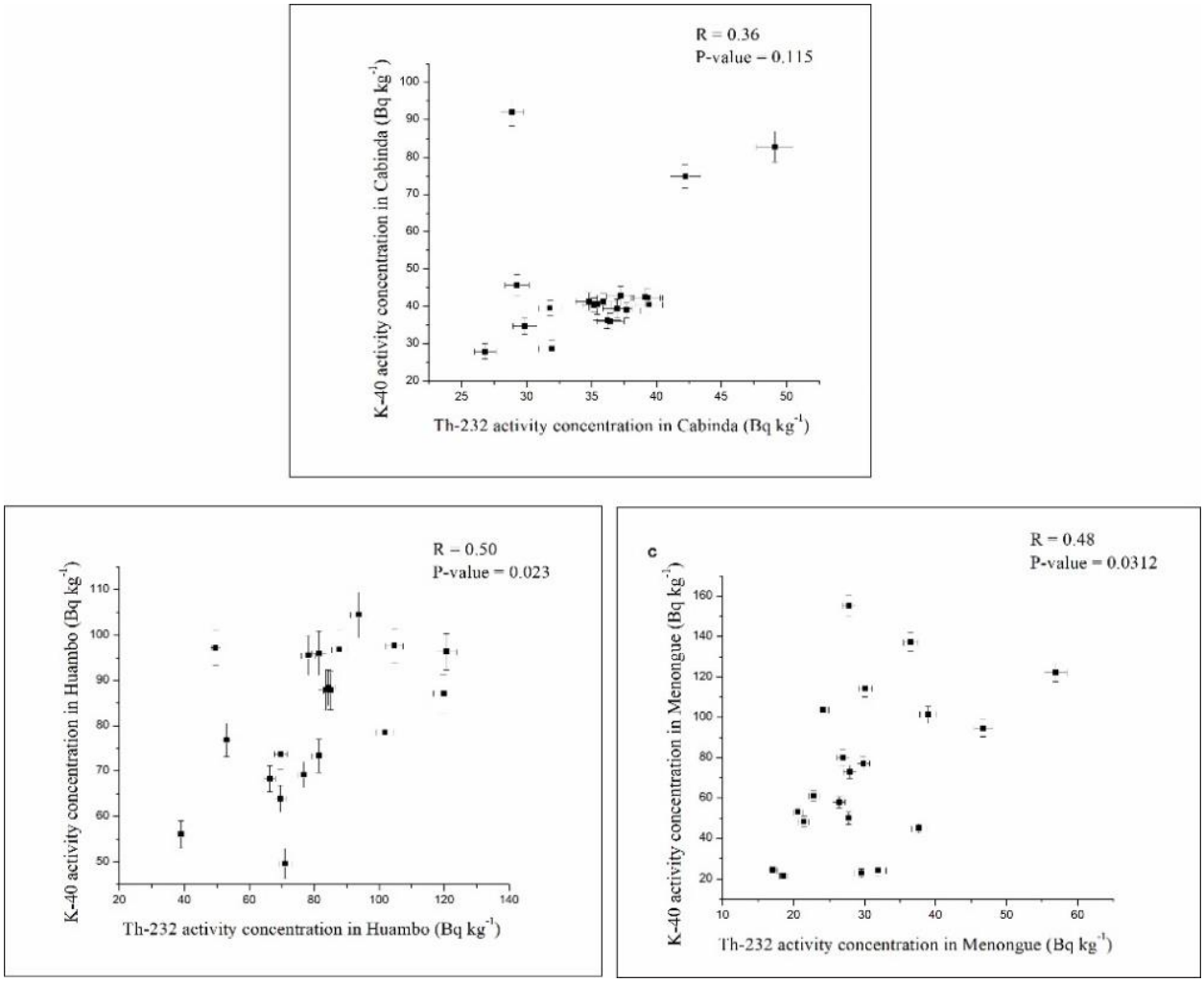

Figure 21. Correlation between Th-232 and K-40 activity concentrations in adobe of the study areas (a) Cabinda, (b) Huambo and (c) Menongue.

5.5. Radiation hazard indices and calculated external doses

5.5.1. Ra_{eq} and I hazard indexes

Averages and standard deviations of the Ra_{eq} index are 81 ± 13 in Cabinda, 209 ± 45 in Huambo and 76 ± 24 Bq kg^{-1} in Menongue, respectively. For the I index, averages and standard deviations are 0.28 ± 0.05 in Cabinda, 0.72 ± 0.15 in Huambo and 0.26 ± 0.08 in Menongue, respectively (*Table 6*; Figure 22).

Location		Ra_{eq} (Bq kg^{-1})	I index	Annual Effective Dose calculated (mSv y^{-1})
Cabinda	Average	81 ± 13	0.28 ± 0.05	0.4 ± 0.06
	Range	56-21	0.19-0.42	0.22-0.50
Huambo	Average	209 ± 45	0.72 ± 0.15	0.8 ± 0.2
	Range	113-273	0.39-0.95	0.47-1.11
Menongue	Average	76 ± 24	0.26 ± 0.08	0.3 ± 0.06
	Range	44-145	0.16-0.51	0.18-0.62

Table 6. Summary of averages, standard deviations and ranges of Radium equivalent index (Ra_{eq}), I index, and calculated annual effective doses in adobe samples of the study areas.

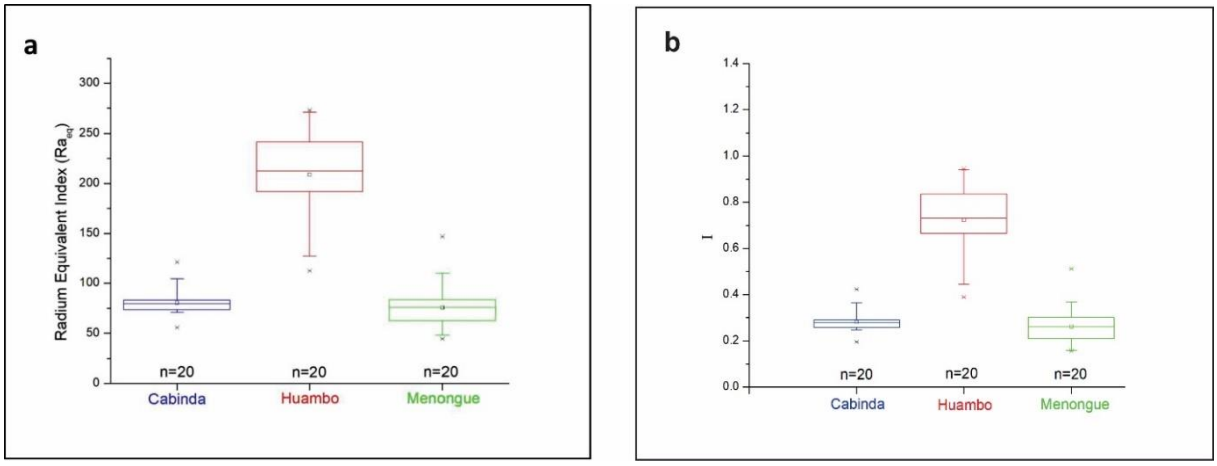

Figure 22. Box and whisker plots of (a) the Radium Equivalent Index and (b) the unitless activity concentration index I recommended by the RP 112 (EC, 1999) at the three study areas.

5.5.2. Calculated external doses

Averages of the annual effective doses calculated from the activity concentration of the radionuclides in building materials at the three study areas with respective standard deviation are: 0.4 ± 0.06, 0.8 ± 0.2 and 0.3 ± 0.06 mSv y^{-1} in Cabinda, Huambo and Menongue, respectively (Table 6). The results are visualized in Figure 23 together with the values based on in-situ gamma dose equivalent rate measurements (already presented separately in Section 5.1).

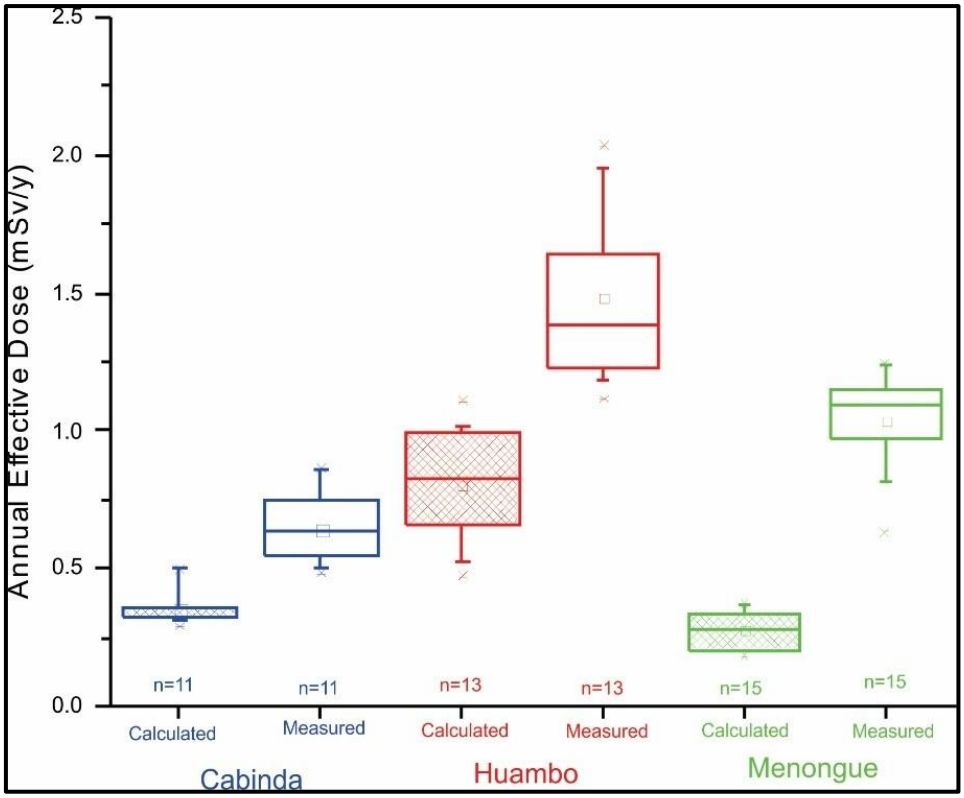

Figure 23. Comparison between the annual effective dose values calculated from Ra-226, Th-232 and K-40 activity concentrations of the building materials at the three study areas (AED-calculated) and measured in-situ (AED-measured).

5.6. Radon and thoron emanations of adobe

Summary statistics of radon and thoron emanation in the three studied areas and all the adobe samples together are in Table 7 and the results are represented in box and whisker plots (Figure 24). Samples from Huambo show the highest emanation for both radon and thoron with 81±39 and 7±2 kg^{-1} s^{-1}. In Cabinda, the same values are 34±30 and 5±3 and in Menongue 50±9 and 4±1 kg^{-1} s^{-1}, respectively. It is important to note that, because of the big leakage noticed in the measurement of the radon emanation, from the 30 measured samples only 12 are available for the evaluation. Based on the so called "growth curve" method, which is described and evaluated in detail by Szabó (2013) and also used in this work, the α, the measure of radon leakage (Eq. 6 and 7), should not exceed 0.02 h^{-1}. Rejected results for the radon emanation had α raging between 0.024 and 0.061 h^{-1} (Section 4.2.5). The total number of evaluated data for radon and thoron emanation is 82.

		Count	Min.	L. quartile	Median	Av.	St. dev.	U. quartile	Max.	Range	St. skewness	St. kurtosis
Cabinda	Radon	2	13	13	34	34	30	55	55	42		
	Thoron	10	2	4	4	5	3	5	12	9	2.50	2.78
Huambo	Radon	5	50	56	75	81	39	76	148	98	1.61	1.55
	Thoron	9	3	5	7	7	2	8	9	7	-0.55	-0.36
Menongue	Radon	5	37	47	50	50	9	53	61	24	-0.28	0.44
	Thoron	10	2	3	4	4	1	4	5	3	-0.42	0.07
All adobe samples	Radon	12	13	49	54	60	32	68	148	135	2.61	3.88
	Thoron	29	2	4	4	5	2	5	12	10	2.50	1.07

Table 7. Basic statistics of the emanation of radon and thoron in adobe samples in Cabinda, Huambo and Menongue, and for all the study areas together (kg^{-1} s^{-1}).

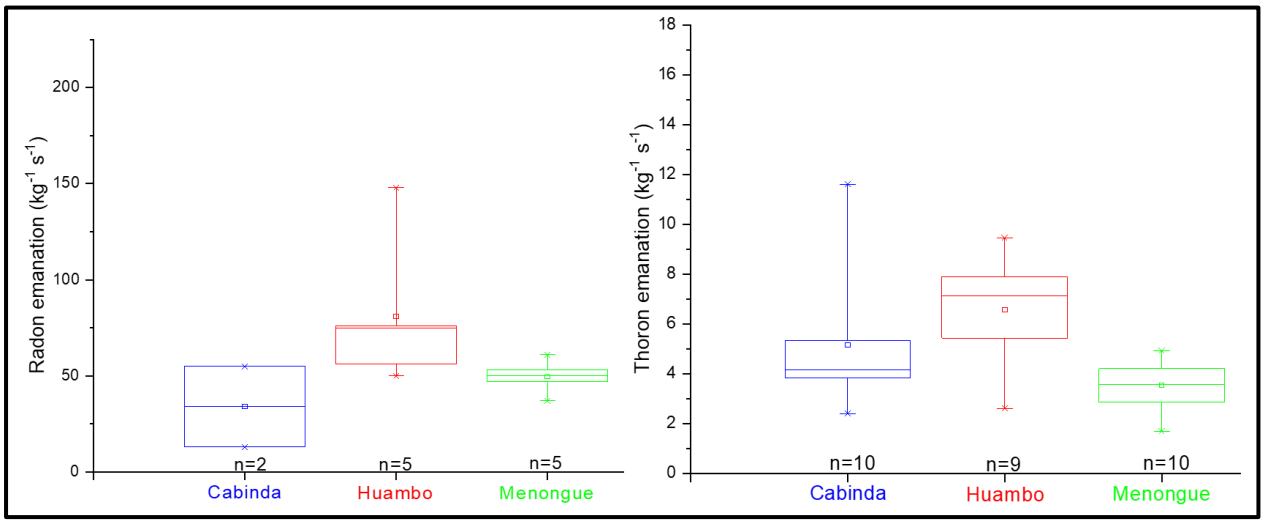

Figure 24. Box and whisker plots of radon and thoron emanation (kg^{-1} s^{-1}) in adobe samples at the study areas (Cabinda, Huambo and Menongue).

5.7. Radon and thoron emanation fractions of adobe

Summary statistics of radon and thoron emanation fraction in the three studied areas and for all the samples together are in Table 8 and these results are represented in box and whisker plots (Figure 26). Samples from Huambo have the lowest values of the emanation fraction for both radon and thoron with 12±4 and 8±2 %. In Menongue, the values of radon emanation fraction are the highest with 28±9 %. Thoron emanation fraction in Menongue is 14±5 %. In Cabinda, the emanation fraction of radon and thoron are 16±11 and 14±7 %, respectively.

		Count	Min.	L. quartile	Median	Av.	St. dev.	U. quartile	Max.	Range	St. skewness	St. kurtosis
Cabinda	Radon	2	8	8	16	16	11	24	24	15		
	Thoron	10	8	11	11	14	7	13	31	23	2.79	3.073
Huambo	Radon	5	9	9	10	12	4	14	17	9	0.89	-0.473
	Thoron	9	4	7	8	8	2	10	11	7	-0.86	0.121
Menongue	Radon	5	16	23	30	28	9	31	39	23	-0.30	0.001
	Thoron	10	6	12	13	14	5	16	27	21	1.63	2.342
All adobe samples	Radon	12	8	9	17	19	10	27	39	30	0.89	-0.517
	Thoron	29	4	10	11	12	6	13	31	27	3.95	4.478

Table 8. Basic statistics of the emanation fraction of radon and in Cabinda, Huambo, Menongue and for all areas together (%).

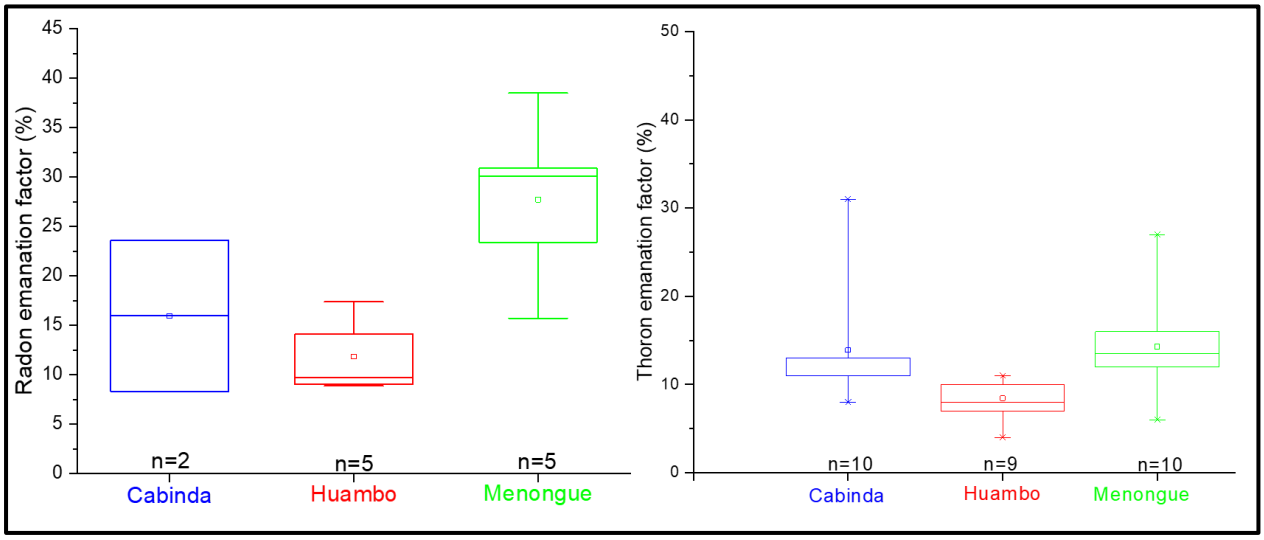

Figure 25. Box and whisker of radon and thoron emanation fraction (%) in adobe samples at the study areas (Cabinda, Huambo and Menongue).

5.8. Grain size distributions

Nineteen selected and representative adobe soil samples were analyzed for grain size distribution by laser diffraction. Based on the results, Cabinda adobe samples have sand fraction present ranging between 44-74 %, silt fraction between 20-36 % and clay fraction between 6-20 % with the following medians in mass %: 62 of sand, 25 of silt and 9 of clay. Huambo adobe samples have sand fraction present ranging between 4-75%, silt fraction between 12-57 % and clay fraction between 8-83 % with the following medians in mass %: 48 of sand, 34 of silt and 19 of clay. Menongue adobe samples have sand fraction present ranging between 5-58 %, silt fraction between 21-42 % and clay fraction between 17-53 % with the following medians in mass %: 49 of sand, 26 of silt and 26 of clay (Table 9). Data from the

different study areas present different tendencies: the highest sand fraction were measured at Cabinda, silt fraction at Huambo and clay fraction at Menongue sampling sites (Table 9).

Individual data of sampling sites were plotted on the widely used USDA (USDA 1999) soil texture classification triangle (Figure 26). Sandy loam and loam texture classification can be recognized at each study area with dominancy of Cabinda adobe soil samples. Only Menongue samples show sandy clay loam and clay loam texture classification. Additionally, loam texture is also characteristic for this study area. Adobe soil samples from Huambo typically display a sandy loam texture (Figure 28).

Area			Sand (%)	Silt (%)	Clay (%)
		C1L2	74.037	19.888	6.075
		CS2	67.792	23.383	8.825
Cabinda	Sample ID	CS7L2	61.002	31.334	7.664
		Cs8L2	62.361	25.416	12.223
		Cs10L2	44.068	36.085	19.847
	Average±st.dev.		**62±11**	**27±7**	**11±6**
	Median		**62**	**25**	**9**
	Range		**44-74**	**20-36**	**6-20**
		Hs6	5.785	11.623	82.592
		Hs1	3.711	35.527	60.762
		Hs1L2	60.184	26.617	13.199
Huambo	Sample ID	Hs5	3.936	57.082	38.982
		Hs5L2	47.46	33.91	18.63
		Hs8L2	74.60	17.27	8.131
		Hs17L2	50.11	36.84	13.052
	Average±st.dev.		**35±30**	**31±15**	**34±29**
	Median		**48**	**34**	**19**
	Range		**4-75**	**12-57**	**8-83**
		Ms1	48.66	33.91	17.436
		Ms1B	44.04	36.69	19.272
		Ms2L2	39.55	24.88	35.572
Menongue	Sample ID	Ms3L2	58.34	24.77	16.89
		Ms4L2	54.13	20.47	25.404
		Ms4L2	50.88	26.03	23.093
		Ms5L2	4.60	41.98	53.425
	Avegare±st.dev.		**43±18**	**30±8**	**27±13**
	Median		**49**	**26**	**23**
	Range		**5-58**	**21-42**	**17-53**

Table 9. Grain size distribution in selected adobe soil samples with respective averages, standard deviations and medians from Cabinda, Huambo, Menongue sampling sites (st.dev.- standard deviation).

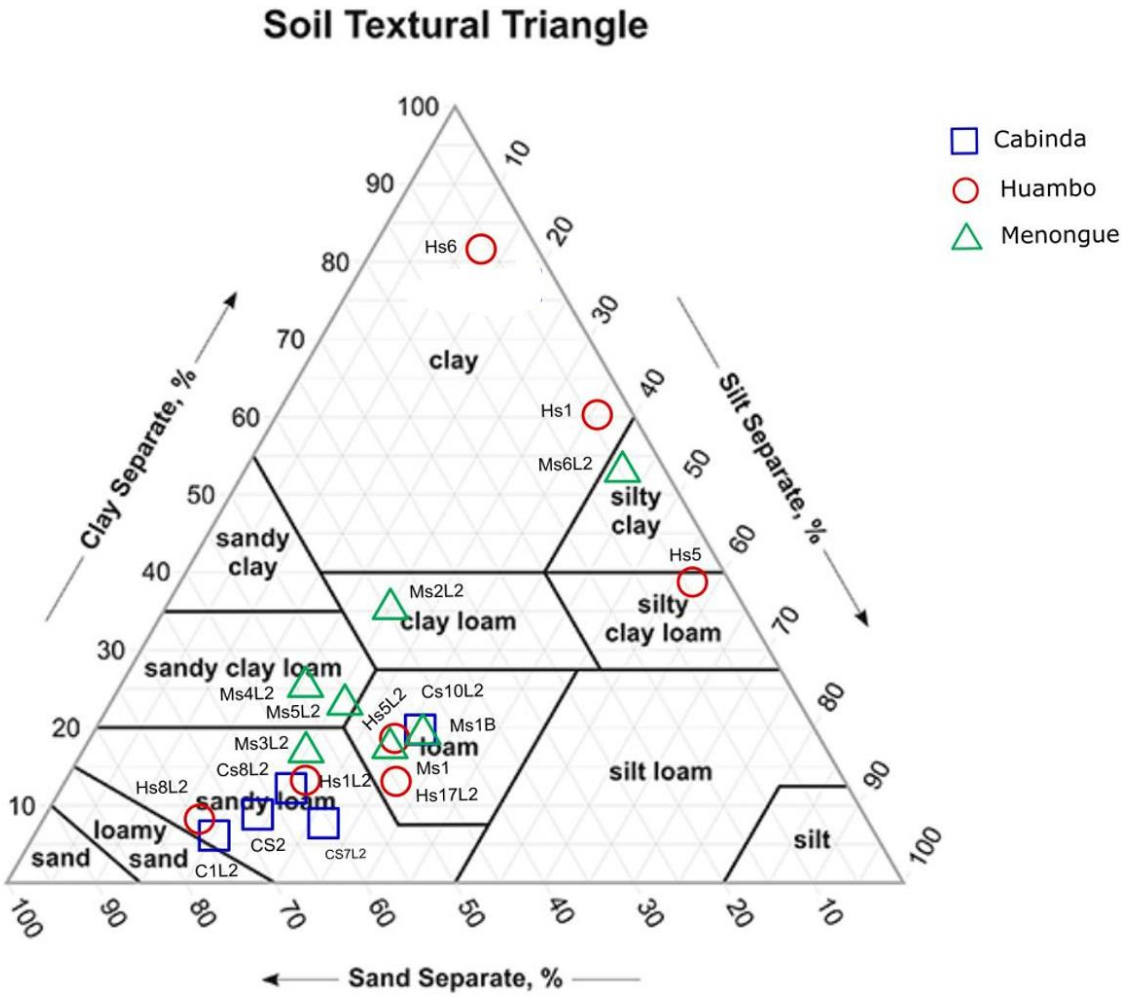

Figure 26. USDA soil texture classification triangle of the adobe soil samples from Cabinda (blue), Huambo (red) and Menongue (green) indicating sampling site codes at the corresponding symbols (initial letter of C - Cabinda, of H - Huambo and of M - Menongue). The legend of the triangle is as follows: 1) Clay, 2) Silt clay, 3) Silt clay loam, 4) Silt loam, 5) Clay, 6) Clay loam, 7) Loam, 8) Sandy clay, 9) Sandy clay loam, 10) Sandy loam, 11) Loamy sand, 12) Sand (USDA 1999).

5.9. Identified phases by XRD

For the mineral and phase determination, 29 adobe samples were analyzed by XRD (Table 10). Studied areas present different mineralogical compositions. Averages and standard deviations (ranges) of the mineral proportions in m/m % unit are presented in Table 11 and described below.

All of the studied adobe soil samples contain quartz and kaolinite. The former is the dominant mineral showing a decreasing quantity in the following order for the studied areas (range, average±standard deviation %): Cabinda (66.0-84.9, 76.2±6.2), Huambo (56.2-86.0, 68.5±9.1)

and Menongue (39.8-68.3, 56±10). In contrast, kaolinite shows opposite order: Menongue (15.2-29.1, 21±4.9), Huambo (4.3-23.4, 16.8±5.9) and Cabinda (8.0-16.6, 12.4±3.4). Except one sample from Huambo (Hs7), goethite and amorphous phase were also identified in all collected adobe samples showing the highest amounts (range, average±standard deviation %) in Menongue (1.4-11.6, 6.5±3.2 for goethite and 4.6-11.5, 6.9±2.4 for amorphous phase) and lowest values in Huambo (0.4-6.6, 2.6±2.5 for goethite and 1.2-13.5, 4.5±3.8 for amorphous material). In Cabinda, the adobe soils have goethite and amorphous phase present in the following values (range, average±standard deviation %): 2.0-7.6, 3.6±1.7 and 2.0-10.65, 2±3.3, respectively.

The following additional minerals were frequently identified in several adobe samples: illite, hematite, gibbsite, cristobalite. Illite is present in all samples from Menongue in the following proportions (range, average±standard deviation %) of 0.5-4.1, 1.7±1.1, in samples from Huambo (with one exception) of 1.5-3.5, 2.3±0.8 and in half of the Cabinda adobe soils of 0.4-4.8, 2.7±1.6. Hematite is generally present in Huambo (0.1-2.0, 0.8±0.7), Menongue (2.7-10.9, 6.2±2.9) and in the half of Cabinda samples (0.3-0.7, 0.5±0.2) expressed as range and average±standard deviation %. Gibbsite occurs in all Huambo samples (0.9-5.6, 3±1.5) and very rarely in Menongue (Table 10, 11). Small amount of cristobalite is characteristic for only Huambo samples (0.3-2.6, 1.0±0.7).

Adobe samples from Huambo (central part of the country) present the highest variety of minerals. This is the only area where gibbsite and anatase were present in all samples. Some minerals in < 1 m/m % quantities are exclusively found in Huambo as well, like rutile, andradite, zircon, Mg-calcite, nacrite. Amorphous material is also present in considerable amounts in all Huambo adobe samples. Menongue area very rarely also has some specific minerals, namely smectite, akaganeite, calcite and gypsum.

Sample ID	Quartz	Kaolinite	Goethite	Hematite	Anatase	Amorphous	Illite	Cristobalite	Gibbsite	Ti-magnetite	Rutile	Andradite	Zircon	Mg-calcite	Nacrite	Smectite	Akaganeite	Calcite	Gypsum	Biotite 1M
Cs1	72.8	12.8	4.6			9.7														
Cs2	78.6	10.3	4.0		0.6	4.0	2.4													
Cs5	66.0	15.8	7.6			10.6														
Cs8	75.2	11.1	5.0			8.7														
Cs9	69.9	16.6	3.3		1.3	3.0	4.8	1.1												
Cs10	71.4	16.3	2.2	0.4	1.7	2.0	4.1	1.7		0.2										
Cs11	78.3	15.2	2.6	0.7	0.7	2.5														
Cs13	80.0	9.0	2.4	0.3	0.6	5.0	2.5													0.2
Cs14	84.9	8.5	2.0	0.4	0.6	2.0	1.7													
Cs17	84.7	8.0	2.4		0.4	4.0	0.4													
Hs1	78.8	11.2	0.9	0.4	1.2	1.2	2.2	1.0	3.0	0.2										
Hs3	66.4	17.2	2.5	2.0	1.1	3.4	3.1	0.8	2.1		0.5	0.8								
Hs5	86.0	4.3	1.0	1.2	0.5	4.4	1.8		0.9											
Hs6	71.7	13.1	3.9	1.9	0.8	4.5	1.5		1.9		0.2		0.6							
Hs7	67.9	20.7		0.4	1.8		1.6	2.6	4.0	0.5	0.3									
Hs8	67.7	19.5	0.4	0.5	1.2	2.7	3.5	1.1	3.1		0.2									
Hs11	58.0	19.6	6.6	0.7	1.2	6.9	3.1	0.8	2.6				0.3	0.2						
Hs17	70.5	15.9	1.4	0.4	1.1	1.5	2.7	0.7	5.3											
Hs18	56.2	23.4	0.4	0.1	0.6	13.5	1.5	0.3	1.7						2.2					
Hs19	61.5	23.0	6.4		1.5	2.0			5.6											
Ms3	58.6	17.9	11.6	3.3	1.1	5.2	2.4													
Ms4	53.0	22.8	5.6	5.6	0.8	11.5	0.8													
Ms5	39.8	27.4	11.1	8.7	1.8	9.8	1.3													
Ms7	49.7	19.4	7.0	10.9	1.4	6.0	2.5		2.0							0.3	0.3	0.6		
Ms10	59.6	16.2	6.5	7.7	0.8	5.0	1.4		1.2								0.4	1.2		
Ms11	44.7	29.1	6.1	7.0	2.1	4.6	4.1		1.3								1.0			
Ms12	68.3	18.2	1.4	2.7	1.1	6.3	1.0	0.6											0.5	
Ms13	68.0	15.2	4.8	3.5	1.2	6.1	1.1													
Ms17	62.6	23.7	4.5		0.6	8.0	0.5													

Table 10. Mineralogical composition (m/m %) of adobe soil samples from Cabinda (Cs), Huambo (Hs) and Menongue (Ms) determined by XRD.

Minerals	Average m/m % (range)		
	Cabinda	Huambo	Menongue
Quartz	76±6.2 (66–85)	69±9.1 (56–86)	56±10 (40–68)
Kaolinite	12±3.4 (17–8)	17±5.9 (4.3-23)	21±4.9 (15–29)
Goethite	3.6±1.7 (2–7.6)	2.6±2.5 (0.4–6.6)	6.5±3.2 (1.4–12)
Hematite	0.5±0.2 (0.3–0.7)	0.8±0.7 (0.1–2)	6.2±2.9 (2.7–11)
Anatase	0.8±0.5 (0.4–1.7)	1.1±0.4 (0.5–1.8)	1.2±0.5 (0.6–2.1)
Amorphous material	5.2±3.3 (2–11)	4.5±3.5 (1.2–14)	6.9±2.4 (5–11)
Illite	2.7±1.6 (0.4-4.8)	2.3±0.8 (1.5–3.5)	1.7±1.1 (0.5–4.1)
Cristobalite	1.4±0.4 (1.1–1.7)	1.0±0.7 (0.3–2.6)	0.6
Gibbsite	------	3.0±1.5 (0.9–5.6)	1.5±0.4 (1.2–2)
Ti-magnetite	0.2	0.4±0.2 (0.2–0.5)	------
Rutile	------	0.3±0.1 (0.2–0.5)	------
Andradite	------	0.8	------
Zircon	------	0.5±0.2 (0.3–0.6)	------
Mg-calcite	------	0.2	------
Nacrite	------	2.2	------
Smectite	------	------	0.3
Akaganeite	------	------	0.6±0.4 (0.3–1)
Calcite	------	------	0.9±0.4 (0.6–1.2)
Gypsum	------	------	0.5
Biotite	0.2	------	------

Table 11. Averages ± standard deviations (ranges) of mineral abundances (m/m %) in adobe samples per study area (blue – Cabinda, red – Huambo, green – Menongue) determined by XRD.

The presented mineral assemblage (Table 11) is common in tropical areas (e.g., Segalen, 1974; Dosseto et al. 2006) where soils go through several chemical processes mainly hydrolyzation and oxidation, which transform the original silicate minerals into kaolinite, alumina hydroxide (gibbsite and amorphous products) and different iron oxides and hydroxides (goethite, hematite and amorphous products; Da Costa et al. 2015; Dosseto et al. 2006). The amorphous material fixes iron and transforms to goethite and hematite (Da Costa et al. 2015) or in case of high Al-content it forms alumina hydroxides (Segalen, 1974). Kaolinite is also a typical product during acidic chemical weathering process; however presence of illite suggests newly formed clay mineral (Da Costa et al. 2015). Commonly occurring anatase, a secondary origin of titanium-dioxide, clearly indicates a highly weathered soil formation process (Okusami et al. 1997). Gibbsite is present only in Huambo and some Menongue sampling sites (Table 10), where the necessary high alumina content is present in the metamorphic and igneous bad rock (Figure 4).

Among the most abundant four phases (i.e. quartz, amorphous material, kaolinite and goethite) in the studied samples, the highly dominant quartz is considered as a constant and inert component. Therefore, ignored in the followings. By adding the amounts of gibbsite, illite+nacrite+smectite and hematite respectively to the rest major phases (amorphous material, kaolinite and goethite), a triplot of sensitive mineral assemblage can be drawn (Figure 27). This displays specific variations in the presence of clay minerals and Fe- and Al-phases of each study area. In Cabinda adobe samples, the decrease of clay mineral content goes together with an increase in Al-containing phases and a slighter decrease of the proportion of the Fe-phases. Half of the Huambo samples show diminished Fe-mineral content. In contrast, the majority of soils collected from Menongue are enriched in Fe-minerals.

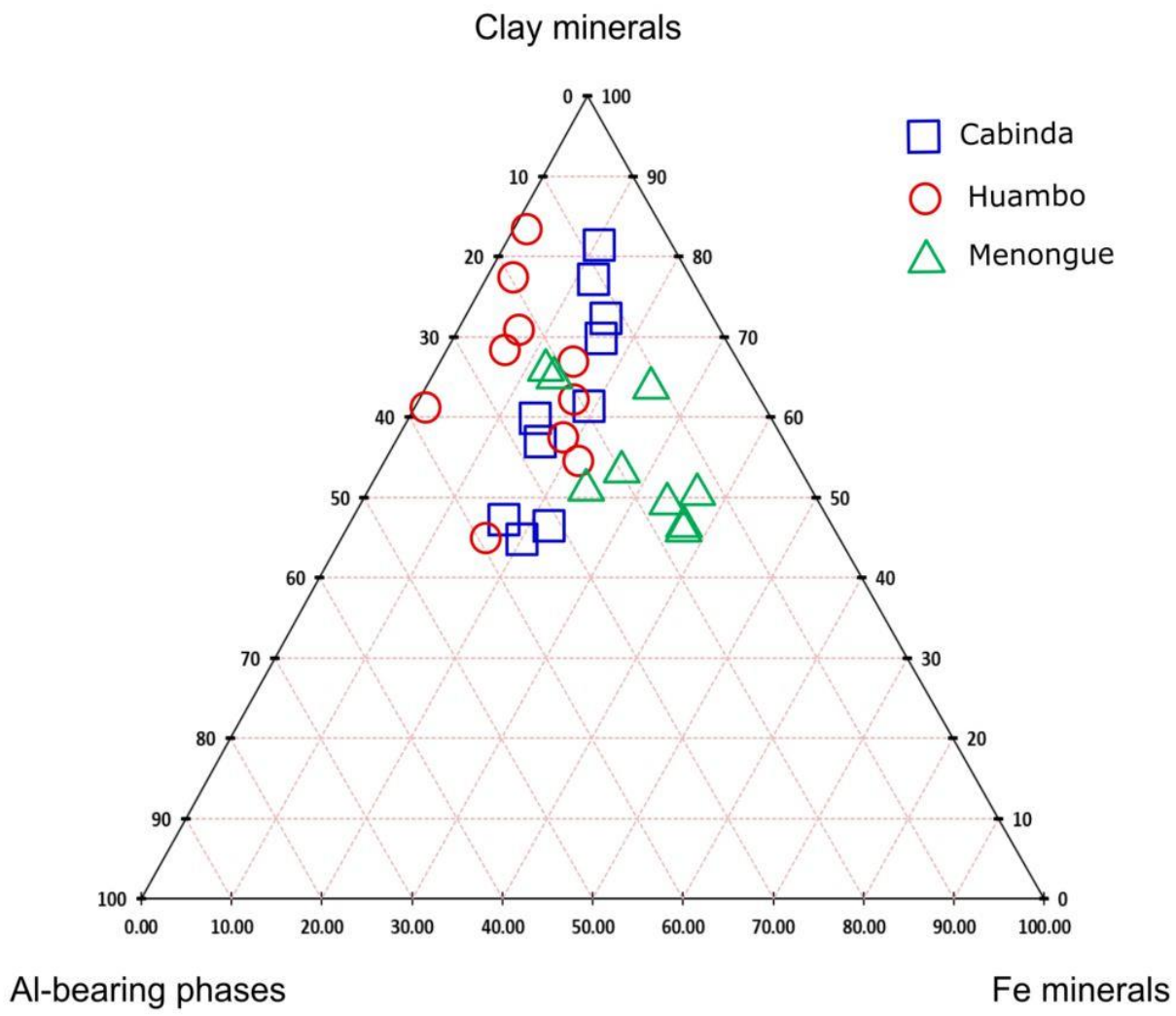

Figure 27. Triplot diagram of clay minerals (kaolinite+illite+nacrite+smectite), Al-bearing phases (gibbsite+amorphous phase) and Fe minerals (goethite+hematite) in Cabinda (blue square), Huambo (red circle) and Menongue (green triangle).

6. Discussion

6.1. Environmental radiation risk in Angolan adobe houses

6.1.1. External risk evaluation

6.1.1.1. Measured and estimated external annual effective doses

The annual effective dose was determined according to two different procedures. In one hand, it is calculated from the radionuclides activity concentration of the building material and the other hand, it is the result of an in-situ measurement. It is obvious that the measured values are influenced by many other factors than the building material. In this section the comparison is done to see how big the difference is and what is the contribution of the building material.

Although some values from Huambo are high, all averages of the estimated dose, calculated from the radionuclides activity concentration of the building material, are lower than the recommended criterion by the European Commission of 1 mSv y^{-1} (EC 1999 , Figure 23).

As expected, in all cases the measured averages are higher than the calculated ones by a ratio of 1.8, 1.9 and 3.9 in Cabinda (north), Huambo (central) and Menongue (south), respectively (Salupeto-Dembo et al. 2020, Figure 12, 23). This result shows the influence of other sources than the building material, namely cosmic rays and radionuclides from the soil (Beck and De Planque 1968; Bossew et al. 2017). Moreover, results from the Mann-Whitney test shows statistically significant differences when comparing values from Huambo to those from the two other study areas for both measured and calculated values, respectively. However, when comparing results from Cabinda (north) and from Menongue (south), statistically significant differences depend on measured values. Those are much higher in Menongue when it comes to measured values, but higher in Cabinda concerning calculated values.

In other hand, medians of the outdoors equivalent external annual effective doses (section 5.1, Figure 13) have also been compared by the Mann-Whitney test. Results of the comparison of Cabinda to Huambo and Cabinda to Menongue, as well as Huambo to Menongue give a P-value < 0.05 what shows statistically significant differences among the compared medians of the background radiation with highest values in Huambo and lowest values in Cabinda (section 5.1,

Figure13). The above observations suggest that the altitude (1 m in Cabinda, 1700 m in Huambo and 1 350 m in Menongue) is the most important contributor to the difference between the measured and the estimated external annual effective doses indoors This is similar to the results of Achola et al. (2012), who reported very different ratios between the directly measured outdoors values and those calculated from radionuclide concentrations varying generally from 1.3 to 7.3 mSv y^{-1} up to 45.5 mSv y^{-1} in one particular case. Furthermore, it has also been demonstrated and confirmed by studies made in different parts of the world that dose exposure highly depends on the altitude (UNSCEAR 2008).

Contribution of the adobe building material in Angola to the external annual effective dose depends on the geological background of the area, as it will be demonstrated in section 6.2.1. even though in this study the contribution was not significant. However, an attention has to be paid in areas located in high altitude.

6.1.1.2. Building material indexes compared to international and recommended limits

Average values of the Radium equivalent index (Ra_{eq}) are the highest in Huambo the central part of the country and the lowest in Menongue at the south part (Figure. 22, Salupeto-Dembo et al. 2020). None of the results is higher than the recommended value of 370 Bq kg^{-1} (OECD 1979; Salupeto-Dembo et al. 2020).

Values of Ra_{eq} from the present study are compared to those of other countries as seen in Table 12. Values of the adobe from the central part (Huambo) are higher (209 Bq kg^{-1}; Figure 22) than most chosen reference countries, being only lower than the clay bricks from Finland (241 Bq kg^{-1}, OECD 1979) and those from Australia (218 Bq kg^{-1}, Beretka and Mathew 1985).

As for the external dose (I index), results show average values three times higher in Huambo (0.72) than in both other studied areas (Cabinda: 0.28 and Menongue: 0.26; Figure 22). All calculated values are lower than the recommended limit of 1. However, the highest values from Huambo (0.95, 0.94) are very close to the recommended limit (Salupeto-Dembo et al. 2020, Figure 22). Comparing to other studies as shown in Table 12, averages from the central part, Huambo, are just lower than the red clay bricks from Bangladesh (0.91, Chowdhury et al. 1998) and higher than all others, whereas from Cabinda (0.28) and Menongue (0.26) the averages are lower compared to

values published in all other studies (Table 12, Figure 22). If we consider the average of the I index for all samples (0.42), the value is higher than that of Hungarian adobes (0.35) and Nigerian soils (0.33) (Szabó et al. 2013; Ademola et al. 2014). However, it is lower than values reported in Egypt and Bangladesh (El-Tahawy and Higgy 1995; Chowdhury et al. 1998) (Table 12, Figure 22).

From the results of the present study, adobe building material from Angola is not hazardous (Salupeto-Dembo et al. 2020). Nevertheless, adobes from Huambo belong to the range of high values compared to used references in this study. These results draw the attention to more investigation regarding adobe building material from areas with the geology known for potential high radioactivity (De Araújo 1992).

Type of building material	Country	Locality	Number of samples	Average activity concentration (Bq kg^{-1})			Ra_{eq} (Bq kg-1)	I	references
				Ra-226	Th-232	K-40			
Adobe	Angola	Cabinda	20	26 ±7	36 ± 5	45 ± 17	81	0.28	Current study
		Huambo	20	87 ± 20	81 ± 21	82 ± 15	209	0.72	
		Menongue	20	27 ± 10	30 ± 10	73 ± 40	76	0.26	
		All samples	60	47 ± 30	49 ± 26	67 ± 30	122	0.42	
	Hungary		20	27 ± 3	30 ± 5	339 ± 36	95±10	0.35±0.04	Szabó et al. (2013)
Red-soil brick	Cameroon		4	------	81±2	-------	153	------	Ngachin et al. (2007)
Mud brick	Australia		4	22	81	447	173	------	Beretka and Mathew (1985)
	Nigeria	OGBOMOSO	2	6.81±2.26	6.78±2.58	66.34±6.66	22	------	Ayinmode et al. (2012)
	Egypt		10	53 ± 18	14 ± 10	325 ± 202	98 ±48	------	Tahir et al. (2005)
Red clay brick	Algeria		12	65±7	51±5	675±4	190 ±9.5		Amrani and Tahtat (2001)
	Bangladesh		10	29±6	53±12	292±45	127.14 ±9.85	0.91±0.07	Chowdhury et al. (1998)
	Zambia		--------	-------	81±7	412±19	180 ± 22	-------	Hayumbu et al. (1995)
	Egypt		21	24	24	258	78	0.5	El-Tahawy and Higgy (1995)
	Cameroon	Yaounde	4	----	81±2	----	193.34	----	Ngachin et al. (2007)
Clay brick	U.K		25	52	44	703	169	-------	OECD (1979)
	Australia		25	40	88	680	218	-------	Beretka and Mathew (1985)
	Finland		33	78	62	962	241	-------	OECD (1979)
	Algeria		8	47±6	35±4	425±3	130 ±7.8	-------	Amrani and Tahtat (2001)
Soil	Worldwide average			35	30	400			UNSCEAR (2000)
	Nigeria		20	-------	26.4	505.1	31.75	0.33	Ademola et al. (2014)
	Namibia	Windhoek	160	-------	35.2 ± 9.9	517.9 ± 117.4	----------	-------	Oyedele et al. (2006)
	Namibia	Different localities	200	-------	67.3 ± 42.5	706.1 ± 214.6	195.3 ± 79.3	----------	Shimboyo et al. (2016)
	Cameroon	Douala-Bassa Zone,	18	24.50 ± 1.80	66.72 ± 7.91	28.19 ± 20.72	122.08 ±11.80		Ndontchueng et al. (2014)
	Italy	Lombardia region	156	-------	48 ± 8.9	640 ± 150	-------	-----	Guidotti et al. (2015)
	Thailand	Chao Phraya river basin	51	-------	30	400	46.2 ± 0.7	--------	Santawamaitre et al. (2014)
	Norway	Kongsfjord	17	43.3 ±29.2	21.1 ±13.2	282.7 ±175.9	---------	----------	Dowdall et al. (2003)
	Spain	Central Pyrenees	-------	20.8-34.9	23.7-49.4	446-799	---------	-------	Navas et al. (2011)

Table 12. Comparison of the Ra-226, Th-232 and K-40 activity concentrations, radium equivalent (Ra_{eq}) and I index of different materials in different countries (Salupeto-Dembo et al. 2020).

6.1.2. Internal risk evaluation

6.1.2.1. Radon and thoron inhalation radiation risk in Angolan adobe houses

According to the results (Figure 17), the annual radon inhalation dose is particularly significantly higher in Huambo (2.83±0.8 mSv y^{-1}, Salupeto-Dembo et al. accepted) than the worldwide average (1.15 mSv y^{-1}, UNSCEAR 2008). The other two studied areas show values are below the reference numbers. Moreover, when thoron is included in the inhalation dose, total inhalation dose is about two times higher than the reference value of 1.25 mSv y^{-1} (Figure 17, UNSCEAR 2000). As already mentioned by Tokonami et al. (2001) when they tested the contribution of thoron on passive detectors, thoron may have an important contribution to the inhalation dose. In the present study, the average thoron contribution to the inhalation dose is 50 %. Other studies also shed light on significant thoron contribution to the inhalation dose. In traditional (made of soil) Chinese houses, thoron contributed up to 57 % to the total dose (Shang et al. 2005). Hungarian adobe houses showed an average thoron contribution of 30 % (Szabó et al. 2014). A study on radon and thoron in houses made of soil bricks carried out in Cameroon showed a thoron contribution of up to 79 % (Saïdou et al. 2015). From the referred results, it is clear that radon is not enough to access the total annual inhalation dose in adobe or similar houses, and that the total radon and thoron radiation risk in Angolan adobe houses is not negligible and worth further considerations.

6.1.2.2. Number of dwellings with radon and thoron activity concentrations above recommended values

Both radon and thoron activity concentrations show lognormal distributions (Figure 8). Therefore, a lognormal probability plot for both isotopes can be drawn with the 95 % confidence intervals (Figure 16). The plot for annual radon average, therefore, indicates that there is a 95 % probability that 10 to 32 % of adobe houses in Angola, assuming the representativity of our sampling, are above the recommended limit for indoor radon concentration of 100 Bq m^{-3}(Figure 28, WHO 2010). However, none of the houses exceed the stronger recommendation of 300 Bq m^{-3} annual average radon activity concentration (WHO 2010).

For thoron, the lognormal probability plot (Figure 28) shows that there is a 95 % confidence that 59 to 81 % of adobe houses in Angola are over 100 Bq m^{-3} and 6 to 28 % are over 300 Bq m^{-3}.

Despite the fact that many studies are reporting high levels of indoor thoron (Schery 1990; Doi and Kobayashi 1994; Chung et al. 1998; Tokonami et al. 2001; Chege et al. 2015; Saïdou et al. 2015), as well as its high contribution to the inhalation dose, no limit concentration was yet recommended for thoron.

From the above stated, one can conclude that a certain percentage of houses made of adobe in Angola have relatively high radon concentrations even though in the range of international recommendations. Regarding thoron, the values are higher and the percentage of involved dwellings is higher (Figure 28).

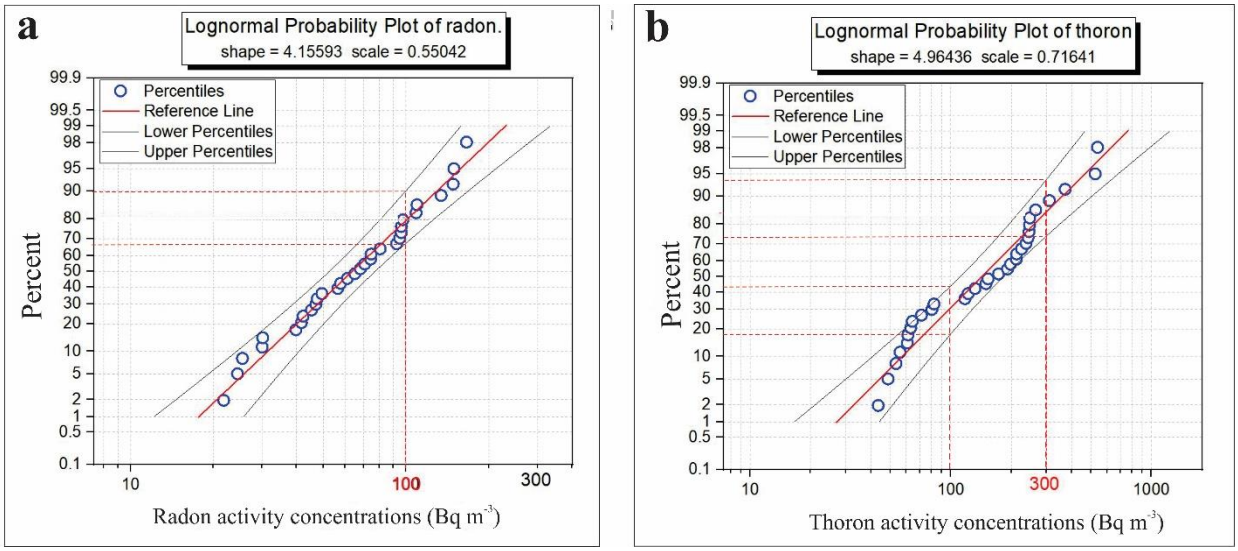

Figure 28. Lognormal probability plots of annual average (a) radon and (b) thoron activity concentrations in Angolan adobes from the study area (Cabinda, Huembo, Memongue) with estimates of the number of dwellings above certain levels (Salupeto-Dembo et al. accepted).

6.1.2.3. Comparison of indoor radon and thoron levels with other countries

The results of the present study are compared to those made in other countries (Table 13). The type of building material is similar to adobe, but in some places (Otawa in Canada, Douala in Cameroon, Gumma in Japan, Kővágószőlős in Hungary, Macedonia, Mexico, Table 13) the investigation was a general survey in dwellings or workplaces, where the type of building material was not taken into account. An effort was made to choose studies, where passive detectors were used for a better comparison.

Comparing indoor radon activity concentration averages, results of Huambo (112±31 Bq m^{-3}) are among the four greatest values showing only Kővágószőlős (Hungary; former uranium mining

area; 154 Bq m^{-3}, Kávási et al. 2007), the southeastern part of the Great Hungarian Plain (Hungary; 194 Bq m^{-3}, Szabó et al. 2014) and Douala (Cameroon; 139±47 Bq m^{-3}, Takoukam S. et al. 2019) higher values (Table 13). Results from Cabinda and Menongue sampling sites are among the lowest values (30±8 and 59±16 Bq m^{-3}, respectively), but still higher than those of Gumma (Japan; 22±14 Bq m^{-3} Tokonami et al. 2005), Hiroshima (26±11 Bq m^{-3}, Doi and Kobayashi 1994) and South Korea (22 Bq m^{-3}, Table 6, Chung et al. 1998).

Indoor thoron activity concentration averages give different classifications. Studies carried out on adobe or similar building materials have much higher activity concentrations than Cabinda (162±93 Bq m^{-3}) and Menongue (92±55 Bq m^{-3}) building materials. However, values from Huambo (278±13 Bq m^{-3}) adobes are still among the highest after Mirma Hill (Kenya; 652 Bq m^{-3}, Chege et al. 2015) and Shanxi and Shaanxi (China; 351 Bq m^{-3}, Table 6, Tokonami et al. 2004).

Country	Building material	Location	Radon activity concentrations ($Bq.m^{-3}$)			Thoron activity concentrations ($Bq.m^{-3}$)			Reference
			Average	Geometric mean	Range	Average	Geometric mean	Range	
Angola	Adobe	Cabinda	30±8	29	21-45	162±93	130	26-310	Present study
		Huambo	112±31	108	71-166	278±134	252	118-539	
		Menongue	59±16	57	40-95	92±55	81	44-213	
		All samples	65±39	55	21-166	172±121	134	26-539	
Hungary	Adobe	SE Great Hungarian Plain	194	166	45-609	245	211	33-576	Szabó et al. (2014)
Cameroon	Adobe	Poli and Lolodorf	92±3	72	27-937	260±13	213	48-700	Saïdou et al. (2015)
China	Earthen building material**	Many different locations	72±59	58±2	x*-427	318±368	162±4	x*-1860	Shang et al. (2005)
China	Earthen building material**	Shanxi and Shaanxi	91	57	19-195	351	153	10-865	Tokonami et al. (2004)
Canada	Building material non identified	Ottawa	110	74±2	8-1525	56	19±4	5-924	Chen et al. (2008)
Cameroon	Building material non identified	Douala	139±47	118±1	31-436	80±52	62±2	4-246	Takoukam et al. (2019)
Japan	Wooden houses with soil walls	Hiroshima	26±11	------	------	85±16	------	------	Doi and Kobayashi (1994)
Korea	Mud walls	Six different cities	22	------	------	82	------	------	Chung et al. (1998)
Japan	Building material non identified	Gumma	22±14	------	11-93	22±18	------	3-97	Tokonami et al. (2005)
Hungary	Building material non identified	Kövágószölös	154	------	17-1083	98	------	1-741	Kávási et al. (2007)
Germany	Clay houses	Bavaria	20-160	------	------	------	------	10-90	Gierl et al. (2014)
Macedonia	Building material non identified	Regional survey	------	------	------	37±36	28±2	3-272	Stojanovska et al. (2013)
Mexico	Building material non identified	Regional survey	------	------	------	82	55	8-234	Martinez et al. (2004)
Kenya	Earthen building material**	Mirma Hill	35	------	16-56	652	------	132-1295	Chege et al. (2015)

*Table 13. Comparison of radon and thoron activity concentrations of adobe and similar building materials from different countries. * - data not available. ** - earthen building materials are those made of soil, clay or similar materials (Salupeto-Dembo et al. accepted).*

6.2. Effect of environmental factors on radiation levels

6.2.1. Geology and geochemistry

6.2.1.1. Influence of geology on the abundance of radionuclides in adobe

The influence of geology on the spatial distribution of natural radiation has been proven by numerous studies (e.g. Tzortzis et al. 2003; Mehra et al. 2011; Odumo et al. 2011; Maxwell et al. 2013) a dose values can relate to different geological backgrounds (e.g. Bossew et al. 2017; Szabó et al. 2017; Torres et al. 2018). It is important to recall that the studied adobe building material is made of the local soil, which develops via heavy tropical chemical weathering process from the surrounded rocks (Coffman 1990). The composition of the source rock eventually controls the natural radioactivity of the soils of the area (Navas et al. 2011) and, therefore, of adobes. Results of present study were published by Salupeto-Dembo et al. (2020) and have shown different levels of radioactivity at the three studied areas of Angola (Figure 18) that have different geological backgrounds (De Araújo 1992; Salupeto-Dembo et al. 2020). As seen in the results, the North part (Cabinda) and the South part (Menongue) reveal the lowest average activity concentrations (Table 4; Figure 18) : 26 ± 7, 36 ± 5, 45 ± 17 and 27 ± 10, 30 ± 10, 73 ± 40 Bq kg^{-1} for Ra-226, Th-232 and K-40, respectively. Adobe samples collected in Cabinda are mostly made of soils derived from rocks belonging to Pleistocene marine sediment formations consisting mostly of sand deposits. It is supported by the grain size analyses (Figure 26) and XRD study of the samples (Table 10, 11). Adobe samples from Menongue are basically from soils formed from rocks belonging to Eocene-Pliocene sandstone formations. In contrary, the central part of the country (Huambo) with Archean metamorphic (gneiss and micaschist) and Proterozoic metasedimentary formations (De Araújo 1992) have the highest average activity concentrations (Figure 18a, b, c). The above described formations are known for their potential to contain elevated concentrations of radioactive minerals zircon and other thorium uranium rich minerals (Boyle 1982; Bourdon et al. 2003). Based on the XRD analyses, the adobe soil samples collected from Huambo show the widest spectrum of mineral species and identification of zircon and rutile in <1 m/m % was also successful. These samples also have large variability of minerals having high specific surface (e.g. goethite, gibbsite, clay minerals) (Table 10, 11).

6.2.1.2. Geochemistry of Ra-226, Th-232 and K-40 based on their correlations

In order to understand the reliance of the three studied radionuclides, Ra-226, Th-232 and K-40, it is important to analyze their correlations and, consequently, their relationships (Salupeto-Dembo et al. 2020). The strongest correlation between Ra-226 and Th-232 is found in Menongue (R = 0.8, Table 5, Figure 19-21). The lithology made up of Eocene-Pliocene sediment formations in Menongue is rather homogeneous (De Araujo 1992). In areas with such a characterization, correlations between Ra-226 and Th-232 are expected to be high (Fairbridge 1972). This strong correlation found between Ra-226 and Th-232 may be explained by the similar geochemical behavior of the parent and progeny nuclides, which infers similar responses to the soil and different environmental processes that affect their distribution (Navas et al. 2011). Uranium and thorium have the same replacement capacity of a nucleus in the lattice of a mineral because of their similar radius. Moreover, despite the fact that uranium tend to be more mobile than thorium during aqueous chemical weathering processes, studies have proven the immobility of uranium due to adsorption or co-precipitation by amorphous Fe-oxyhydroxides (Bourdon et al. 2003). Based on our XRD analyses, the majority of adobe soil samples collected at Menongue sampling sites has Fe-minerals, like goethite+hematite (Table 10, 11, Figure 27) in the highest proportion with high specific surface area. It is more than interesting that Dequincey et al. (2002) had the same result of uranium and thorium accumulation in the indurated ferruginous cap of kaya laterites from northern Burkina Faso, and of their secondary redistribution into the profile.

Regarding the correlation between Ra-226 and K-40, the only area with a statistically significant relationship is Cabinda (Table 5). Samples from Cabinda were taken at the littoral part where chemical weathering is not profound, whereas, in the interior part of the country (Huambo, Menongue), not only the rocks but the soils are highly weathered (Diniz 2006; Jones, A. et al. 2015). It is confirmed by the XRD analyses (Table 10, 11) showing > 50 m/m % quartz content in the all the studied adobe soil samples. Both studies by Wilford et al. (1997) and Dickson and Scott (1997) explain the influence of the weathering process and the topography on the radionuclide distribution (IAEA 2003). Potassium is more easily weathered and leached out than radium in soils because of its higher solubility and probably hygroscopic feature. Moreover, upper horizons in soils are poor in potassium because of the plant uptake (Fujiyoshi and Sawamura 2004) despite the fact that its natural abundance is much higher than that of uranium (or radium).

Contrariwise to the results from the correlation between Ra-226 and K-40, statistically significant relationship exists between Th-232 and K-40 in Huambo and Menongue, but not in Cabinda (Table 5, Figure 19-21). In some cases, for instance, when thorium is hydrated (Bourdon et al. 2003), the behavior of potassium and thorium is similar during the chemical weathering process under low pH value. In these cases, both elements are mobile during alteration as demonstrated on the study of Dickson and Scott (1997). Consequently, the average potassium and thorium content of soils reflect the average of the rocks content on the same elements from which they are derived. However, the differences in soil radioelement concentrations are relatively small (IAEA 2003).

Overall, the correlation among radionuclides is the strongest between Ra-226 and Th-232 in all areas, which was also found in adobes and soils, for instance, by Szabó et al. (2013) and El Afifi et al. (2006). However, as extensively illustrated and explained by Wilford et al. (1997), in the study about different Australian soils, weathering processes and topography might have principal factors on the behavior of the radionuclides and, consequently, their distribution in the soil (IAEA 2003).

6.2.1.3. International comparison of Ra-226, Th-232 and K-40 activity concentrations of adobe

As studies about radiation of building materials have not carried out in Angola, it was more adequate to compare the results of our study to similar materials in other countries (Table 12, Salupeto-Dembo et al. 2020). In that regard, apart from adobe, we used soil, red-soil bricks, mud-bricks, soil and clay bricks since the conservation of the radionuclides content is similar considering that the manufacturing process does not change the initial composition of the building material (Szabó et al. 2013). It is also important to note that studies related to the radiological assessment of the adobe building materials are scarce. The worldwide median concentrations in soils (35, 30, 400 Bq kg^{-1} for Ra-226, Th-232 and K-40, respectively) determined by UNSCEAR (2000) will be also used as reference values.

Amongst all the studied radionuclides, highest average values are found in Huambo, at the central part of the country (Table 4, Figure 18). Measured activity concentrations of Ra-226 and Th-232 in adobes are lower in Cabinda (26 ±7, 36 ± 5 Bq kg^{-1}) and Menongue (27 ± 10, 30 ± 10 Bq kg^{-1}), but more than two times higher in Huambo (87 ± 20, 81 ± 21 Bq kg^{-1}) than the reference values

(30, 40 Bq kg^{-1}, UNSCEAR 2000, Table 4, Figure 18). Regarding K-40, all measured samples are below the worldwide average reference (UNSCEAR 2000, Table 4, Figure 18).

Average values of Ra-226 in Cabinda and Menongue adobes are the same within standard deviation as Hungarian adobe (Szabó et al. 2013), Australian mud-bricks (Beretka and Mathew 1985), Bangladesh and Egyptian red clay bricks (Chowdhury et al. 1998; El-Tahawy and Higgy 1995), as well as Cameroonian and Spain soils (Ndontchueng et al. 2014; A. Navas et al. 2011), whereas in Huambo they show elevated value. If the average number is considered for all samples together (47 ± 30 Bq kg^{-1}), the value is higher than the world reference one found in UNSCEAR (2000, 35 Bq kg^{-1}).

Regarding the values of Th-232 in Table 12, Huambo (central) belongs to the group with the highest averages (above 81 Bq kg^{-1}), i.e. the red soils brick from Cameroon (Ngachin et al. 2007), the clay brick from Australia (Beretka and Mathew 1985), the red clay bricks from Zambia and Cameroon (Hayumbu et al. 1995; Ngachin et al. 2007). Cabinda and Menongue adobe values are in the same range as those from most of the countries summarized in Table 5., but lower than the worldwide average reference value. The average of all Angolan adobe samples together (49 ± 26 Bq kg^{-1}) is slightly higher than the reference value (UNSCEAR 2000).

All activity concentrations of K-40 from present study are much lower compared to most values contained in Table 12, except of the studied soils in Cameroon (28 ± 21 Bq kg^{-1}) with the lowest values (Ndontchueng et al. 2014) and the mudbrick from Nigeria (66 ± 7 Bq kg^{-1}; Ayinmode et al. 2012), which are lower than concentrations in adobes from Huambo (82 ± 15 Bq kg^{-1}) and Menongue (73 ± 40 Bq kg^{-1}), but higher than from Cabinda (45 ± 17 Bq kg^{-1}). The distribution of K-40 can be highly variable because it can be controlled by physical processes such as soil redistribution (erosion/deposition) and by processes of leaching/sorption in the soil complex (Dickson and Scott 1997; Navas et al. 2011; Wilford et al. 1997). These reveal significance of geology, local climatic conditions and physical processes, which are crucial to the radionuclide distribution.

6.2.1.4. Structural properties of adobe influencing emanation properties

Radon and thoron emanation of rocks, soils and building materials is reported to be affected by many influencing factors such as moisture (Greeman and Rose 1996; Bossew 2003), temperature

(Stranden et al. 1984), specific surface area (Somlai et al. 2008) and the content of the parent radionuclide. Its value in soils and rocks is usually around 20 % as average, in the range of 5 to 70 % (UNSCEAR 2000; Sakoda et al. 2010). A detailed study on adobe building materials in Hungary showed that radon gets emanated in an average 28±7 % probability and in a range of 12-53 % and that thoron leaves the grains of the samples with an average 18±7 % probability in the range of 7-38 % (Szabó 2013).

In the current studied adobe building material from Angola, radon and thoron emanation results (Table 7, Figure 24) show the highest values in Huambo which can be explained by the elevated amount of Ra-226 and Th-232 in samples from this area (Table 4, Figure 18). Parent radionuclide content in the material is unquestionably essential for the emanation of radon and thoron (Bossew 2003, Sakoda et al. 2010). This is sustained by the good linear correlation between radon emanation and Ra-226 with R= 0.76 and P-value = 0.006 (Figure 27a), as well as between thoron emanation and Th-232 with R = 0.81 and P-value < 0.001 (Figure 27b).

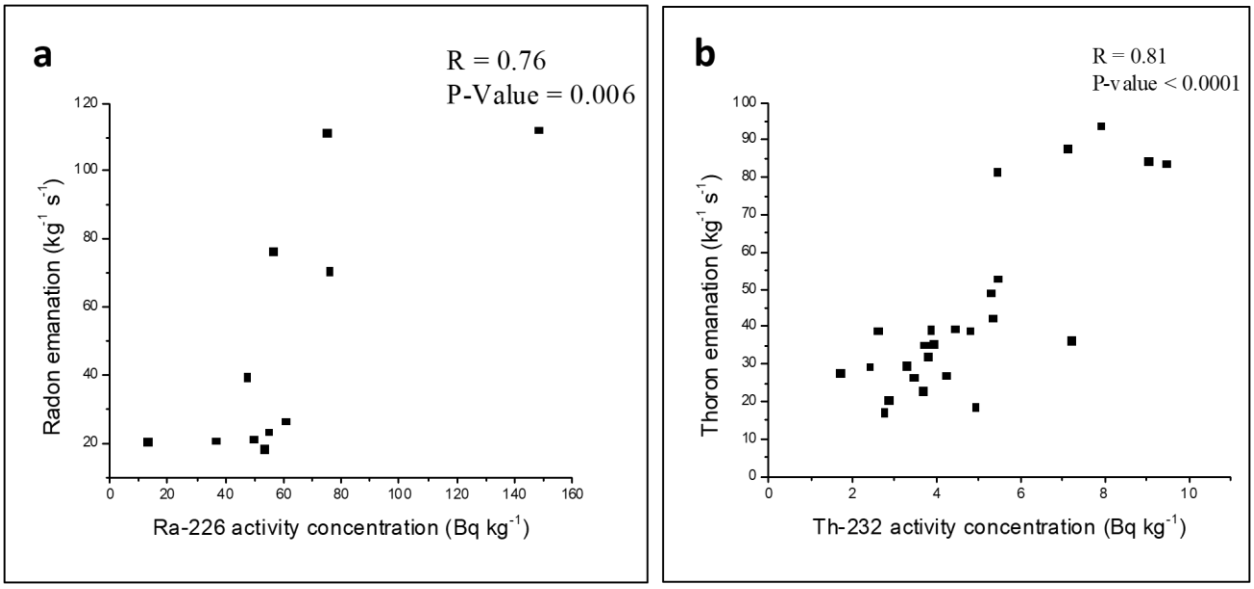

Figure 27. Correlation between a) radon emanation (kg^{-1} s^{-1}) and Ra-226 activity concentration (Bq kg^{-1}) and b) thoron emanation (kg^{-1} s^{-1}) and Th-232 activity concentration (Bq kg^{-1}) in Angolan adobes from all the studied sampling sites in Cabinda, Huambo and Menongue)

Radon and thoron emanation fraction of all samples from Angola displayed averages and standard deviations (ranges) as follows, 19±10 % (8-39 %) and 12±6 % (4-31 %), respectively, which are lower than values of Hungarian adobe building material (Szabó 2013). Emanation fraction is the

lowest in Huambo 12±4% (9 – 17%) and 8±2% (4 – 11%) and the highest in Menongue 28±9% (16 – 39%) and 14±5% (6 – 27%) for radon and thoron, respectively (Table 8, Figure 25), which shows a very different picture than radon and thoron emanations. Emanation is connected mainly to the Ra-226 and Th-232 radionuclide contents (Figure 27), whereas emanation fraction is rather connected to the structure of the building material like the grain size distribution among other physical properties (Szabó 2013).

Properties studied which may influence emanation fraction in the studied samples are the grain size distribution and the mineralogical composition, where the radionuclides are located within grains (Table 9, 10, 11). It is seen earlier that Angolan adobe samples in general contain mostly quartz (Table 10, 11). Sakoda et al. (2010) demonstrated when studying the emanation in isolated minerals (quartz, goethite, microcline, muscovite) that quartz had the lowest emanation fraction among the studied minerals. Specific surface area, however, is a factor, which highly influences emanation (Somlai et al. 2008). Coarse grained sand, suspecting high quartz proportion, have low specific surface area. Among Angolan adobe samples, the ones from Cabinda have the highest proportions of sand (Table 9, Figure 26), thus high emanation fraction should not be expected. Nevertheless, Huambo has lower emanation fraction than Cabinda. The explanation for that is similar to that reported by Krupp et al. (2017), who studying the emanation coefficient in 14 different minerals, demonstrated that zircon and other U-238 and Th-232 rich minerals have even lower emanation fraction compared to quartz. This is the only area among the study areas with minerals like zircon and rutile (Table 10, 11), which are well-known minerals with potentially elevated radioactivity. Higher radioactivity in Huambo certainly comes from other minerals than the most frequent ones, in Table 10. These minerals together with other accessory minerals coming from granitic bed rock (Figure 4), can be present in quantities undetectable by XRD, may cause the increase of the radioactivity (Leal et al. 2020; Esan et al., 2020) in adobes and the differences in emanation fraction.

Menongue adobe samples show the highest emanation fractions (Figure 25.), as well as the highest amount of clay grain size fraction (Table 9, Figure 26) indicating an increase in specific surface area. In the already mentioned study by Sakoda et al. (2010) it is also shown that emanation fraction in goethite was considerably high. Samples from Menongue also contain the highest amount of goethite (Table 10), Figure 27). The lowest emanation fraction results characteristic for Huambo adobe samples, where the radionuclide contents are the highest, which observation might

be connected to the distribution of radionuclides within grains and, therefore, might refer to different source minerals.

6.2.1.5. Spatial variation of indoor radon and thoron activity concentrations

Box and whisker plots in Figure 15a and b show the annual average indoor radon and thoron activity concentrations at the three studied areas. As seen in results the Mann-Whitney test ascertains that activity concentrations in Huambo, the central part of the country, are the highest among the study areas (Salupeto-Dembo et al. accepted). These results can be explained by the differences in geology. In fact, in this area, the geology is composed of metamorphic (gneiss, micaschist, metasediments) and igneous (granite, rhyolite to andesites) rocks, which can contain the higher abundance of mother nuclides of radon and thoron in the studied fields as we explained earlier. The highest values of Ra-226 and Th-232 in adobe building materials (116 and 121 Bq kg^{-1}, respectively; Figure 10; Salupeto-Dembo et al. 2020) confirms the above stated. Radon and Ra-226 show a correlation coefficient of 0.46 with a P-value of 0.0042 (Figure 28a). This proves that there is a relationship between radon and its source. However, it worth taking into consideration that the correlation would be better if we had radon coming specifically from the building material. As known, most indoor radon derives from the underlying dwelling foundation and some studied dwellings are without coverage on the floor. In these cases, radon, migrating from the floor, may considerably contribute to the indoor levels. This result is consistent with those of Saidou et al. (2015), who studied adobe dwellings from Cameroon. Contrary to the case of radon, there is not a statistically significant linear relationship between thoron and its source, Th-232 (Salupeto-Dembo et al. accepted), which show a correlation coefficient of 0.29 and a P-value of 0.08 (Figure 28b). Thoron measurements are more disturbed by other factors, like ventilation and humidity because of its short half-life (Dwivedi et al. 2001; Szabó et al. 2014). The equilibrium factor of thoron is, generally, influenced by indoor atmospheric parameters such as ventilation more strongly than that of radon (Gierl et al. 2014). Because thoron diffuses very slowly (1 to $3x10^{-6}$ m^2 s^{-1}, Szabó 2013), any ventilation can prevent its accumulation near the walls which disturbs the measurements. Thus, it is hard to have the full amount of thoron originating from the building. For this reason, the correlation between thoron and the source is expected to be even less significant than between radon and its source.

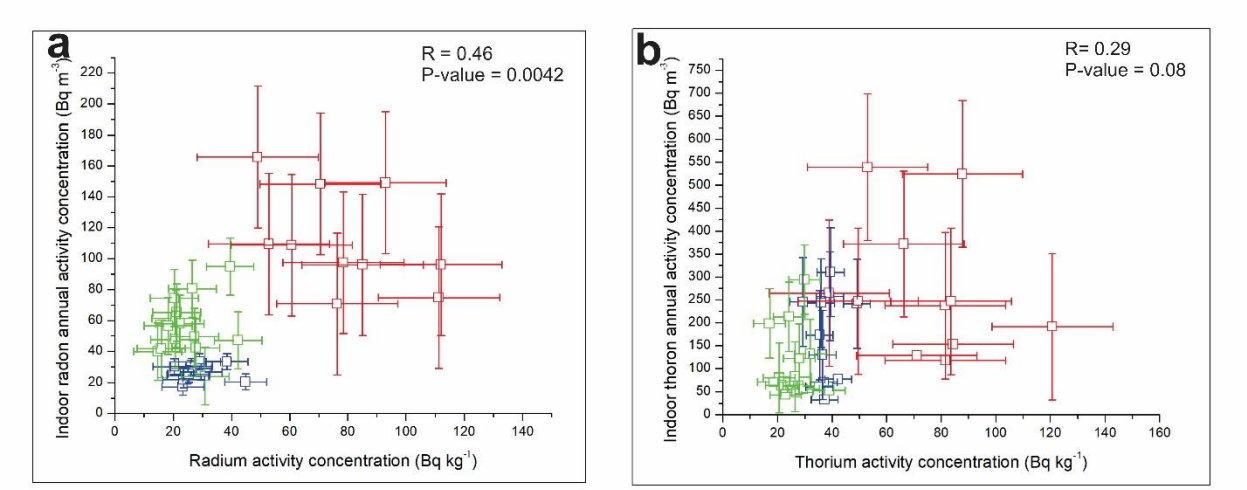

Figure 28. Correlation between (a) radon and Ra-226 and (b) thoron and Th-232 indoors and in adobes, respectively, from study areas of Cabinda (blue), Huambo (red) and Menongue (green) (Salupeto-Dembo et al. accepted).

6.2.2. Effects of climatic conditions

With the aim of evaluating the effect of climatic conditions on indoor radon and thoron activity concentrations in Angolan adobe houses, the one-year survey period was divided into two seasons: rainy and dry. As seen in Figure 14 and proven by Mann-Whitney tests (P-value <0.05 in Cabinda and in Huambo), medians of the indoor radon during the rainy season indicate statistically significantly higher values than in the dry season in Cabinda and Huambo. The elevated indoor radon activity concentrations during rainy seasons can be explained by the influence of rain precipitation. Adobe building material, showing soil properties, has the ability to absorb water (Szabó et al. 2014). It is also important to emphasize that most indoor radon moves from the ground under the dwellings. The moist content of pore spaces both in the adobe and the soil may increase the emanation coefficient and consequently the exhalation of radon (Thamer et al. 1981; Sasaki et al. 2004), thus the level of radon activity concentration in the rainy season. Another factor might be the common behavior of the residents, who tend to seal their homes when the weather is worse. Results of the present study are consistent with studies carried out in Ghana (Otoo et al. 2018b) and in Cameroon (Bineng et al. 2020) where radon levels were also elevated during the rainy season (medians of rainy and dry seasons were respectively found to be 39.3 and 26.9 Bq m-3 in Ghana and 131 and 80 Bq m-3 in Cameron). Both comparative studies explained

the difference by the common practice of inhabitants of closing windows during rainy season. Regarding Menongue, the difference is statistically not significant (P-value equals 0.067). The possible explanation of this variance is that having a semi-desert climate, diurnal temperatures of Menongue are very high (above 35˚C) causing rapid evaporation of the water accumulated in the soil. Consequently, only a small amount of water can accumulate in the pore space influencing radon exhalation. Another reason can be explained by the less probability of the inhabitant to close their windows during this period. Although temperature could play a principle role in seasonal variations of the indoor radon levels, the differences in the average temperatures among seasons are generally very small in Angola as it was the case during the monitored period (4℃ in Cabinda and 1℃ in Huambo and Menongue, Figure 5). A comparison of the medians of the annual averages of the indoor thoron, on the other hand, does not show significant differences in values between the two seasons (P-value equals 0.73 in Cabinda, 0.74 in Huambo and 0.92 in Menongue; Figure 14). Because of its short half-life there is no expectation of thoron coming from the floor as it was the case for radon. Moreover, thoron diffuses very slowly (Csige et al. 2013), any ventilation can prevent its accumulation near the walls, which disturbs the measurements. Thus, it is difficult to have the full amount of thoron deriving from the building (Salupeto-Dembo et al. accepted).

7. Conclusions

From the three studied areas in Angola, Cabinda (north) and Menongue (south) show Ra-226 and Th-232 activity concentrations in adobe building material in the same range as most international works focusing on similar type of materials. Whereas, Huambo (central) shows elevated values (116 – 49 and 121 – 39 Bq kg^{-1} for Ra-226 and Th-232, respectively). Regarding K-40, values from all studied areas are low compared to other countries. From the correlations among the studied radionuclides, it is concluded that their geochemical behavior is an important factor determining their abundance. Based on the determined Ra_{eq} and I building material qualification indexes, adobe houses in Angola are safe to use in radiological point of view. However, a closer look at the geology of the source material is strongly recommended when old metamorphic and acidic igneous rocks are present. The annual effective doses showed different ranges for different methods of determination. Values determined from direct measurements are higher than those estimated from the activity concentrations of the building materials. It is because, apart from the geology influences to the external radiation dose of the population living in adobe houses, there is other influences among which the altitude of the settlement. Despite of the spatial variability and the differences between the two methods of estimations, it is confirmed by all results that external radiation dose from adobe building material in Angola does not mean any significant risk for the residents of adobe houses (Salupeto-Dembo et al. 2020).

Seasonal and spatial variations of the radon and thoron activity concentrations in adobe houses at the three investigated areas were also examined in this study (Salupeto-Dembo et al. accepted). Radon activity concentrations are higher during the rainy season than in the dry season, whereas no statistically significant differences were detected for thoron. Annual average radon and thoron activity concentrations are also the highest in Huambo (central part of the country) like Ra-226 and Th-232 activity concentrations. Seasonal variations are essentially most probably due to precipitation variability, and spatial variations are mostly due to differences in geology and the mother nuclide content of adobe. Radon and thoron activity concentrations are sampled from a lognormally distributed population based on hypothesis testing. Regarding radon activity concentrations, 10 to 32 % of adobe houses in Angola are above the recommended limit of 100 Bq m^{-3} and when it comes to thoron activity concentrations, 59 to 81 % of adobe houses are expected to be over 100 Bq m^{-3}, and 6 to 28 % of them are over 300 Bq m^{-3} with 95 % probability. The

inhalation dose in Huambo (4.5±1.5 mSv y^{-1}) is above the worldwide average (1.15 mSv y^{-1}). The contribution of thoron to the inhalation dose is shown to be 50 %. The total inhalation dose received by residents is not expected to be negligible and it is worth further investigations. The results of this study are valuable information on radon and thoron as well as on Ra-226, Th-232 and K-40 content of soils in Africa in general and in Angola in particular.

Results regarding the structure, mineralogy and radon and thoron emanation properties show that samples from Huambo have the lowest radon and thoron emanation fractions, Menongue the highest and Cabinda in the middle. These differences are attributed to the grain size distribution and the mineralogical composition of the samples. The grain size distribution shows samples from Cabinda with the highest sand contribution and Menongue with the highest clay content among the studied areas, which explain observations through considering the specific surface areas. The highest radioactivity, but lowest emanation fraction results in Huambo might be connected to the differences in source minerals. This is the only area with minerals, like zircon and rutile and potentially other accessory minerals, from granitic bed rock with elevated radionuclide contents.

Thesis points

1. My doctorate project is the first to investigate natural radiation in Angolan adobe dwellings measuring ambient gamma dose equivalent rate, Ra-226, Th-232 and K-40 activity concentrations in building materials (following experiences published with my participation in Völgyesi et al., 2016) and indoor radon and thoron levels at three areas of the country with different geological background, geographical location and microclimate. These areas are Cabinda in the north, Huambo in the central and Menongue in the south part of the country. The results show a spatial distribution: most of the values from Huambo are significantly the highest compared to the other studied areas, which is explained by its geological background composed mostly of granitic rocks (Salupeto-Dembo et al. accepted; Salupeto-Dembo et al. 2020).

2. I concluded that external radiation from adobe building material in Angola is not hazardous for the local population. This is confirmed by calculated radium equivalent (Ra_{eq}), activity concentration (I) indexes of 45 samples from the three studied areas and also by calculated and measured external doses. The influence of the altitude on the elevated external dose was also clearly demonstrated (Salupeto-Dembo et al. 2020).

3. I described a seasonal variation of indoor radon and thoron activity concentrations in adobe dwellings of Angola. Radon showed higher values in the rainy season than in the dry season, whereas thoron showed no statistically significant variation between the two seasons. I concluded that the moist content of the soil during rainy season and the behavior of the residents are the main reasons of elevated radon activity concentrations during rainy season (Salupeto-Dembo et al. accepted).

4. I estimated the percentage of adobe houses in Angola with annual radon and thoron activity concentrations above reference values. For this, I described the statistical distributions of results. Accepting a lognormal distribution for both radioactive noble gas isotopes, I concluded that for annual radon activity concentration average there is a 95 % probability that 10 to 32 % of adobe houses in Angola are above the recommended 100 Bq m^{-3}, assuming the representativity of sampling. However, none of the houses exceed the stronger recommendation of 300 Bq m^{-3}. For

thoron, no limit exists, but it is estimated that 59 to 81 % of adobe houses in Angola are over 100 Bq m^{-3} and 6 to 28 % are over 300 Bq m^{-3} at around 9 cm from the walls with 95 % confidence (Salupeto-Dembo et al. accepted).

5. I have estimated the internal radiation dose of the Angolan population living in adobe houses and confirmed that radon and thoron may cause a non-negligible contribution to the radiation exposure. The residents of Huambo have a higher radon inhalation radiation risk (2±0.8 mSv y^{-1}) than the world average (1.15 mSv y^{-1}). The presently best available estimation shows that thoron contribution to the inhalation dose is significant, around 50 % in average in adobe houses of Angola. With thoron contribution, the average inhalation dose for the population living in adobe houses in Huambo rises up to 4.5±1.5 mSv y^{-1} (Salupeto-Dembo et al. accepted).

Publications of the author

Salupeto-Dembo J, Szabó-Krausz Z, Völgyesi P, Kis Z, Szabó Cs (2020) External radiation exposure of the Angolan population living in adobe houses. J Radioanal Nucl Chem 32: 353-364. doi: 10.1007/s10967-019-06920-z

Salupeto-Dembo J, Szabó-Krausz Z, Völgyesi P, Szabó Cs (accepted) Radon and thoron radiation exposure of the Angolan population living in adobe houses. J Radioanal Nucl Chem doi: 10.1007/s10967-020-07215-4

Völgyesi P, Szabó Z, Salupeto-dembo J, Kis Z, Szabó Cz, (2016) Gamma-spektrometriai módszer magyarországi salakminták Ra-226 aktivitáskoncentrációinak meghatározására a 186 keV-os csúcs használatával aktivitáskoncentrációinak meghatározására a 186 keV-os csúcs használatával. Sugárvédelem, IX: 25–32.

Bibliography

Achola SO, Patel JP, Mustapha AO, Angeyo HK (2012) Natural radioactivity and external dose in the high background radiation area of Lambwe East,Southwestern Kenya. Radiat Prot Dosimetry 152: 423–8. doi: 10.1093/rpd/ncs047

Ademola AK, Bello AK, Adejumobi AC (2014) Determination of natural radioactivity and hazard in soil samples in and around gold mining area in Itagunmodi, south-western, Nigeria. J Radiat Res Appl Sci 7: 249–255. doi: 10.1016/j.jrras.2014.06.001

Ajayi OS, Olubi OE (2016) Investigation of indoor radon levels in some dwellings of southwestern Nigeria. Environ Forensics 17: 275–281. doi: 10.1080/15275922.2016.1230909

Amrani D, Tahtat M (2001) Natural radioactivity in Algerian building materials. Appl Radiat Isot 54: 687–689. doi: 10.1016/S0969-8043(00)00304-3

Ateba JFB, Ateba PO, Ben-Bolie GH, et al (2010) Natural background dose measurements in South Cameroon. Radiat Prot Dosimetry 140: 81–88. doi: 10.1093/rpd/ncq035

Avrami E, Guillaud H, Hardy M (2008) Terra Literature Review: An Overview of Research in Earthen Architecture Conservation. The Getty Conservation Institute, Los Angeles, J. Paul Getty Trust, pp: 174.

Ayinmode BO, Famakinwai RO, Ajayi JO (2012) Assessment of natural radioactivity in concrete block, extruded clay brick, and mud brick taken from Ogbomoso, Southwestern, Nigeria. Anadolu Univ J Sci Technol -A 13: 23–29.

Beck H, De Planque G (1968) The radiation field in air due to distributed gamma-ray sources in the ground. HASL Rep 1: 1–53. PMID: 5192267

Beltrán-Torres S, Petrik A, Szabó KZ, Jordan G, Yao J, Szabó Cs (2018) Spatial relationship between the field-measured ambient gamma dose equivalent rate and geological conditions in a granitic area, Velence Hills, Hungary: An application of digital spatial analysis methods. J Environ Radioact 192: 267–278. doi: 10.1016/j.jenvrad.2018.07.001

Beretka J, Mathew PJ (1985) Natural radioactivity of australian building materials, industrial

wastes and by-products. Health Phys 48:87–95. doi: 10.1097/00004032-198501000-00007

Bineng GS, Tokonami S, Hosoda M (2020) The importance of direct progeny measurements for correct estimation of effective dose due to radon and thoron. Front Public Health 8: 1–12. doi: 10.3389/fpubh.2020.00017

Bongenaar, J. J. T. M., Kossen, N. W. F., Metz, B., & Meijboom, F. W. (1973). A method for characterizing the rheological properties of viscous fermentation broths. Biotechnology and Bioengineering, 15(1), 201–206. doi:10.1002/bit.260150115

Bossew P (2003) The radon emanation power of building materials, soils and rocks. Appl Radiat Isot 59: 389–392. doi: 10.1016/j.apradiso.2003.07.001

Bossew P, Cinelli G, Hernandez-Ceballos M, et al (2017) Estimating the terrestrial gamma dose rate by decomposition of the ambient dose equivalent rate. J Environ Radioact 166: 296–308. doi: 10.1016/j.jenvrad.2016.02.013

Bourdon B, Lundstrom CC, Henderson SP, Turner GM (2003) Reviews in Mineralogy & Geochemitry 52, URANIUM – SERIES GEOCHEMISTRY. Geocehmical Sociaty & Mineralogical Society of America, ISBN 10: 0939950642, pp: 656.

Boyle RW (1982) Geochemical prospecting for thorium and uranium deposits. Development in Economic Geology, 16, pp: 493 Elsevier Scientific Publishing Company, ISBN 0-444-42070-3.

Chege M, Hashim N, Nyambura C, et al (2019) Radon and thoron; Radioactive gases lurking in earthen houses in rural Kenya. Front Public Heal 7: 1–6. doi: 10.3389/fpubh.2019.00113

Chege MW, Hashim NO, Merenga AS, et al (2015) Estimation of annual effective dose due to radon and thoron concentrations in mud dwellings of Mrima Hill, Kenya. Radiat Prot Dosimetry 167: 139–142. doi: 10.1093/rpd/ncv231

Chen J, Tokonami S, Sorimachi A, et al (2008) Preliminary results of simultaneous radon and thoron tests in Ottawa. Radiat Prot Dosimetry 130: 253–256. doi: 10.1093/rpd/ncm503

Chowdhury MI, Alam MN, Ahmed AKS (1998) Concentration of radionuclides in building and ceramic materials of Bangladesh and evaluation of radiation hazard. J Radioanal Nucl Chem 231: 117–122. doi: 10.1007/BF02388016

Chung WH, Tokonami S, Furukawa M (1998) Preliminary survey on radon and thoron concentrations in Korea. Radiat Prot Dosimetry 80: 423–426. doi: 10.1093/oxfordjournals.rpd.a032563

Coffman R, Agnew N, Austin G, Doehne E (1990) Adobe mineralogy: characterization of adobes from around the world. In: 6th International Conference on the Conservation of Earthen Architecture: Adobe 90. Las Cruces, New Mexico, U.S.A., October 14-19, 1990. 424–429.

Csige I, Szabó Z, Szabó Cs (2013) Experimental technique to measure thoron generation rate of building material samples using RAD7 detector. Radiat Meas 59: 201–204. doi: 10.1016/j.radmeas.2013.07.003

Da Costa PYD, Nguetnkam JP, Mvoubou CM, et al (2015) Old landscapes, pre-weathered materials, and pedogenesis in tropical Africa: How can the time factor of soil formation be assessed in these regions? Quat Int 376: 47–74. doi: 10.1016/j.quaint.2014.04.062

De Araújo AG (1992) Geologia de Angola: noticia explicativa da carta geológica à escala 1:1.000.000. Serviço Geológico de Angola, Luanda

Dequincey O, Chabaux F, Clauer N, et al (2002) Chemical mobilizations in laterites: Evidence from trace elements and ^{238}U-^{234}U-^{230}Th disequilibria. Geochim Cosmochim Acta 66: 1197–1210. doi: 10.1016/S0016-7037(01)00845-6

Dickson, B.L., Scott KM (1997) Interpretation of aerial gamma-ray surveys – adding the geochemical factors. AGSO Journal of Australian Geology & Geophysics, 17: 187-200.

Diniz AC (2006) Características mesológicas de Angola descrição e correlação dos aspectos fisiográficos, dos solos e da vegetação das zonas agrícolas angolanas. pp:546.Lisboa : IPAD

Doi M, Kobayashi S (1994) Characterization of japanese wooden houses with enhanced radon and tkoron concentrations. Health Phys 66: 274–282. doi: 10.1097/00004032-199403000-00007

Dosseto A, Bourdon B, Gaillardet J, Allegre CJ, Filizola N (2006) Time scale and conditions of weathering under tropical climate: Study of the Amazon basin with U-series. Geochim Cosmochim Acta 70: 71-89. doi:10.1016/j.gca.2005.06.033

Dowdall M, Gerland S, Lind B (2003) Gamma-emitting natural and anthropogenic radionuclides in the terrestrial environment of Kongsfjord, Svalbard. Sci Total Environ 305: 229–240. doi: 10.1016/S0048-9697(02)00478-3

Downs RT, Hall-Wallace M (2003) The American Mineralogist crystal structure database. Am Mineral 88: 247–250. doi: 10.5860/choice.43sup-0302

Durridge Co. (2013) RAD7 Radon Detector User Manual (Revision 7.2.1.). Boston, 77 pages, 49–63.

Dwivedi KK, Mishra R, Tripathy SP, et al (2001) Simultaneous determination of radon, thoron and their progeny in dwellings. Radiat Meas 33: 7–11. doi: 10.1016/S1350-4487(00)00131-1

Eakin M, Brownlee SJ, Baskaran M, Barbero L (2016) Mechanisms of radon loss from zircon: Microstructural controls on emanation and diffusion. Geochim Cosmochim Acta 184: 212–226. doi: 10.1016/j.gca.2016.04.024

EC (1999) Radiological protection principles concerning the natural radioactivity of building materials - Radiation Protection 112. Eur Comm pp: 24. ISNB 92-828-8376-0

Eisenbud M, Gesell TF (1997) Environmental radioactivity : from natural, industrial, and military sources. Fourth Edition, Academic Press pp: 641. ISBN - 10: 0-12-235154-1

El-Tahawy MS, Higgy RH (1995) Natural radioactivity in different types of bricks fabricated and used in the Cairo region. Appl Radiat Isot 46: 1401–1406. doi: 10.1016/0969-8043(95)00220-8

El Afifi EM, Hilal MA, Khalifa SM, Aly HF (2006) Evaluation of U, Th, K and emanated radon in some NORM and TENORM samples. Radiat Meas 41: 6277–633. doi: 10.1016/j.radmeas.2005.09.014

Esan DT, Sridhar MKC, Obed R, Ajiboye Y, Afolabi O, Olubodun B, Oni OM (2020) Determination of residential soil gas radon risk indices over the lithological units of a Southwestern Nigeria University. Sci Report 10: 7368. doi.10.1038/s41598-020-64217-8.

European Union (2013) Council Directive 2013/59/Euratom. Off J Eur Union 56: 216. pp: 73. doi: 10.3000/19770677.L_2013.124.eng

Fairbridge RW (1972) The encyclopedia of geochemistry and environmental sciences. Van Nostrand Reinhold Co., New York, N.Y.

FAO - Unesco (1977) Soil Map of the World 1 : 5 000 000, Volume VI - Africa. pp: 346. ISBN

92-3-101362-9.

Fratini F, Pecchioni E, Rovero L, Tonietti U (2011) The earth in the architecture of the historical centre of Lamezia Terme (Italy): Characterization for restoration. Appl Clay Sci 53: 509-516. doi: 10.1016/j.clay.2010.11.007

Fujiyoshi R, Sawamura S (2004) Mesoscale variability of vertical profiles of environmental radionuclides (^{40}K, ^{226}Ra, ^{210}Pb and ^{137}Cs) in temperate forest soils in Germany. Sci Total Environ 320: 177–188. doi: 10.1016/j.scitotenv.2003.08.007

Gierl S, Meisenberg O, Feistenauer P, Tschiersch J (2014) Thoron and thoron progeny measurements in German clay houses. Radiat Prot Dosimetry 160: 160–163. doi: 10.1093/rpd/ncu076

Gomes MI, Gonçalves TD, Faria P (2014) Unstabilized rammed earth: Characterization of material collected from old constructions in south portugal and comparison to normative requirements. Int J Archit Herit 8: 185–212. doi: 10.1080/15583058.2012.683133

Graulis S, Chateigner D, Downs RT, et al (2009) Crystallography Open Database - An open-access collection of crystal structures. J Appl Crystallogr 42: 726–729. doi: 10.1107/S0021889809016690

Greeman DJ, Rose AW (1996) Factors controlling the emanation of radon and thoron in soils of the eastern U.S.A. Chem Geol 129: 1–14. doi: 10.1016/0009-2541(95)00128-X

Guidotti L, Carini F, Rossi R, et al (2015) Gamma-spectrometric measurement of radioactivity in agricultural soils of the Lombardia region, northern Italy. J Environ Radioact 142: 36–44. doi: 10.1016/j.jenvrad.2015.01.010

Harley N, Chittaporn P, Medora R, Merrill R (2010)Measurement of the indoor and outdoor 220Rn (thoron) equilibrium factor: Application to lung dose. Radiat Prot Dosimetry 141: 357–362

Hayumbu P, Zaman M, Munsanje S (1995a) NATURAL RADIOACTIVITY OF ZAMBIAN COAL AND COAL ASH. Budapest JRadioanalNuclChemLetters 201: 333–346

Hayumbu P, Zaman MB, Lubaba NCH, et al (1995b) Natural radioactivity in Zambian building materials collected from Lusaka. J Radioanal Nucl Chem 199: 229–238. doi: 10.1007/BF02162371

IAEA (2014) The Environmental Behaviour of Radium: Revised Edition, Technical Reports Series No. 476, IAEA, Vienna (2014)

Jones, A., Breuning-Madsen H, Brossard M, et al (2015) Atlas Des Sols D ' Afrique

Kávási N, Németh C, Kovács T, et al (2007) Radon and thoron parallel measurements in Hungary. Radiat Prot Dosimetry 123: 250–253. doi: 10.1093/rpd/ncl102

Kis Z, Völgyesi P, Szabó Zs. (2013) DÖME: Revitalizing a low-background counting chamber and developing a radon-tight sample holder for gamma-ray spectroscopy measurements. J Radioanal Nucl Chem 298: 2029–2035. doi: 10.1007/s10967-013-2691-8

Kitson-Mills D, Sovoe S, Opoku-Ntim I, et al (2019) An assessment of indoor radon level in a suburb of Ghana. Environ Res Commun 1 :061002. doi: 10.1088/2515-7620/ab2af7

Krupp K, Baskaran M, Brownlee SJ (2017) Radon emanation coefficients of several minerals: How they vary with physical and mineralogical properties. American Mineralogist ; 102: 1375–1383. doi: https://doi.org/10.2138/am-2017-6017

Leal AL do C, Lauria D da C, Ribeiro FCA, et al (2020) Spatial distributions of natural radionuclides in soils of the state of Pernambuco, Brazil: Influence of bedrocks, soils types and climates. J Environ Radioact 211: 106046. doi: 10.1016/j.jenvrad.2019.106046

Levinson AA, Bland CJ (1978) Examples of the variability of disequilibrium and the emanation factor in some uraniferous materials. Can J Earth Sci 15: 1867–1871. doi: 10.1139/e78-194

Martinez T, Navarrete M, Gonzalez P, Ramírez A (2004) Variation in indoor thoron levels in Mexico City dwellings. Radiat Prot Dosimetry 111: 111–113. doi: 10.1093/rpd/nch371

Maxwell O, Wagiran H, Ibrahim N, et al (2013) Comparison of activity concentration of 238U, 232Th and 40K in different Layers of subsurface Structures in Dei-Dei and Kubwa, Abuja, northcentral Nigeria. Radiat Phys Chem 91: 70–80. doi: 10.1016/j.radphyschem.2013.05.006

Mehra R, Singh S, Singh K (2011) Assessment of the average effective dose from the analysis of 226 Ra, 232 Th and 40 K in soil samples from Punjab, India. Geochem J 45: 497–503

Mustapha AO, Patel JP, Rathore IVS (1999) Assessment of Human Exposures to Natural Sources of Radiation in Kenya. Radiat Prot Dosimetry 82: 285–292. doi: 10.1093/oxfordjournals.rpd.a032637

Navas A, Gaspar L, Lopez-Vicente M, Machin J (2011) Spatial distribution of natural and artificial radionuclides at the catchment scale (South Central Pyrenees). Radiat Meas 46:2 61–269. doi: 10.1016/j.radmeas.2010.11.008

Nazaroff WW (1992) Radon transport from soil to air. Rev Geophys 30: 137–160. doi: 10.1029/92RG00055

Ndontchueng MM, Mekongtso Nguelem EJ, Simo A, et al (2014) Gamma Emitting Radionuclides in Soils from Selected Areas in Douala-Bassa Zone, Littoral Region of Cameroon. ISRN Spectrosc 2014: 1–8. doi: 10.1155/2014/245125

Ngachin M, Garavaglia M, Giovani C, et al (2007) Assessment of natural radioactivity and associated radiation hazards in some Cameroonian building materials. Radiat Meas 42: 61–67. doi: 10.1016/j.radmeas.2006.07.007

Odumo OB, Mustapha AO, Patel JP, Angeyo HK (2011) Radiological survey and assessment of associated activity concentration of the naturally occurring radioactive materials (NORM) in the Migori artisanal gold mining belt of southern Nyanza, Kenya. Appl Radiat Isot 69: 912–916. doi: 10.1016/j.apradiso.2011.02.016

OECD (1979) Exposure to radiation from the natural radioactivity in building materials. Nuclear Energy Agency Organization for Economic Co-operation and Development, pp: 40

Okusami TA, Rust RH, Alao AO (1997) Red soils of different origins from southwest Nigeria: Characteristics, classification, and management considerations. Can J Soil Sci 77: 295–307. doi: 10.4141/S96-069

OpenWeatherMap (2016) Open Weather Map current weather and forecast. https://openweathermap.org/. Accessed 10 Feb 2020

Otoo F, Darko EO, Garavaglia M, et al (2018a) Public exposure to natural radioactivity and radon exhalation rate in construction materials used within Greater Accra Region of Ghana. Sci African 1: e00009. doi: 10.1016/j.sciaf.2018.e00009

Otoo F, Darko EO, Garavaglia M, et al (2018b) Seasonal indoor radon studies in buildings of Accra Metropolis of Greater Accra region of Ghana. Radioprotection 53: 199–206. doi: 10.1051/radiopro/2018023

Oyedele JA (2006) Assessment of the natural radioactivity in the soils of Windhoek city, Namibia,

Southern Africa. Radiat Prot Dosimetry 121: 337–340. doi: 10.1093/rpd/ncl025

Pacheco-Torgal F, Jalali S (2012) Earth construction: Lessons from the past for future eco-efficient construction. Constr Build Mater 29: 512–519. doi: 10.1016/j.conbuildmat.2011.10.054

Porstendörfer J (1994) Properties and behaviour of radon and thoron and their decay products in the air. J Aerosol Sci 25: 219–263. doi: 10.1016/0021-8502(94)90077-9

Rodgers JL, Nicewander WA (1988) Thirteen Ways to Look at the Correlation Coefficient. Am Stat 42: 59–66. doi: 10.2307/2685263

Saïdou, Tokonami S, Janik M, et al (2015) Radon-thoron discriminative measurements in the high natural radiation areas of southwestern Cameroon. J Environ Radioact 150: 242–246. doi: 10.1016/j.jenvrad.2015.09.006

Saini K, Singh P, Singh P, et al (2016) Seasonal variability of equilibrium factor and unattached fractions of radon and thoron in different regions of Punjab, India. J Environ Radioact. 167: 110-116. doi: 10.1016/j.jenvrad.2016.11.022

Sakoda A, Nishiyama Y, Hanamoto K, et al (2010) Differences of natural radioactivity and radon emanation fraction among constituent minerals of rock or soil. Appl Radiat Isot 68: 1180–1184. doi: 10.1016/j.apradiso.2009.12.036

Salupeto-Dembo J, Szabó-Krausz Z, Völgyesi P, Kis Z, Szabó Cs (2020) External radiation exposure of the Angolan population living in adobe houses. J Radioanal Nucl Chem. 32: 353-364. doi: 10.1007/s10967-019-06920-z

Salupeto-Dembo J, Szabó-Krausz Z, Völgyesi P, Szabó Cs (accepted) Radon and thoron radiation exposure of the Angolan population living in adobe houses. J Radioanal Nucl Chem, doi: 10.1007/s10967-020-07215-4

Santawamaitre T, Malain D, Al-Sulaiti HA, et al (2014) Determination of238U,232Th and40K activity concentrations in riverbank soil along the Chao Phraya river basin in Thailand. J Environ Radioact 138: 80–86. doi: 10.1016/j.jenvrad.2014.07.017

Sasaki T, Gunji Y, Okuda T (2004) Mathematical modeling of radon emanation. J Nucl Sci Technol 41: 142–151. doi: 10.1080/18811248.2004.9715470

Schery SD (1990) Thoron in the Environment. J Air Waste Manag Assoc 40: 493–497. doi:

10.1080/10473289.1990.10466704Selagen P (2071) Metallic oxides and hydroxides in soils of the warm and humid areas of the world: formation, identification, evolution. In: Soils and Tropical Weathering 2: 25-38 Proceedings of the Bandung Symposium, 16-23 November 1969, UNESCO, Paris.

Shang B, Chen Æ Bin, Gao ÆY, Wang ÆY (2005) Thoron levels in traditional Chinese residential dwellings. Radiat Environ Biophys 44: 193–199. doi: 10.1007/s00411-005-0020-5

Shimboyo SA, Oyedele JA, Sitoka SS (2016) Soil Radioactivity Levels And Associated Hazards In Selected Towns In Uranium-Rich Western Namibia. Int Sci Technol J Namibia 7: 73–84. ISSN: 2026-7673

Smith, Cothern (1987) Environmental Radon, 1st Editio. Springer Science + Business Media, New York ISBN 978-1-4899-0475-1, pp: 359, DUI 10.1007/978-14899-0473-7

Somlai J, Jobbágy V, Somlai K, et al (2008) Connection between radon emanation and some structural properties of coal-slag as building material. Radiat Meas 43: 72–76. doi: 10.1016/j.radmeas.2007.10.028

Stojanovska Z, Bossew P, Tokonami S, et al (2013) National survey of indoor thoron concentration in FYR of Macedonia (continental Europe-Balkan region). Radiat Meas 49: 57–66. doi: 10.1016/j.radmeas.2012.11.023

Stoops G, Marcelino V, Mees F (2010) Interpretation of Micromorphological Features of Soils and Regoliths. 2nd Edition, Elsevier pp: ISBN 9780444531568, 9780080932309 pp: 969

Stranden E, Kolstad AK, Lind B (1984) The Influence of Moisture and Temperature on Radon Exhalation. Radiat Prot Dosimetry 7: 55–58. doi: 10.1093/oxfordjournals.rpd.a082962

Szabó KZs, Jordan G, Petrik A, Horváth Á, Szabó Cs (2017) Spatial analysis of ambient gamma dose equivalent rate data by means of digital image processing techniques. J Environ Radioact 166: 309–320. doi: 10.1016/j.jenvrad.2016.07.013

Szabó Zs (2013) TERRESTRIAL RADIOACTIVITY IN HUNGARIAN ADOBE BUILDING MATERIAL AND DWELLINGS WITH A FOCUS ON THORON (^{220}RN). Doctoral Thesis, Eötvös Loránd University, Budapest pp: 128.

Szabó Zs, Jordan G, Szabó Cs, et al (2014) Radon and thoron levels, their spatial and seasonal variations in adobe dwellings - a case study at the great Hungarian plain. Isotopes Environ

Health Stud 50: 211–225. doi: 10.1080/10256016.2014.862533

Szabó Zs, Völgyesi P, Nagy HÉ, Szabó Cs, Kis Z, Csorba O (2013) Radioactivity of natural and artificial building materials - a comparative study. J Environ Radioact 118: 64–74. https://doi.org/10.1016/j.jenvrad.2012.11.008

Tahir SNA, Jamil K, Zaidi JH, et al (2005) Measurements of activity concentrations of naturally occuring radionuclides in soil samples from Punjab province of Pakistan and assessment of radiological hazards. Radiat Prot Dosimetry 113: 421–427. doi: 10.1093/rpd/nch484

Takoukam S. S, Saïdou, Tokonami S, et al (2019) Simultaneous measurements of indoor radon and thoron and inhalation dose assessment in Douala City, Cameroon. Isotopes Environ Health Stud 55: 499–510. doi: 10.1080/10256016.2019.1649258

Thamer BJ, Nielson KK, Felthauser K (1981) The effects of moisture on radon emanation including the effects on diffusion. Bur Mines USA 213, NTIS: PB/83-136358 pp: 213

Tokonami S, Sun Q, Akiba S, et al (2004) Radon and Thoron Exposures for Cave Residents in Shanxi and Shaanxi Provinces. Radiat Res 162: 390–396. doi: 10.1667/rr3237

Tokonami S, Takahashi H, Kobayashi Y, et al (2005) Up-to-date radon-thoron discriminative detector for a large scale survey. Rev Sci Instrum 76: 1–5. doi: 10.1063/1.2132270

Tokonami S, Yang M, Sanada T (2001) Contribution from thoron on the response of passive radon detectors. Health Phys 80: 612–615. doi: 10.1097/00004032-200106000-00014

Trevisi R, Caricato A, D'Alessandro M, et al (2010) A pilot study on natural radioactivity in schools of south-east Italy. Environ Int 36: 276–280. doi: 10.1016/j.envint.2009.12.008

Tzortzis M, Tsertos H, Christofides S, Christodoulides G (2003) Gamma-ray measurements of naturally occurring radioactive samples from Cyprus characteristic geological rocks. Radiat Meas 37: 221–229. doi: 10.1016/S1350-4487(03)00028-3

UNSCEAR (2000) Exposures from natural radiation sources (Annex B). Sources Eff Ioniz Radiat 84–141. doi: 10.1097/00004032-199907000-00007

UNSCEAR (2008) Sources and effects of ionizing radiation 1 pp: 143

UNSCEAR (2010) Exposures of the Public and Workers from Various Sources of Radiation. Annex B. In: Sources and effects of ionizing radiation. pp: 281

USDA (1999) Soil Taxonomy. A Basic System of Soil Classification for Making and Interpreting Soil Surveys. Agriculture Handbook No. 436. Soil Conservation Service, U.S. Department of Agriculture. From Superintendent of Documents, U. Agric Handb Number 436, pp: 869 . doi: 10.1017/S0016756800045489

Valentin, J. (2007) Annal of the ICRP Publication 3, The 2007 Recommendations of the International Commission on Radiological Protection. doi: 10.1016/j.icrp.2007.11.001, pp: 328

Varga G., Gresina F., Újvári G., Kovács J., Szalai Z. (2019) On the reliability and comparability of laser diffraction grain size measurements of paleosols in loess records. Sedimentary Geology 389: 42-53, ISSN 0037-0738, doi: 10.1016/j.sedgeo.2019.05.011

Völgyesi P (2015) Environment geochemical and radiometric study of building material and attic dust samples affected by industrial activity in Hungary. Doctoral Thesis, Eötvös Loránd University, Budapest pp:155

Völgyesi P, Szabó Z, Salupeto-Dembo J, Kis Z, Szabó Cs (2016) Gamma-spektrometriai módszer magyarországi salakminták 226 Ra aktivitáskoncentrációinak meghatározására a 186 keV-os csúcs használatával. Sugárvédelem, IX: 25–32.

Wells DF, Brown CW (2009) Processing Powder X-ray Diffraction Patterns with a Fourier Transform Digital Band Pass Filter. Instrum Sci Technol 37: 89–101

WHO (2010) Indoor Radon a Public Health Perspective. Int J Environ Stud 67: 108. doi: 10.1080/00207230903556771

Wilford, J.R.; Bierwirth, P.N.; Craig MA, Citation (1997) Application of airborne gamma-ray spectrometry in soil/regolith mapping and applied geomorphology. AGSO J Aust Geol Geophys ISSN 1320-1271; Worldcat; CODEN AJGGEF; 17, 28: 201–216

World Health Organization (WHO) (2016) Radon and health. https://www.who.int/news-room/fact-sheets/detail/radon-and-health. Accessed 26 Mar 2020

Table of Figures

Tables

Summary

NATURAL RADIOACTIVITY IN ANGOLAN ADOBE HOUSES AND BUILDING MATERIALS

Measurement of environmental radioactivity in Angola is a novelty despite of a growing interest in determining radiation exposure of human populations worldwide. This study is the first aiming to investigate the radioactivity in Angolan adobe houses, a widely used building material representing the radioactivity of the soil and the source rock. In one hand indoor radon and thoron activity concentrations are investigated in this study. Activity concentrations were recorded by passive detectors in rainy and dry seasons in 40 adobe dwellings located at three areas with different climatic and geological backgrounds (Cabinda in the North, Huambo in the central and Menongue in the South). Seasonal and spatial variations were investigated showing higher values in the rainy than in the dry season and both radon and thoron levels are the highest in Huambo, the central part of the country. The number of adobe houses above certain radon and thoron levels were predicted for Angola (10-32 % of houses are predicted to be above 100 Bq m-3 radon activity concentration, and 59-81 % would be above 100 Bq m-3 and 6-28 % above 300 Bq m-3 thoron activity concentration at the 95 % confidence level). The contribution of thoron to the inhalation dose was estimated to be 50% in average. The study confirmed that radon and thoron may cause a non-negligible contribution to the internal radiation exposure. In other hand, sixty adobe samples have been collected. Activity concentrations of Ra 226, Th 232 and K 40 have been determined by gamma-ray spectroscopy. These values were used to calculate radiation hazard indexes of these building materials and to estimate external doses of residents. Estimated external doses were compared to in-situ measured ambient gamma dose equivalent rates as well. Average Ra-226, Th-232 and K-40 activity concentrations in Bq kg-1 are 26 ± 7, 36 ± 5, 45 ± 17 in Cabinda, 87 ± 20, 81 ± 21, 82 ± 15 in Huambo and 27 ± 10, 30 ± 10, 73 ± 40 in Menongue, respectively. Huambo shows elevated Ra 226 and Th 232 values which can be explained by its older geological formations. Regarding K-40, values are low compared to other countries. Based on the determined Raeq and I indexes, and also measured and calculated external doses, adobe building material from Angola does not represent an external radiation risk. The altitudes of settlements significantly contribute to in-situ measured ambient gamma dose equivalent rates.

The structural properties of the studied adobe connected to the aim of the study have been analysed by determining the emanation fraction, grain size distribution by laser diffraction, and mineralogical composition by XRD. Averages with standard deviation (range) of radon and thoron emanation (in kg^{-1} s^{-1}) are 60±32 (13-148) and 5±2 (2-12) respectively. The same values from respective studied areas are 34±30 (13-55) and 5±3 (2-12) in Cabinda, 81±39 (50-148) and 7±2 (3-9) in Huambo, 50±9 (37-61) and 4±1 (2-5) in Menongue respectively. As for the emanation factor in % values for radon and thoron accounted for all areas are 19±10 (8 – 39) and 12±6 (4 – 31) for all samples. In the three study areas, those values for radon and thoron, respectively, correspond to 16±11 (8 – 24) and 14±7 (8 – 31) in Cabinda, 12±4 (9 – 17) and 8±2 (4 – 11) in Huambo and 28±9 (16 – 39) and 14±5 (6 – 27) in Menongue. Samples from Huambo have the highest radon and thoron emanations but the lowest emanation fractions while those from Menongue basically show the opposite, which puts Cabinda into the middle. Emanations were shown to connect to radionuclide contents and the emanation fractions are explained by the grain size distributions and the mineralogical compositions of the samples. Cabinda has the highest sand contribution and Menongue the highest clay content. The exceptional results in Huambo are connected to differences in source minerals, like the presence of zircon and rutile and other accessory minerals from the granitic bed rock.

DOI Nr: 10.15476/ELTE.2020.057